AD-A110 306 TRW DEFENSE AND SPACE SYSTEMS GROUP REDONDO BEACH CA F/G 20/5
FREE ELECTRON LASER THEORETICAL STUDY.(U)
NOV 81 M Z CAPONI, C SHIH, J DAWSON, T LIN F49620-80-C-0079
UNCLASSIFIED FEL-27R AFOSR-TR-81-0889 NL

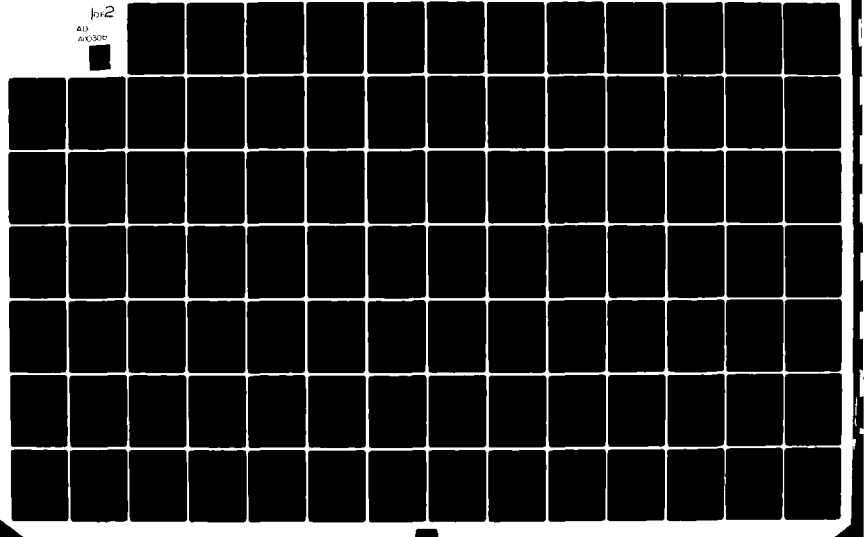

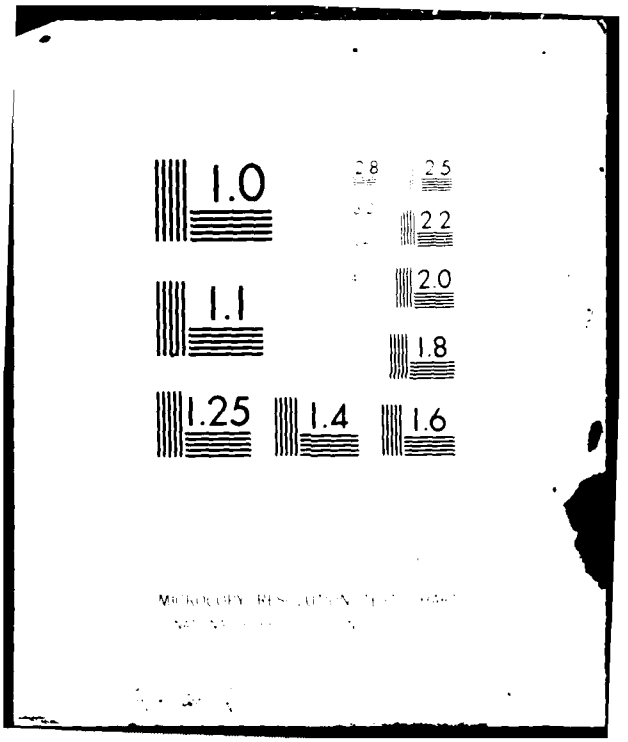
1.0
1.1
1.25
1.4
1.6
1.8
2.0
2.2
2.5

AD A110306

DTIC FILE COPY

UNCLASSIFIED

SECURITY CLASSIFICATION OF THIS PAGE (When Data Entered)

REPORT DOCUMENTATION PAGE		READ INSTRUCTIONS BEFORE COMPLETING FORM
1. REPORT NUMBER AFOSR-TR-82-0889	2. GOVT ACCESSION NO. AD-A110 306	3. RECIPIENT'S CATALOG NUMBER
4. TITLE (and Subtitle) Free Electron Laser Theoretical Study; Investigation of finite geometry effects, small signal gain enhancement and parasitic instabilities		5. TYPE OF REPORT & PERIOD COVERED Final, 80 Jul 01 to 81 Sept. 30
		6. PERFORMING ORG. REPORT NUMBER 81. FEL-27R
7. AUTHOR(s) M. Zales Caponi, C. Shih; TRW and J. Dawson, T. Lin, K. Whang; UCLA		8. CONTRACT OR GRANT NUMBER(s) F49620-80-C-0079
9. PERFORMING ORGANIZATION NAME AND ADDRESS Energy Research Center, TRW, One Space Park, Redondo Beach, CA. 90278		10. PROGRAM ELEMENT, PROJECT, TASK AREA & WORK UNIT NUMBERS 61102F 2301/A1
11. CONTROLLING OFFICE NAME AND ADDRESS Director, Physical and Geophysical Sciences, Air Force Office of Scientific Research, CODE F98671 Building 410, Bolling AFB, D.C. 20332		12. REPORT DATE 81 Nov. 30
		13. NUMBER OF PAGES 106
14. MONITORING AGENCY NAME & ADDRESS(if different from Controlling Office)		15. SECURITY CLASS. (of this report) Unclassified
		15a. DECLASSIFICATION/DOWNGRADING SCHEDULE

LEVEL II

16. DISTRIBUTION STATEMENT (of this Report)

Approved for public release - unlimited distribution

DTIC ELECTE FEB 1 1982 S H

17. DISTRIBUTION STATEMENT (of the abstract entered in Block 20, if different from Report)

18. SUPPLEMENTARY NOTES Section II, III & IV of this report have been presented in part at the IEEE International Conference in Plasma Physics, May 1981 & APS, Div. of Plasma Physics Oct. 1981. Section III has been accepted for publication in almost identical form in Physics Review A. Section IV will be sent for publication to Physics Review A. Section V has been published in part in (over)

19. KEY WORDS (Continue on reverse side if necessary and identify by block number)

Free Electron Laser, Tapered Wiggler Free Electron Laser, Multicomponent Wiggler Free Electron Laser, High Power Source, Visible radiation, Small Signal gain.

82

20. ABSTRACT (Continue on reverse side if necessary and identify by block number) This is the final report of the Free Electron Laser Theoretical Study carried out by TRW for the AFOSR during the period July 80 to September 81. Four distinct but interrelated problems that play an important role in the characteristics of a Free Electron Laser oscillator were investigated: 1) Transverse Effects: The effect of wiggler field inhomogeneity as well as the influence of different transverse profiles of the signal field and the electron beam on the FEL characteristics were studied in detail. A dramatic decrease in gain and efficiency is found with increasing value of the ratio of electron beam radius to photon beam (over)

DD FORM 1 JAN 73 1473 EDITION OF 1 NOV 65 IS OBSOLETE

UNCLASSIFIED

SECURITY CLASSIFICATION OF THIS PAGE (When Data Entered)

407 631

18. Physics Review Letters, 1981.

20. radius. 2) Small Signal (SS) Gain: A1-D investigation of the small signal gain for a Tapered Wiggler Free Electron Laser was performed analytically for cold electron beams and numerically for cold and warm electron beams. It was found that the small signal gain spectrum shifts and decreases in amplitude as a function of increasing wiggler taper. 3) Multicomponent Wiggler Free Electron Laser (MCWFEL): The results from 1) and 2) motivated the development of a new FEL configuration that could have high small signal gain and sufficiently high efficiency at high powers with nearly the same output frequency. The new FEL is a combination of several wiggler components. 4) Finite Pulse Length Simulations and Kinetic Effects of Trapped Particle Instabilities in Free Electron Lasers: A 1-D finite pulse code was developed and the effects of pulse slippage detrapping of electrons at the beam edge and parasitic instabilities investigated for a tapered wiggler Free Electron Laser.

4

FREE ELECTRON LASER THEORETICAL STUDY

FINAL REPORT

F49620-80-C-0079

Prepared for the AFOSR

FOR THE PERIOD OF PERFORMANCE

COVERING JULY 1980 to SEPTEMBER 1981

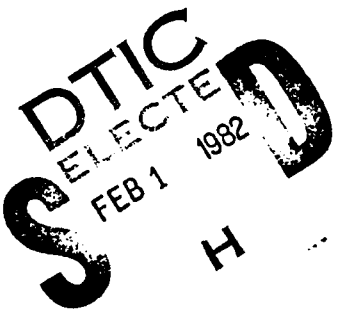

by

M. ZALES CAPONI and C. SHIH

TRW, Energy Research Center, One Space Park

Redondo Beach, California 90278

and

J. DAWSON, T. LIN and K. WHANG

UCLA, Plasma Simulation Group

(Under TRW subcontract No. J76648 DCOE)

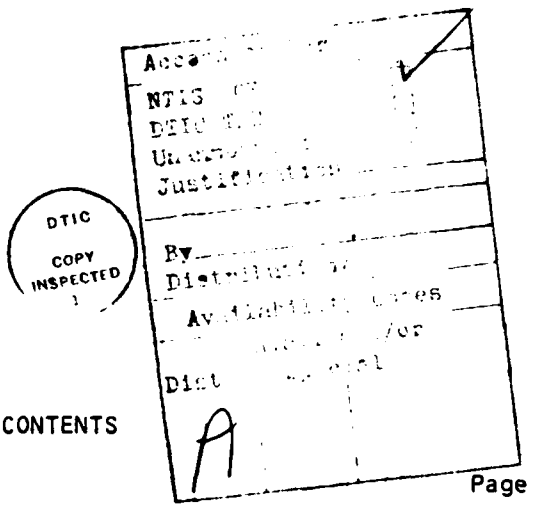

TABLE OF CONTENTS

TABLE OF CONTENTS (Continued)

I. INTRODUCTION

A Free Electron Laser (FEL) device[1] generates stimulated radiation by the interaction of a relativistic electron beam and an external electromagnetic wave or pump. The intensity of the emission increases with the pump amplitude and it is advantageous to use an external ripple magnetic field ("wiggler") as the external pump. The FEL with a wiggler of constant pitch and amplitude (CWFEL) has a large small signal (ss) gain, but a low high signal (hs) gain and efficiency ($\eta < 0.1\%$) for optical wavelengths.[2,3,4] By adiabatically tapering the wiggler field amplitude and/or wavelength (tapered wiggler FEL, TWFEL), the predicted hs gain and efficiency can be dramatically enhanced.[2,5] A considerable amount of theoretical work has been carried out to describe the TWFEL characteristics. However, until recently most of the studies utilized simplified models that assumed one dimensional, infinite length electron beams, single mode excitation, single pass and amplifier (hs) operation. Although these simplifications are quite useful to understand the TWFEL mechanisms, they limit the range of applicablity of the theories, mainly to predict the characteristics of practical FEL devices. In addition, the validity of most of the assumptions have to be reevaluated to study FEL oscillators.

It was the purpose of the FEL theoretical study reported here to investigate the influence of relaxing some of these simplifying assumptions on the TWFEL characteristics. In particular, the investigations were focussed on the following problems: 1) transverse effects; wiggler field inhomogeneity, electron and photon beam radial profiles; 2) small signal behavior as a function of taper; 3) small signal gain enhancement for TWFEL; reduction of the number of photon passes to design a practical

oscillator; 4) finite electron beam pulse effects and parasitic instability growth and saturation. The results of these investigations are described in detail in Sections II through V, respectively, of this report. Each section is self-contained, describing the problem, the objective of the research, the approach taken and the results obtained in detail. Section V was performed by UCLA under subcontract to TRW. In what follows, we briefly summarize the contents of each section.

In Section II, the transverse effects are described. For an optical FEL, the electron beam is of the order of a few millimeters in the transverse direction. The electron beam radius is chosen so that the beam is in equilibrium with the high amplitude wiggler field. This dimension is quite different than that of a propagating electromagnetic wave. Due to the betratron oscillations caused by the wiggler field, the electrons sample different amplitudes of wiggler and radiation field. Since the TWFEL efficiency and gain strongly depend on the amplitude of the wiggler field and the power density of the radiation, these effects can play an important role in the final gain value, its spectrum and its radial dependence. In this report, the influence of the wiggler field inhomogeneity on the electron beam dynamics and hence on the FEL characteristics is investigated in detail and compared with the effective energy spread approximation.[6] An analytical formula was calculated for the particle orbits in the transverse direction that includes the nonlinear wiggler tapering and the untrapping of particles at the edges of the bucket in the interaction region. This formula will permit the development of a cost-effective 3-D oscillator code. In the present investigation it was utilized to predict the behavior of a TWFEL that utilizes a finite emittance electron beam, as a function of input power and to study the effect on the TWFEL characteristics, (gain, gain spectrum and efficiency) of Gaussian versus square profiles for both electrons and photons. These initial studies provide the building blocks for the possible formulation of numerically cost-effective 3-D analyses valid for small signal as well as high signal gain.

The effects of the wiggler inhomogeneities were found to be well represented (withing 10-15%) by an effective energy spread as long as this effective energy spread is smaller than the ponderomotive force bucket

height. Thus, it is a bad representation for small signal gain calculations, even for very small emittance electron beams resulting in a problem of importance for oscillator start-up. For amplifier operation, the analysis shows that the combination of the wiggler inhomogeneity and the initial electron velocity cancels the effect of the betatron oscillations in the phase equation for the electrons and only the effect of their initial transverse coordinates remains. That is, once the initial increase in energy spread due to electrons starting at different positions, with different amplitude of the wiggler field, is taken into account no additional untrapping is introduced by the betatron oscillations.

The effect in the deceleration efficiency, and hence in gain introduced by the fact that, due to their betatron oscillations, the electrons sample different values of radiation power density, is found to depend on the ratio of the total equilibrium electron beam radius (R_e) to the optical beam radius at the waist (R_{pw}). The maximum effect, however, that occurs for $R_e/R_p \simeq 0.6$ corresponds to an increase in gain when betatron oscillations are included of less than 15%. A dramatic decrease in gain and efficiency is found as the ratio R_e/R_{pw} increases from zero. In particular, the gain decreases from G_o at $R_e = 0$, to $G_o/1.6$ at $R_e = 0.7\ R_{pw}$, to $G_o/4$ for $R_e = R_{pw}$.

These results will be submitted for publication as a technical note and have been presented at the IEEE International Plasma Conference (Santa Fe, May 1981) and at the FEL Workshop in Idaho, June 1981.

In Section III, the small signal gain studies are presented. The results from this investigation were submitted for publication to Physics Review A and has been accepted subject to small revisions. For a TWFEL, the gain is enhanced over that of a CWFEL only at a given optimum amplifier operation, input radiation power. For other powers, the gain decreases and this unusual behavior becomes of concern for oscillator operation. Further, the gain spectrum itself varies as a function of radiation power and therefore problems like frequency hopping or multimode operation that can either delay or completely impossibilitate the arriving of the oscillator saturation state may happen. In this report, a 1-D analytical and numerical investigation of the TWFEL small signal gain is presented. An analytical formula for the gain was derived that

is valid for any "type" of wiggler tapering, including multicomponent wigglers (Section IV). A parametric study of the small signal gain spectrum for different wiggler tapers was carried out in detail.

The small signal gain for a TWFEL was found (as expected) to have the same general characteristics as for the CWFEL. The unusual result, however, is that the spectrum shifts and decreases in amplitude as a function of increasing wiggler taper. Thus, it can be either negative or positive for $\gamma = \gamma_r$. The maximum positive small signal gain in general occurs for $\gamma \leq \gamma_r$. For increasing input power, the value of γ (or output frequency) that correspondends to maximum gain for a given taper varies. At the "optimum" input power for amplifier operation (that at which the gain is maximum for a given taper), the maximum gain occurs for $\gamma = \gamma_r$. For input powers higher than this (where saturation occurs for oscillator operation), the optimum energy is $\gamma > \gamma_r$.

This variation of the gain curve with input power becomes crucial for an oscillator, since it will determine if the oscillator can be started at either low input powers for an electron beam with $\gamma = \gamma_r$ or if large input powers are necessary, making the oscillator impractical. Further, if the oscillator is started from noise, it will start at a frequency that is shifted from the optimum one at saturation. This will result in very long times to reach equilibrium if it can be reached at all, and an increase in the output frequency bandwidth.

The results from the small signal gain study motivated the development of a new FEL configuration that could have high small signal and large signal gain at the same radiation frequency. This configuration is described in Section IV. The new FEL scheme is a combination of several wiggler components: multicomponent wiggler FEL (MCWFEL). The scheme is similar in certain aspects to the optical klystron for CWFEL that consists of a "prebuncher" and a "radiator" section separated by a drift section. The main difference with a MCWFEL is that the unusual behavior of the tapered wiggler gain curve requires a different arrangement of the components and more than one radiator. In this manner, each component operates at its optimum input power and is transparent at others. The components are in general a couple of constant wigglers, a drift space and a tapered wiggler of appropriate lengths and ordered in an appropriate manner. Encouraging

preliminary results were obtained for a 10.6 μm device of characteristics similar to those of the TRW experiment and also for 1 μm. The results for 10 μm are presented in this report. The investigations of gain and efficiency enhancement by a MCWFEL were performed with a 1-D code that assumed a Gaussian optical beam propagation for both input and excited wave. Initial studies were also performed of the characteristics of the different wiggler components and its influence in the small gain.

The better MCW configurations were found to be composed of a small prebuncher section, a drift section, followed by a constant wiggler or very small taper section for operation at small signal followed by a small drift section for phase adjustment and followed by a tapered section for operation at high signal. A number of different configurations and their main characteristics are also presented in Section IV. The results from these investigations will be submitted to Physics Review A for publication and have been presented at the IEEE International Conference on Plasma Physics (Santa Fe, May 1981) and the October APS Meeting of the Division of Plasma Physics, New York, 1981.

The investigations carried out by UCLA under subcontract from TRW for the AFOSR are presented in Section V of this report. The excited radiation pulse, although initially of the same length than the electron beam, changes shape as a function of time due to the difference in velocity between both pulses. This change in shape due to slippage can untrap electrons reducing the gain. The effect, that can be small for an amplifier, becomes quite large in an oscillator. In order to study these effects as well as those due to the possible growth of parasitic (trapped particles) instabilities, a 1-D finite pulse code was developed. The code was tested also for CWFEL. A unique feature of the code, in addition to the possibility of variable tapering, is the self-consistent description of the pulse density and of D.C. space charge effects. The space charge field is due to the large density of the microbunch electron pulse and there was initially a concern that it could cause untrapping due to an increase in the effective energy spread. To date, slippage and space charge effects as well as the influence of different electron and optical beam profiles have been analyzed with this code for amplifiers of the characteristics of the TRW 10.6 μm experiments and for higher

gain ones. A multimode description that will permit to study harmonic growth and sideband instability in detail has been included in the code recently. In addition, the nonlinear mechanisms which limit the enhancement process of the parasitic instabilities were observed with the use of an infinite electron beam code and the linear growth of the instabilities was analytically calculated with a kinetic treatment. Some of the results from these investigations were published in a Physical Review Letters paper, a copy of which is attached to this section.

For a TWFEL amplifier, where the gain is moderate, it was found that the "slippage" and "edge" effect as simulated by the 1-D finite electron and optical beam pulse TWFEL code do not play a very important role. The electron dynamics is dominated by the input laser pulse that is modeled after the TRW experiment. Thus, the input optical pulse is much longer (1.3 nsec) than the electron beam pulse (30-40 psec). Still, the overall (averaged) gain of the system was found to be a factor of two smaller than the gain at the center of the pulse due to the Gaussian (in length) shape of the electron pulse and hence of the excited optical pulse. For larger gains, however, it was found that even for an amplifier the untrapping of the electron at the edge plays an important role. For example, for a total gain G = 100 percent, the overall gain is decreased by a factor of 10 with respect to what is predicted by the periodic code. The space charge effects were found to be negligible in situations similar to the TRW experiment. This effect, however, can play a role for some of the planned 1 μm experiments if the bunched electron beam has to drift more than 50 meters between the source and the interaction region. In addition, the influence of both space charge and slippage for oscillators where small effects are enhanced by the large number of bounces of the optical beam is still in progress.

REFERENCES I

1. H. Motz, J. Appl. Phys. 22, 527 (1951)

2. P. Sprangle, R. Smith, NRL Memorandum Report 9033, Jan. 1977; also P. Sprangle, C.K. Tang, W.H. Hanheimer, Phys. of Q. Elec. 7, 207 (1980)

3. M. Za'es Caponi, J. Munch, H. Boehmer, Phys. of Q. Elec. I, 523 (1980)

4. E.B. Colson, Phys. Q. Elec. 5, 157 (1977)

5. N.M. Krall, P. Horton and M. Rosenbluth, J. of Q. Elect. 7, 113 (1980)

6. U.K. Neil, "Emittance and Transport of Electron Beams in a Free Electron Laser", JASON Technical Report JSR-79-10, SRI Internat., Dec. 1979

II. STUDY OF THE INFLUENCE OF TRANSVERSE EFFECTS ON THE CHARACTERISTICS OF A TAPERED WIGGLER FREE ELECTRON LASER

In the Free Electron Laser interaction, the amplitude of the wiggler magnetic field, the radiation field and the electron beam current density play a crucial role. Due to the finite geometry of the system, all of these parameters vary not only along the direction of propagation of the electron beam but also perpendicular (transverse) to it. Hence, in order to obtain a detailed description of the FEL characteristics it would be necessary to develop a three or at least two dimensional analysis of the FEL system. Because of the complexity of the problem, these analysis are in general numerical. In particular, what is required is a two or three dimensional numerical simulation that self-consistently solves the equations of motion of the particles and the Maxwell Equations for the fields. Unfortunately, this type of sophisticated numerical study is extremely expensive and time consuming even for the fast computers of today, and therefore only very few and isolated results for a few sets of parameters could be obtained.

Until recently, in order to obtain parametric studies of the characteristics of a FEL system, the transverse effects were neglected and a simplified, and fast one-dimensional analysis and/or numerical simulation was performed. After these initial investigations, a number of formulations[1,2] were developed to include the influence of transverse effects in the FEL characteristics. In these formulations, the effect of the transverse nonuniformity of the magnetic field and the particles transverse motion are assumed neglegible. In addition the system is treated as a low gain amplifier, that is the input signal is assumed much larger than the excited one

and in most cases is taken to be a plane wave. These simplifications are necessary in order to make the problem tractable computer-wise. Thus, only the three dimensional behavior of the excited wave needs to be calculated.

The neglected transverse contributions, however, can play an important role for a practical FEL oscillator. For example, the particles execute betatron oscillations and sample different wiggler and radiation fields as they travel along their trajectories. Although this effect has been accounted for up to now as an "effective" energy spread, it is not clear that that is the case for some practical experimental parameters.[3] Further, a practical FEL oscillator should start up from noise or with a very small signal and therefore the "amplifier" assumption will no longer hold. Finally, the diffraction of the input Gaussian beam does play an important role in the FEL characteristics for sufficiently long interaction lengths.

In order to analyze the importance of the transverse effects in their totality and to formulate a method that would permit its inclusion in a numerical code in an effective manner, we initiated a study, the first results of which are reported in this section. An analytical formula was calculated for the particle orbits in the transverse direction that includes a non-linear wiggler tapering and the untrapping of particles at the edges of the ponderomotive potential well (bucket) in the interaction region. This formula permits the development of a cost effective numerical simulation that includes the transverse motion of the particles as well as the details of an input Gaussian beam. The code, however, neglects the effect of the interaction on the diffraction of the excited wave. These effects however would be included with a new formulation that we are devloping at the present time. The code was utilized for parameters typical of the TRW experiment and for a parametric study that shows the change in the FEL characteristics with electron beam emittance and the ratio of the electron beam radius to photon beam radius.

In general, in a realizable wiggler, the transverse wiggler field is sinusoidal on its axis. This behavior has been checked, for example, by measuri the magnetic field on the wiggler axis of the TRW 10.6 μm experiment setup.[4] In this case, it was found that the contribution of higher harmonics in less than 0.1 percent. The fact that the magnetic field is divergenceless shows that the field has to vary as well in the transverse

direction with a similar variation constant. Due to this transverse nonuniformity in the magnetic field, the electrons away from the wiggler axis tend to bend toward the axis. Overall, the electron beam exibits a periodic focusing effect which is usually understood as betatron oscillations.

The negligence of transverse contributions is justifiable only when the electrons are very close to the wiggler axis such that they do not experience transverse variation of both fields. Unfortunately, this is not the case. With a finite emittance, the electron beam diverges in the free space. The smaller the beam waist, the greater the divergence of the electron beam. In order to avoid such problem, the beam has a minimum waist at the wiggler entrance such that the divergence can be balanced by the wiggler focusing. It turns out that this radius is comparable to the characteristic distance of the transverse variation in the wiggler field and radiation field. Therefore, the transverse effect can not be neglected completely without careful justification.

For a plane-polarized (in the x direction) wiggler, the magnetic field can be found easily from $\nabla \cdot A_y(x, z) = 0$ and the assumption that the field is translation invariant in the y direction.

$$A_y(x, z) = A_o \cosh k_w x \cos k_w z \tag{1}$$

where A_o is the vector field amplitude and $k_w = 2\pi/\lambda_w$ is the wave number of the wiggler field. The vector field in equation 1 gives the transverse and longitudinal magnetic field as

$$\begin{aligned} B_x(x, z) &= B_o \cosh k_w x \sin k_w z \\ B_z(x, z) &= B_o \sinh k_w x \cos k_w z \end{aligned} \tag{2}$$

It can be seen that the longitudinal and transverse field variations are not independent of each other. They have the same characteristic constant, k_w, however, the transverse variation is in hyperbolic functions. On the wiggler axis, B_x reduces to a sinusoidal function of z and B_z vanishes.

The field in equation 2 represents correctly the wiggler field near the axis for any wiggler design. For the field far from the axis, it is structure-dependent and has to be determined by boundary conditions. However, the far field is of little use because the field in equation 2 covers well the region of our concern.

In a magnetic field (equation 2), the Lorentz equation describing the electron trajectory is reduced to

$$\frac{d^2x}{dz^2} = -\frac{a_w^2 k_w}{4\gamma^2} \sinh 2k_w x \,(1 + \cos 2k_w z)$$

$$\frac{d^2(\Delta z)}{dz^2} = \frac{a_w^2 k_w}{4\gamma^2} (1 + \cosh 2k_w x) \sin 2k_w z \qquad (3)$$

$$a_w = \frac{eB}{mc^2 k_w}$$

where a_w is a dimensionless wiggler field amplitude and Δz is the position deviation of the electron from a freely propagating beam. In equation 3, we have replaced the time variable with the position variable z.

The term, $\cos 2k_w z$, in equation 3 is a fast oscillating contribution to the trajectory. However, the variation in x is much slower and hardly affected by this fast osciallation. This argument is supported by numerical simulation which shows that the fast oscillating term can be completely neglected without introducing any significant difference in the result. Moreover, for typical experimental parameters[4] x is about 1 mm which gives $2k_w x \approx 0.3$. Therefore, $\sinh 2k_w x$ can be substituted by $2k_w x$ within an error of 2 percent. The resulting equation is quite simple

$$\frac{d^2x}{dz^2} = -\frac{a_w^2 k_w^2}{2\gamma^2} x \qquad (4)$$

Equation 4 is identical to a simple pendulum equation with samll amplitude. All electrons have the same oscillation period

$$\Lambda = \frac{\sqrt{2}\gamma\lambda_w}{a_w} \tag{5}$$

An exact calculation of equation 3 gives a shorter period for the outer electrons. However, the difference from equation 5 is minimum. The electron trajectory is then found to be described best by the equation

$$\begin{pmatrix} x(z) \\ u(z) \end{pmatrix} = \begin{pmatrix} \cos kz & \sin kz \\ -\sin kz & \cos kz \end{pmatrix} \begin{pmatrix} x(o) \\ u(o) \end{pmatrix} \tag{6}$$

$$u = v_x(z)/(kc)$$

$$k = 2\pi/\Lambda$$

where u is a measure of the transverse velocity in units of length, and k is the wave number of the betatron oscillation. Equation 6 indicates that the propagation of electrons in a constant wiggler is only a rigid rotation of its distribution in the phase space x - u. The rotation angle, kz, is directly proportional to the propagation distance. The invariant quantity for individual electrons is $(x^2 + u^2)$. Obviously, the electron distribution is an invariant if the initial distribution is isotropic in the phase space. For a Gaussian distribution, the density can be written as

$$N_e \propto e^{-\left(\frac{x^2}{x_e^2} + \frac{u^2}{u_e^2}\right)} \tag{7}$$

where x_e and u_e are the beam radius in real and velocity space. The condition $x_e = u_e$ defines the equilibrium state for the electron beam where the beam radius remains constant. At this point, the beam divergence due

to finite emittance is exactly balanced by the beam focusing due to the transverse field gradient and the equilibrium radius is obtained as

$$x_e^2 = \frac{\epsilon}{k} \tag{8}$$

where ϵ is the beam emittance.

For $x_e \neq u_e$, the beam divergence and focusing do not exactly balance each other. In this case, the beam profile oscillates at the period of the betatron oscillation with the maximum (minimum) radius equal to the larger (smaller) value of x_e and u_e.

For a tapered wiggler, the situation is complicated by the z - dependence of $b_w(z) = a_w(z)k_w(z)$. However, to a very good approximation, we found that the trajectory of an electron in a tapered wiggler can still be described by the equation

$$\begin{pmatrix} X(z) \\ V(z) \end{pmatrix} = \begin{pmatrix} \cos\theta & \sin\theta \\ -\sin\theta & \cos\theta \end{pmatrix} \begin{pmatrix} X(o) \\ V(o) \end{pmatrix} \tag{9}$$

$$X(z) = [g(z)]^{1/2}\, x(z)$$

$$V(z) = [g(z)]^{-1/2} \left[\frac{v_x(z)}{c} + \frac{g'(z)}{2g(z)} \cdot x(z) \right] / k \tag{10}$$

$$g(z) = b_w(z)/b_w(o)$$

$$\theta = k \int_o^z g(z)\, dz$$

Therefore, the beam propagation can also be described by a rigid rotation of the electron distribution in a new phase space X-V where the coordinates are defined in equation 10. The real space coordinate is scaled down or up according to the square root of the taper function g(z). Except for the scaling factor $[g(z)]^{-1/2}$, the new velocity cooridinate, which is in units of length, has a small mixing part coming from the space coordinate. For

practical applications, this mixing in the velocity coordinate is negligible. The major effect of the tapering on the trajectory is in the scaling factor. Since, $X^2 + V^2$ is an invariant quantity (cf Equation 9), we find that the beam radius increases with the decreasing $b_w(z)$.

Due to the betatron oscillation, the electrons experience different field amplitudes as they propagate down the wiggler. However, the transverse variation of a_w within the electron beam is less than 5 percent. The energy equation describing the electron energy loss rate is hardly affected by the oscillation. The case is different when we consider the phase equation

$$\frac{d\psi}{dz} = k_w - \frac{k_s}{2\gamma^2}\left[1 + \frac{a_w^2(x,z)}{2} + \gamma^2 \frac{v_x^2}{c^2}\right] \tag{11}$$

which has been averaged over the magnetic period. V_x in the square bracket survives the averaging because its variation distance is much longer than λ_w. Using the expression in $a_w(x, z)$, we have

$$\frac{d\psi}{dz} = k_w - \frac{k_s}{2\gamma^2}\left\{1 + \frac{a_w(z)}{2} + \frac{b_w(o)\, b_w(z)}{2} \cdot \left[g(z)\, x^2(z) + \frac{v_x^2}{g(z)c^2k^2}\right]\right\} \tag{12}$$

The quantity in the square bracket is an invariant and depends on the initial conditions of individual electrons. Therefore, the betatron oscillation does not appear explicitly in the phase equation. Equation 12 points out that the invariant quantity represents an equivalent energy distribution and could be replaced in principle with an equivalent "effective energy spread".[5] This approach would present an advantage for the numerical simulation. Since we could transform two degrees of freedom, x and v_x, in the simulation code into one, the energy spread, which can be

further merged with the real energy spread, if any. For an electron beam in equilibrium state, the effective energy spread is given as

$$\left(\frac{\Delta\gamma}{\gamma}\right)_{eff} = \left(\frac{\pi x_e}{\lambda_w}\right)^2 \tag{13}$$

where x_e is the equilibrium radius. This result, however, is not valid for any electron beam emittances. If the effective energy spread is of the order of the height of the ponderomotive potential well, the untrapping of electrons plays an important role in the tapered wiggler FEL at optimum power and this effect has to be included in the description.

In order to study in detail the influence of the various transverse effects and to compare with analytical predictions and simplifications, a numerical code was developed that follows the electron equations of motion in 3-D and assumes an input proton beam that can diffract as a Gaussian beam and can have any initial profile. With this code, numerical simulations were performed for parameters characteristic of the TRW 10.6 μm experiment.

The gain of the system was evaluated and compared for three different profile combinations:

1. Square profile electron beam, square profile photon beam
2. Square profile electron beam, Gaussian profile photon beam
3. Gaussian profile electron beam, Gaussian profile photon beam

Case 1 has been applied up to now most extensively in the scaling and analytical studies for its simplicity.[6] In Figure 1, we show the gain depending on electron beam emittance. The photon beam waist radius R_p is set at 2mm which corresponds to 1cm-mrad emittance for the electron beam. Without the betatron oscillation, it is easy to understand that the gain is a constant when $R_e < R_p$ and decreases quadratically when $R_e > R_p$. With the betatron oscillation, the gain curve becomes smoother. However, the gain drops at $R_e < R_p$ due to the effective energy spread and becomes higher at $R_e > R_p$ because the outer electrons still have the chance of passing the optical beam region.

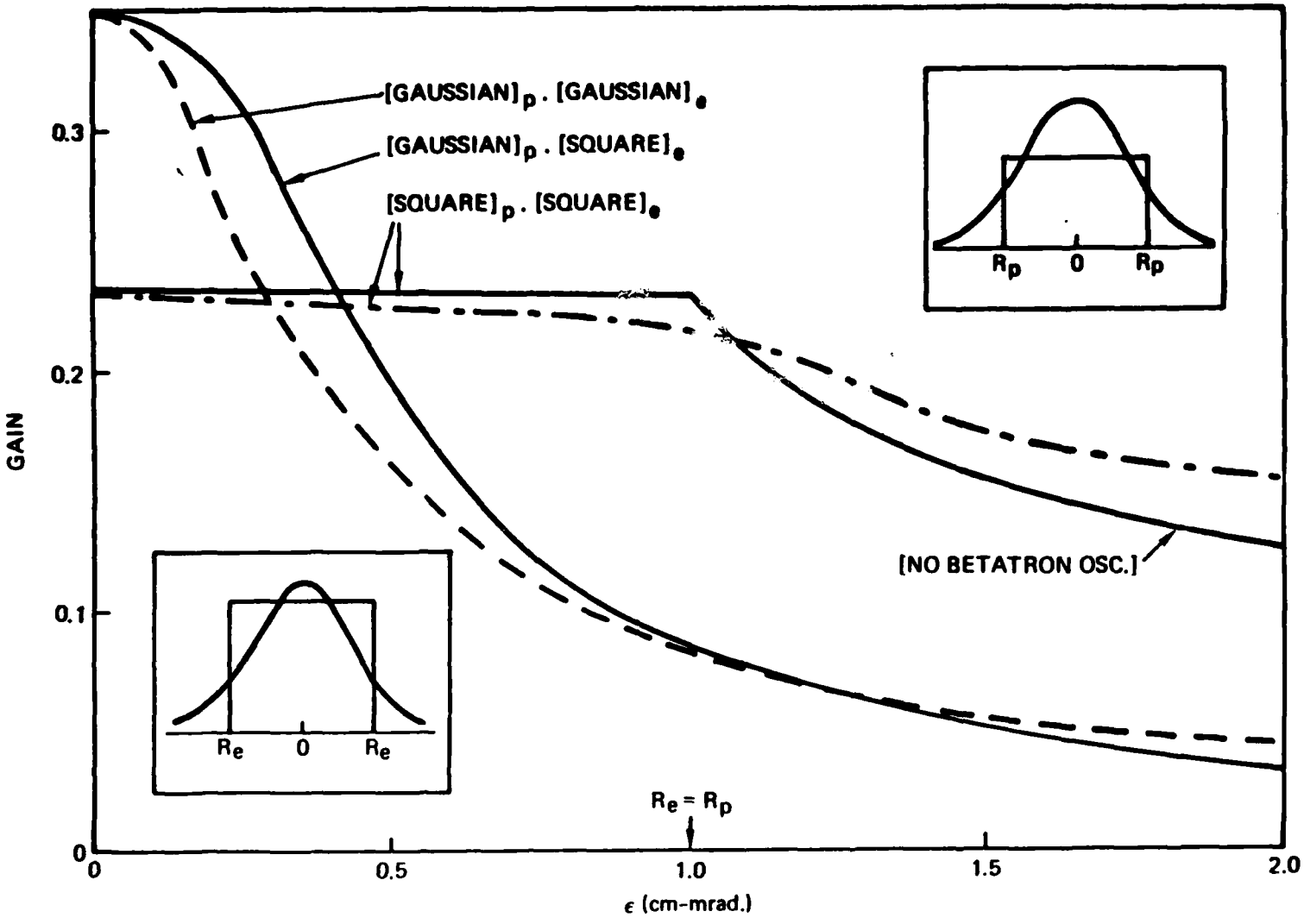

Figure 1. Gain vs. Emittance (or R_e/R_{pw}) for Gaussian and Square Radiation Field Profiles

For cases 2 and 3, the gain curves are similar. The peak gain at zero emittance is about 50 percent higher than the gain for a square photon beam. This is reasonable because the peak intensity of a Gaussian beam is about 50 percent higher than a square beam intensity with the same total power. The gain drops fast as the emittance increases. The gain is only one-fourth of the peak value at $R_e = R_p$ and is close to the value in case 1 only around $R_e = 0.5\ R_p$. Therefore, gross overestimates of the gain are obtained when it is based on case 1. Further, Figure 1 shows that for optimum operation R_e should be $\leq 0.5\ R_p$! As can be seen from the inserts of Figure 1 the square electron beam has more electrons near the center for $R_e < R_p$. Once R_e is larger that R_p, the square electron beam loses electrons faster than the Gaussian electron beam. This is the reason why the gain for a Gaussian electron beam is higher (lower) than the gain for a square electron beam for $R_e > R$ ($R_e < R_p$).

In Figure 2, we show the gain for square electron beam and Gaussian photon beam and compare it to the gain curve if we had used an effective energy spread in Equation 13 for a given emittance. The result proves the validity of using the effective energy spread to replace the effect of beam emittance for small electron beam emittance. However, for large beam emittances this is not the case. The emittance is considered "large" if the "effective energy spread" is larger than the height of the ponderomotive potential well. Even for very small emittance beams this will be the case at small signals. The finite electron emittance small signal gain is analyzed in detail at the end of this section. The case including the photon beam diffraction is also shown in Figure 2 for comparison. These results show that the photon beam profile and ratio of R_e/R_p and effective energy spread (emittance)/bucket height play a more important role than diffraction in determining the FEL gain.

From the above series of results we conclude that in a number of cases the effective energy spread and square photon beam profile can not be utilized to simplify the code. However, instead of following every electron down to the wiggler, the numerical simulation of a free electron laser can be much simplified by assuming that every electron follows the analytical trajectory obtained in equation 6, for a tapered wiggler. To apply directly this trajectory equation in the code, a preliminary knowledge of g(z)

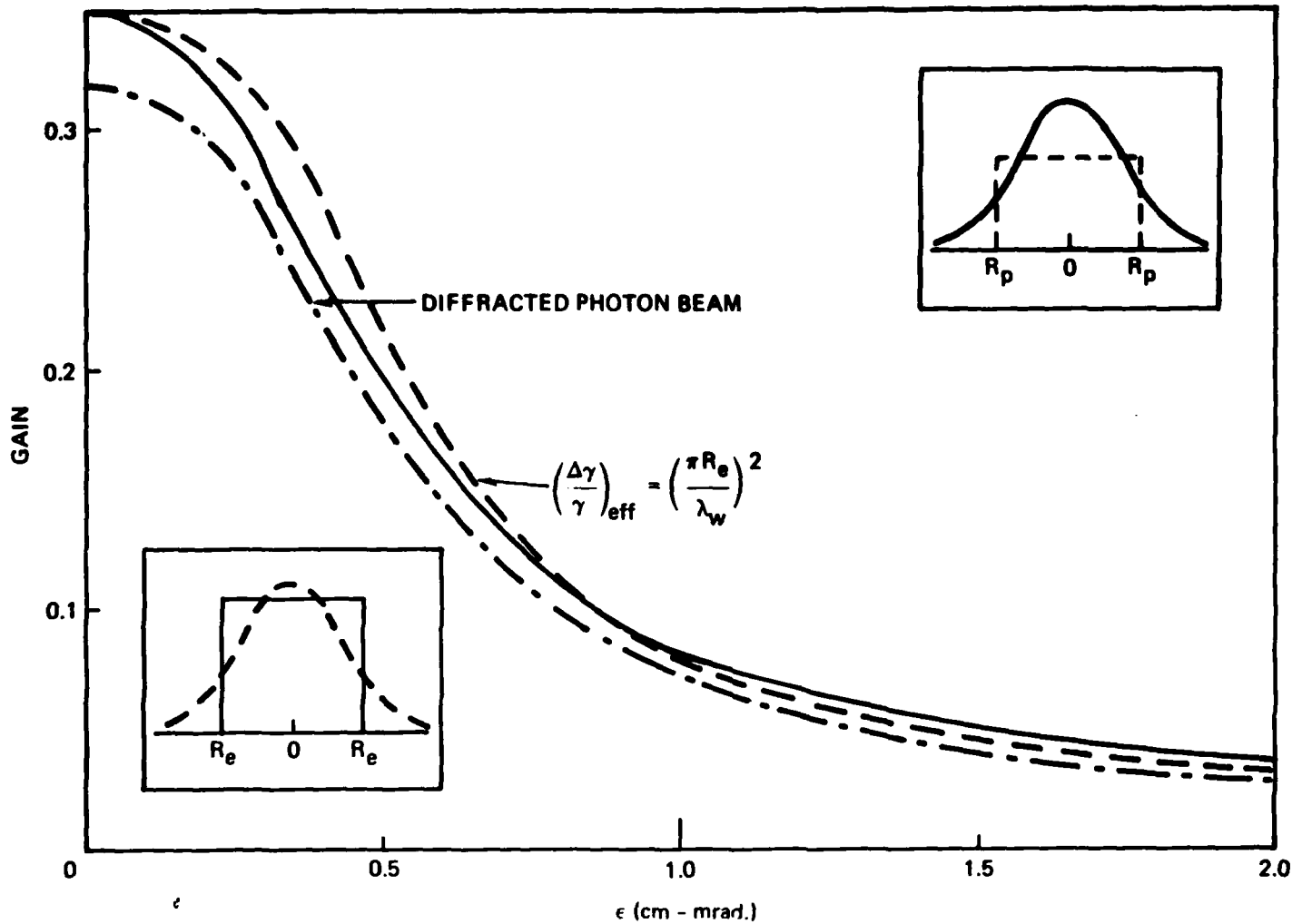

Figure 2. Gain vs. Emittance (or R_e/R_{ow}) using: 1) a defracted photon beam and betatron oscillations (---), 2) no diffraction and betatron oscillations (—),3) no defraction and "effective energy spread" (---).

and optical beam profiles have been analyzed with this code for amplifiers of the characteristics of the TRW 10.6 μm experiments and for higher

becomes necessary. In the low gain limit where a_s is assumed to be constant, it is well knows that $a_w(z)$ or $\lambda_w(z)$ is linearly decreasing. In the high gain regime, the growth of a_s has to be considered in the self consistent equations

$$\frac{da_s^2}{dz} = - \frac{2\omega_p^2}{\omega^2} < \frac{d\gamma}{dz} >|_\phi \tag{14}$$

The ensemble average $< >|_\phi$ can be represented by the fraction of trapped particles assuming that the untrapped particles have no contribution at all

$$< \frac{d\gamma}{dz} >|_\phi = \frac{d\gamma_r}{dz} \frac{N_t(z)}{N_e} \tag{15}$$

The simplest approximation is that the number of trapped particles does not change, i.e. $N_t(z)$ = constant. However, this does not lead to an analytical solution of the equations. In order to obtain an exact solution for the self-consistent equations, we allow detrapping of particles and assume

$$N_t(z) = N_t(o) \cdot \frac{\gamma_r(z)}{\gamma_r(o)} \tag{16}$$

Using Equation (16), we solve self-consistently $a_w(z)$ as

$$a_w(z) = a_w(o) \cos Kz - \frac{2k_w a_s \sin\psi_r}{K} \sin Kz \tag{17}$$

$$K = \frac{\omega_{pt} \sin\psi_r}{\sqrt{\gamma_r \omega_s \omega_w}}$$

In Figure 3 we compare the behavior of $a_w(z)$ for the linear variation, actual simulation ($\psi_r = 35^o$) and the nonlinear variation given by Equation (17). It shows that the prediction of $\gamma_r(z)$ and gain is much better for the nonlinear $a_w(z)$.

USING ANALYTICAL FORMULAS (- - -, - · - · -) AND FORMULATION (—)

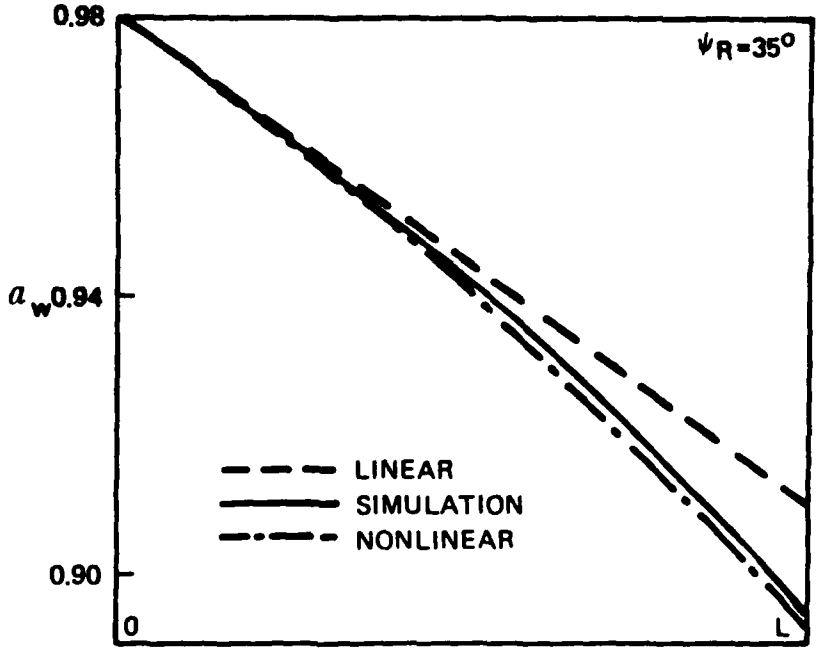

	$a_w(0)$	$a_w(L)$	$\gamma_R(0)$	$\gamma_R(L)$	GAIN
SIMULATION	0.980	0.894	49.83	48.45	1.31
LINEAR	0.980	0.910	49.83	48.70	1.14
NONLINEAR	0.980	0.893	49.83	48.44	1.38

Figure 3. a_w Variation, Deceleration Efficiency and Gain (λ_w=.const).

For variable magnitude period, the assumption for the z-dependence of $N_t(z)$ can be more justifiable. Since the height of trapping potential is

$$\text{Bucket height} = \frac{2a_w a_s \gamma_r}{\mu} \Gamma(\psi_r) , \tag{18}$$

it is reasonable to assume that the number of trapped particle is proportional to the bucket height:

$$N_t(z) = N_t(o) \cdot \frac{\gamma_r(z)}{\gamma_r(o)} \frac{\overline{a_s(z)}}{\sqrt{a_s(o)}} \tag{19}$$

Using (19), we obtain a self-consistent tapering in the wiggler pitches

$$\lambda_w(z) = \lambda_w(o) \left\{ 1 - \frac{2a_s a_w k_w \sin\psi_r}{\mu^2} \; z \; \left[1 + \rho z + 1/3(\rho z)^2 \right] \right\} \tag{20}$$

$$\rho = \frac{\omega_{pt}^2 k_s \mu^2}{4 \gamma_r^2 \omega_s^2}$$

In Figure 4, we compare $\lambda_w(z)$ for the linear variation, actual simulation ($\phi_r = 35^o$) and the nonlinear variation given in Equation (20).

Since Equations (17) and (14) are analytical and integrable and describe much better the real tapering of the wiggler, they can be used in Equations (9) and (10) for the electron trajectories.

Since an electron's initial conditions, $x(o)$ and $V_x(0)$, determine its equivalent energy, γ, in the phase equation, it is important to check the dependence of the gain spectrum on the electron transverse distribution. In particular, we are interested in the small-signal gain because it plays an important role in the oscillator start up. This spectrum is well known analytically for a zero emittance electron beam. Based on the phase Equation (12) and the energy equation. We can obtain the small-signal

USING ANALYTICAL FORMULA (– –, – · – · –) AND SIMULATIONS (—)

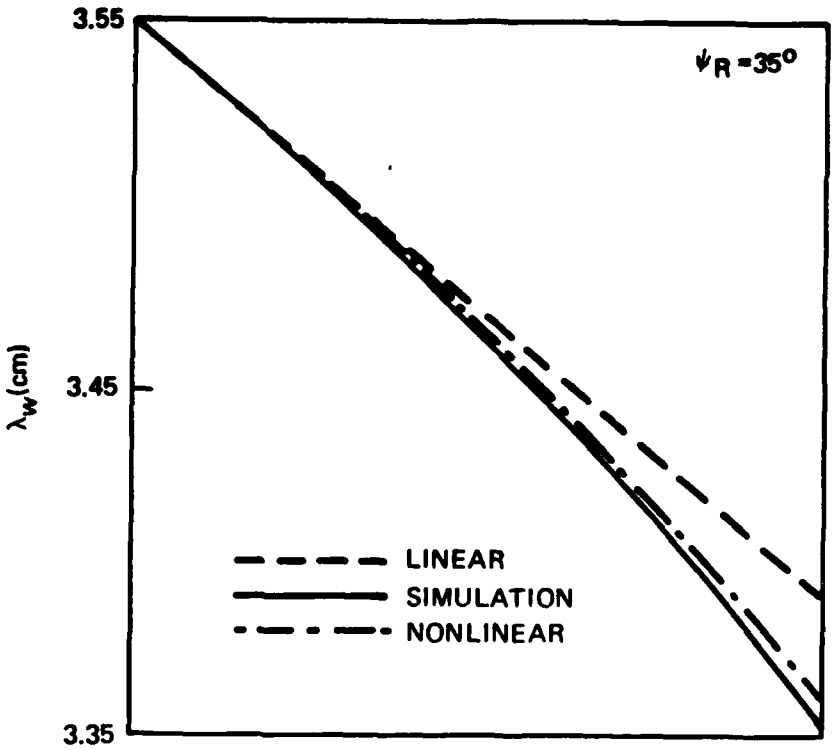

	$\lambda_w(0)$	$\lambda_w(L)$	$\gamma_R(0)$	$\gamma_R(L)$	GAIN
SIMULATION	3.556	3.352	49.83	48.38	1.38
LINEAR	3.556	3.391	49.83	48.66	1.19
NONLINEAR	3.556	3.360	49.83	48.44	1.41

Figure 4. λ_w Variation, Deceleration Efficiency and Gain (a_w = const).

energy loss of each electron from a general 1-D small-signal theory (7) (see section III). The energy loss is proportional to the derivative of the spontaneous spectrum generated by that particular electron

$$\Delta \varepsilon = \varepsilon \frac{\partial}{\partial h} |Q|^2 \tag{21}$$

$$h = \left.\frac{d\psi}{dz}\right|_{z=0}$$

where Q is the far field amplitude, $|Q|^2$ is the spontaneous emission spectrum and h is the initial detuning constant.

In order to obtain the total energy loss of electrons, we integrate $\Delta\xi$ over the initial electron distribution. For the case of a helical wiggler the total energy loss is

$$\Delta\varepsilon_T = \int_0^\infty \Delta\varepsilon(r)\, f(r)\, r\, d\, r \tag{22}$$

$$\int_0^\infty f(r)\, rdr = 1$$

where f(r) is the normalized electron distribution. If the wiggler is sinusoidal, elliptical coordinates must be used to describe the electron beam distribution. Assuming that all the energy extracted from the electron is converted to radiation, the radiation gain will have the same energy spectrum as the energy loss in Equation (22).

As a demonstration of this calculation we assume that the electron beam has a uniform distribution in the phase space up to the circle $X^2 + V^2 = R^2$. The integration (22) results in

$$\Delta\varepsilon_T = \frac{2}{R^2} \int_0^R \varepsilon_o \frac{\partial}{\partial h} |Q|^2\, r\, dr \tag{23}$$

where r is the radial distance from the origin in phase space. Since

$$h = k_w - \frac{k_s}{2\gamma^2}\left(1 + a_w^2 + b_w^2 r^2\right) \tag{24}$$

we obtain

$$\Delta\varepsilon_T = -\frac{\varepsilon_o \gamma^2}{R^2 k_s b_w^2}\int \frac{\partial}{\partial h}|Q|^2 \, dh$$

$$= \frac{\varepsilon_o \gamma^2}{R^2 k_s b_w^2}\left[|Q|^2_{\gamma=o} - |Q|^2_{\gamma=R}\right] \tag{25}$$

where R is the beam equilibrium radius. Therefore, the gain spectrum is a Raman-type which is the difference of two spontaneous spectra with a relative shift equivalent to the beam radius. This result is demonstrated by a numerical simulation of a 10.6 μm experiment with zero tapering. The electron beam radius is 2mm which results in an energy shift of about 1.75 percent. The simulation is done at 0.01 Mev input radiation power which is within the small-signal regime. The gain spectrum (Figure 5) clearly indicates the theoretical prediction in (25). As the electron beam radius approaches to zero, the dip and peak of the gain curve will move close to each other. At the zero limit, it reduces to the well known gain spectrum.

For a plane-polarized wiggler, we have a similar result. The gain spectra for different emittance are shown in Figure 6. It can be seen that the gain curves are antisymmetric. The peak gain drops and shifts to the right as the emittance increases. The negative gain almost stays stationary. It shifts from hL = -2.6 to approximately hL = 0.

It is interesting to compare these curves with the corresponding results for gaussian electron beam (Figure 7). The peak gain is smaller for the gaussian beam and the gain curves are highly asymmetric. However, we observe a long tail of positive gain on the side of positive hL. Hence, the effects of finite emittance plays a large role at small signals where the effective energy spread assumption is not valid.

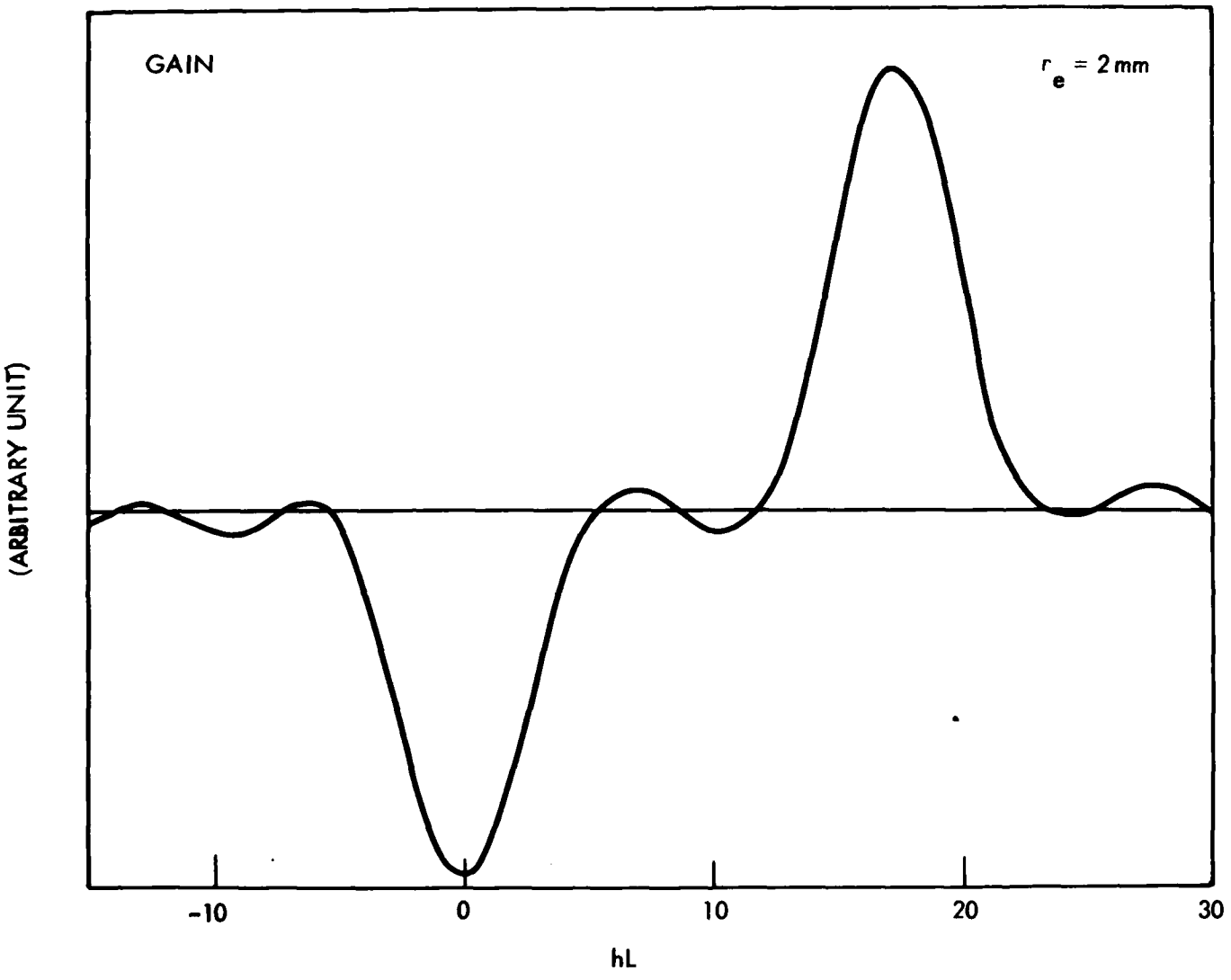

Figure 5. Small Signal Gain Spectrum for a Constant Wiggler Free Electron Laser Including A Finite Electron Beam Emittance.

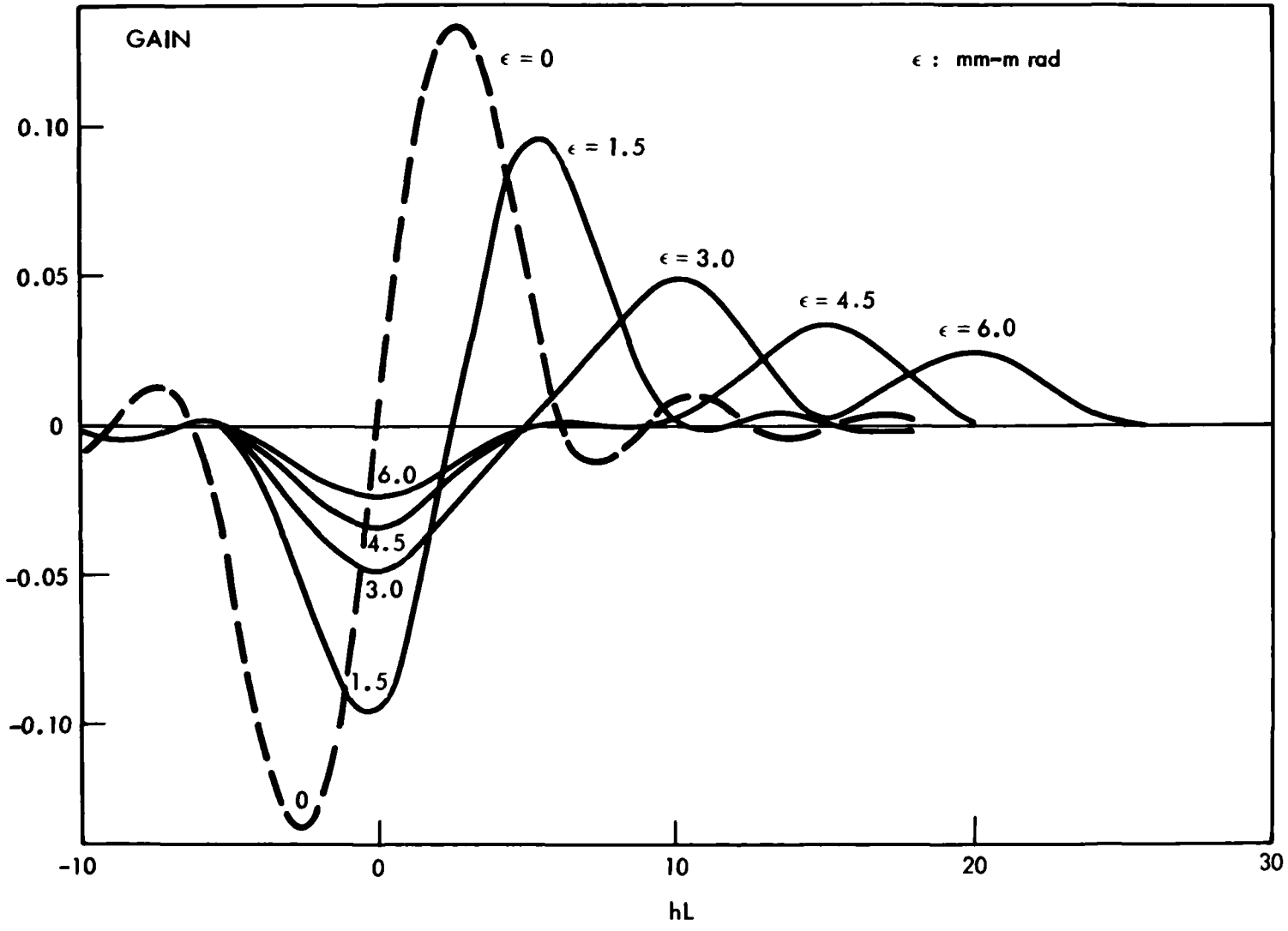

Figure 6. Gain Spectrum for Uniform Electron Beam

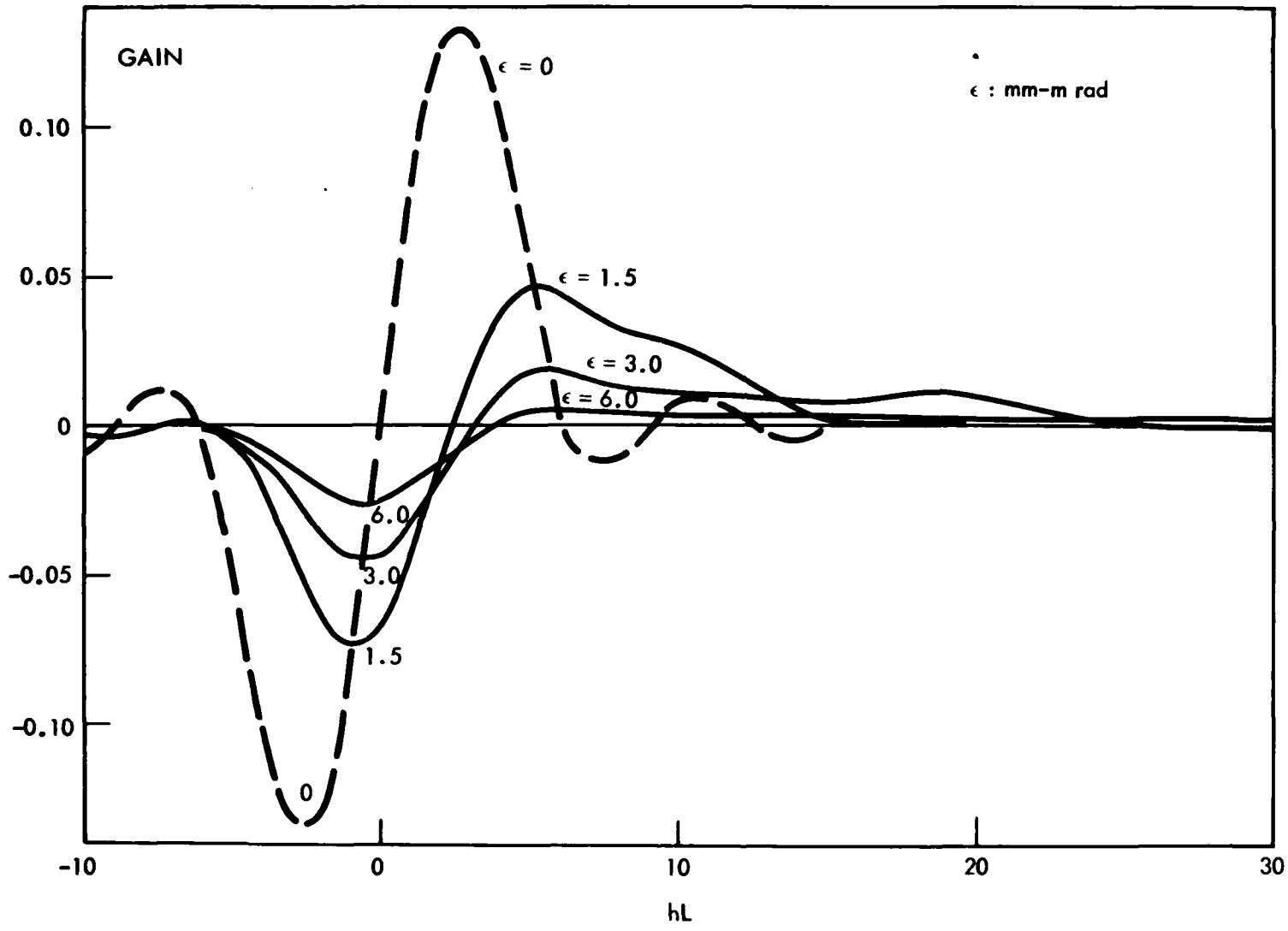

Figure 7. Gain Spectrum for Gaussian Electron Beam

REFERENCES II

1. P. Sprangle and Cha-Mei Tang, "The Three-dimensional Nonlinear Theory of the Free Electron Laser Amplifier". NRL Memorandum Report 4280 (1980).

2. L.R. Elias and J. Gallardo, "Coherent Linenard-Wiechert Fields Produced by Free Electron Lasers". To be published in Phys. Rev A, Dec (1981).

3. C. Shih and M.Z. Caponi, "Influence of the Transverse Variation of a Sinusoidal Wiggler on the Variable Wiggler Free Electron Laser Characteristics". Presented at IEEE International Conference on Plasma Science, Santa Fe, New Mexico, May 18-20, 1981.

4. H. Boehmer, M.Z. Caponi, J. Edighoffer, S. Fornaca, J. Munch, G.R. Neil, B. Saur and C. Shih. "Variable Wiggler Free Electron Laser Experiment". Accepted for publication in Phys. Rev. Lett. (1981)

5. V.K. Neil, "Emittance and Transport of Electron Beams in a Free Electron Laser". JASON Technical Report JSR-79-10. SRI International, Dec, 1979.

6. N.M. Kroll, P. Morton and M.N. Rosenbluth, "Free Electron Lasers with Variable Parameter Wiggler", JASON Technical Report JSR-79-01. SRI International, Feb, 1980.

7. C. Shih and M.S. Caponi, "Theory of Multicomponent Wiggler Free Electron Laser in the Small-Signal Regime", Accepted for publication in Phys. Rev A, (1981).

III. GENERAL I–D THEORY OF MULTI–COMPONENT WIGGLER FREE ELECTRON LASERS IN THE SMALL–SIGNAL REGIME

III-1. INTRODUCTION

It is well-known that a properly tapered wiggler can extract more electron energy than an untapered wiggler to amplify the input signal of a high frequency free electron laser (FEL).[1] The physical principle is based on keeping the phase velocity of the ponderomotive potential well, formed by the interaction of the wiggler field with the electrons and the radiation field, in pace with the electron mean velocity in such a way that the energy extraction process can be continued down the wiggler. This is accomplished by either spatially varying the phase velocity of the potential well (bucket) or by replenishing the longitudinal energy lost by the electron beam to radiation. The phase velocity can be varied in a controlled manner by adiabatically tapering the wiggler period whereas the longitudinal electron energy can be replenished by either adiabatically tapering the wiggler amplitude or introducing a d.c. longitudinal electric field. The electrons that are initially trapped in the bucket tend to remain trapped if the motion is sufficiently adiabatic. As the bucket energy or its amplitude decreases, the mean energy of the trapped electrons is reduced. The extracted electron beam energy provides the amplification of the input laser signal.

The appropriate taper of the wiggler depends on the rate of change of the electron beam energy which is in turn strongly related to the radiation field strength. Therefore, a wiggler with a given taper is optimum only for certain input laser power level. The single-pass gain decreases

for either higher or lower input power. At low input powers (small signal), the gain can drop to a much lower value than at high powers and, in some cases, can become negative. This could present serious problem for the start-up of a free-electron laser oscillator.

If the oscillator is started by injecting a low power signal at the desired wavelength, the system will be practical only if the injected power is less, at least, than one-tenth of the optimum power. Usually, this power level is well within the small-signal regime. If the roundtrip cavity loss, including the output coupling, is larger than the single-pass gain, the oscillator can never start. The characteristics of the tapered wiggler FEL at optical frequencies are such that even in cases where the small-signal gain is higher than the threshold value, the net gain is usually too small for the radiation field to reach its saturation within a finite number of passes (typically, for a high current accelerator, there are only several hundred micropulses in an electron macropulse). Recently, it has been suggested that the small-signal gain, as well as the large-signal gain could be enhanced by utilizing multicomponent devices[2-4] or optical klystrons.[5-6] (next section IV)

If the oscillator is started from the noise level, it will oscillate at the wavelength where the gain is maximum. The maximum energy extraction occurs when there is maximum overlap in the interaction region between the electron mean velocity and the bucket phase velocity (resonant). However at small signals, the electron energy loss is slower than the rate for which the tapered wiggler is designed. Thus, to obtain higher gain at small signal levels the starting electron energy would have to be lower than the resonant energy. For fixed electron energy, this means that the wavelength at which the maximum gain occurs varies with the input power. This effect can produce a shift of the operating radiation wavelength as the radiation builds up inside the cavity. In addition, it also suggests that injected oscillators should be started with a signal at the maximum gain wavelength instead of the final, desired wavelength. Although this might solve the start up problem, it can delay the time to reach steady state beyond acceptable limits. The adiabatic condition for the shift and how it proceeds at the expense of the interaction gain need to be studied carefully.

In order to analyze these two aspects of a tapered wiggler FEL oscillator, we undertook the study of the more fundamental problem that is reported in this paper: the analysis of the small-signal gain spectrum which determines the gain magnitude as well as the operating wavelength. The result from these studies motivated a full investigation of the novel multicomponent wiggler scheme.[3] The analysis of this scheme is reported in detail in the next Section IV where the characteristics of the Tapered Wiggler FEL as a function of cavity or input radiation power are discussed

III-2. SPONTANEOUS SPECTRUM

In this subsection, we calculate the classical radiation due to the periodic electron motion in a tapered wiggler. The wiggler is assumed to have plane polarization and the vector potential can be written as:

$$\underset{\sim}{A}_{\perp}(z) = A(z)\,\cos\left(\int_0^z k_w(z)dz\right)\,\hat{x} \tag{1}$$

The calculations can be easily generalized to any field polarization. Far away from the wiggler, the energy received at the detector, dW, per unit angle, $d\Omega$, per unit frequency interval, $d\omega$, is[7]

$$\frac{dW}{d\Omega d\omega} = \frac{e^2\omega^2}{4\pi^2 c}\left|\int_0^L \hat{n}\times\left[\hat{n}\times\vec{\beta}(z)\right]\; e^{i\frac{\omega}{c}\int_0^z [1-\hat{n}\cdot\vec{\beta}(z)]}\,dz\right|^2 \tag{2}$$

where $\hat{n}$ is the direction of observation, L is the wiggler length $\vec{\beta}(z)$ is the electron velocity at position z in units of the light velocity in vacuum, c, and ω the emission frequency.

The integral in (2) represents the complex field amplitude and contains all the informations of the electron motion inside the wiggler. We are especially interested in the forward spontaneous spectrum where $\hat{n} = \hat{z}$. In this direction, the complex amplitude becomes

$$Q = \int_0^L \beta_\perp(z)\, e^{i\frac{\omega}{c}\int_0^z [1 - \beta_z(z)]\, dz}\, dz \qquad (3)$$

$$\beta_\perp(z) = -\frac{eA(z)}{\gamma mc^2} \cos\left(\int_0^z k_w(z)dz\right)$$

In the integrand in (3), $\beta_\perp(z)$ is the electron transverse velocity indicating the radiation strength at position z while $\{\omega/c \int_0^z[1 - \beta_z(z)]dz\}$ is the relative phase delay of the radiation arriving at the detector. If the longitudinal velocity, β_z, is a constant, (for example, in a constant helical wiggler), the complex amplitude is the Fourier transform of the electron transverse motion. If β_z is not a constant, the situation is more complicated. However, the fast oscillation in β_z can be averaged over to obtain:

$$Q = -\frac{1}{2\gamma} \int_0^L a_w(z) e^{-if(z)}\, dz \qquad (4)$$

where; $f(z) = \int_0^z g(z)\, dz$

$$g(z) = k_w(z) - \frac{k_s}{2\gamma^2}\left(1 + \frac{a_w^2(z)}{2}\right)$$

$$a_w(z) = \frac{eA(z)}{mc^2}\ ;\ k_s = \frac{\omega}{c}$$

g(z) is the local detuning function between the electron and the ponderomotive potential. f(z) is the accumulated phase factor. For given $a_w(z)$ and $k_w(z)$, the spontaneous spectrum can be obtained by calculating the integral in (4). The detailed result for several wiggler schemes is shown in III-4.

III-3. SMALL-SIGNAL GAIN

The interaction of an electron with the radiation inside the wiggler can be described by the following one-dimensional equations of motion

$$\frac{d\xi}{dz} = - k_s a_s a_w(z) \sin \psi \tag{5a}$$

$$\frac{d\psi}{dz} = k_w(z) - \frac{k_s}{2\xi} \left[1 + \frac{a_w^2(z)}{2} - a_s a_w(z) \cos \psi \right] \tag{5b}$$

$$\psi = \int \left(k_w + k_s \right) dz - \omega_s t$$

$$\xi \equiv \gamma^2$$

$$a_s \equiv \frac{eEk_s}{mc^2}$$

where E is the radiation field amplitude and ψ is the phase position of the electron in the ponderomotive potential well. In Equations (5a) and (5b), we have averaged over the fast oscillations of the electron motion at the radiation and wiggler period. The term ($a_s a_w \cos\psi$) in (5b) is small and usually neglected in the calculation of the gain. However, we find this term is essential in providing an exact relation between the small-signal gain and the spontaneous spectrum as it will be shown later.

In the small-signal regime, the dynamic variables ξ and ψ can be expanded in powers of a_s

$$\begin{aligned} \xi &= \xi^{(0)} + \xi^{(1)} + \xi^{(2)} + \ldots \\ \psi &= \psi^{(0)} + \psi^{(1)} + \ldots \end{aligned} \tag{6}$$

where $\xi^{(n)}$ and $\psi^{(n)}$ represent the terms proportional to a_s^n. Substituting (6) into (5), we have the following iterative equations

$$\frac{d\psi^{(0)}}{dz} = k_w(z) - \frac{k_s}{2\xi^{(0)}}\left[1 + \frac{a_w^2(z)}{2}\right] \tag{7a}$$

$$\frac{d\xi^{(1)}}{dz} = -k_s a_s a_w(z)\sin\psi^{(0)} \tag{7b}$$

$$\frac{d\psi^{(1)}}{dz} = \frac{k_s\xi^{(1)}}{2\xi^{(0)2}}\left[1 + \frac{a_w^2(z)}{2}\right] + \frac{k_s a_s a_w(z)}{2\xi^{(0)}}\cos\psi^{(0)} \tag{7c}$$

$$\frac{d\xi^{(2)}}{dz} = -k_s a_s a_w(z)\ \psi^{(1)}\cos\psi^{(0)} \tag{7d}$$

with the initial condition $\xi^{(0)} = \gamma^2$, $\xi^{(1)}$ and $\xi^{(2)}$ can be obtained by straightforward integrations of (7)

$$\xi^{(1)} = -k_s a_s \int_o^L a_w(z)\sin\left[\psi_o + f(z)\right]\ dz \tag{8a}$$

$$\xi^{(2)} = -\frac{k_s^2 a_s^2}{4\gamma^2}\left\{\int_o^L a_w(z)\ \cos\left[\psi_o + f(z)\right]dz\right\}^2$$

$$+\frac{k_s^3 a_s^2}{2\gamma^4}\int_o^L a_w(z)\cos\left[\psi_o + f(z)\right]\ dz \int_o^z \left[1 + \frac{a_w^2(z')}{2}\right]\ dz$$

$$\int_o^{z'} a_w(z'')\ \sin\ \left[\psi_o + f(z'')\right]\ dz'' \tag{8b}$$

where ψ_o is the initial phase of the electron and f(z) has been given in (4). We are interested in the electron energy in units of the electron rest mass, γ, which is related to she dynamic variable ξ as

$$\gamma^{(1)} = \frac{\xi^{(1)}}{2\gamma} \tag{9a}$$

$$\gamma^{(2)} = \frac{1}{2\gamma}\left\{\xi^{(2)} - \frac{\xi^{(1)^2}}{4\gamma^2}\right\} \tag{9b}$$

Substituting (8) into (9), we obtain the first and second order corrections to the electron energy. We can then go on to calculate the ensemble averages (over the initial phase ψ_o) of two quantities: the phase averaged energy change $<\Delta\gamma>$ and the phase averaged energy spread $<(\Delta\gamma)^2>$ that are related to the small-signal gain and the spontaneous spectrum respectively for small gain systems and monoenergetic beams.

$$<(\Delta\gamma)^2> = <\gamma^{(1)^2}> \tag{10a}$$

$$= \frac{k_s^2 a_s^2}{8\gamma^2}\int_o^L dz_1 \int_o^L dz_2 a_w(z_1)a_w(z_2)\cos\,[f(z_1) - f(z_2)]$$

$$<\Delta\gamma> = <\gamma^{(2)}> \tag{10b}$$

$$= \frac{k_s^2 a_s^2}{16\gamma^2}\int_o^L dz_1 \int_o^L dz_2 \left[\frac{2}{\gamma} - \frac{\partial}{\partial\gamma}\right]\left\{a_w(z_1)a_w(z_2)\cos\,[f(z_1) - f(z_2)]\right\}$$

Comparing (10b) with (10a), we prove Madey's theorem [8,9]

$$<\Delta\gamma> = \frac{1}{2}\frac{\partial}{\partial\gamma}<(\Delta\gamma)^2> \tag{11}$$

It has to be emphasized that we have proved this theorem for any wiggler configuration. Further, the wiggler variation does not need to be symmetric as the assumption given in the original paper.[8] Since there is essentially no restriction on $a_w(z)$ and $k_w(z)$, the theorem is also

applicable to the multicomponent wiggler or the optical klystron as long as $a_w(z)$ and $k_w(z)$ are slowly varying.

The small-signal gain in the radiation power, $\xi = cE^2/8\pi$, can be derived from the extraction efficiency, η, if it is assumed that all the energy lost by the electron beam goes into electromagnetic energy;

$$\eta \equiv -\frac{\langle \Delta\gamma \rangle}{\gamma} = -\frac{k_s^2 a_s^2}{\gamma} \frac{\partial}{\partial\gamma} |Q|^2 \tag{12}$$

$$G \equiv \frac{\mathcal{E}(L) - \mathcal{E}(0)}{\mathcal{E}(0)} = \eta \cdot \frac{\text{Input e-beam Power}}{\text{Input Radiation Power}} = -\frac{\omega_p^2}{2c^2} \frac{\partial}{\partial\gamma} |Q|^2 \tag{13}$$

where $|Q|^2$ was given in (4). From (9), we find that the small-signal gain is exactly proportional to the slope of the spontaneous spectrum. Note that if the small term in (5b) would have been neglected, the small-signal gain would be

$$G' = -\frac{\omega_p^2}{2c^2} \left\{ \frac{\partial}{\partial\gamma} + \frac{2}{\gamma} \right\} |Q|^2 \tag{14}$$

Although $(2/\gamma)$ is much smaller than $(\partial/\partial\gamma)$ in the relativistic limit, it violates the exact relation that follows from Madey's theorem.

The gain expression in (13) is completely general. It is derived for arbitrary variation in the magnetic amplitude and period including multicomponent devices and optical klystrons. In these devices, the drift space can be represented by $a_w(z) = k_w(z) = 0$. As it will be shown in the next section, an optical klystron is a particular case of the multicomponent device. Instead of its physical drift distance, we have to apply the effective drift distance which is due to the use of dispersion magnets.

III-4. APPLICATIONS

In this subsection the formulas derived in Section III-2 and III-3 for the spontaneous spectrum and small signal gain are applied to particular devices. We first show that for constant wiggler the standard result is obtained and afterwards generalize to tapered wiggler and multi-component wiggler. In order to obtain a simple analytical result the electron beam is assumed cold (zero energy spread).

A. Constant Wiggler

For a constant wiggler, the complex field amplitude is reduced to

$$Q_c = \frac{a_w}{2\gamma} \int_o^L e^{-ihz}\, dz$$

$$h = k_w - \frac{k_s}{2\gamma^2}\left[1 + \frac{a_w^2}{2}\right] \qquad (15)$$

Hence, its spontaneous spectrum is the well known spherical Bessel function squared

$$\frac{dW}{d\Omega d\omega} = \frac{e^2\omega^2 a_w^2 L^2}{16\pi^2 c\gamma^2}\, j_o^2(x)\Big|_{x=\frac{hL}{2}} \qquad (16)$$

The small-signal gain, obtained as shown in Eq. (13), is

$$G_c = \frac{\omega_p^2 k_w L^3}{2c^2\gamma^3}\, \frac{2 - 2\cos x - x\sin x}{x^3}\Big|_{x=hL} \qquad (17)$$

and it peaks at $hL = 2.6$, yielding the standard formula

$$G_{c,max} = 0.27 \frac{\omega_p^2 k_w L^3 a_w^2}{4c^2\gamma^3} \tag{18}$$

B. Linearly Tapered Wiggler

For a tapered wiggler with the variations $a_w(z)$ and/or $k_w(z)$, Equation (4) and (13) can be used to calculate the gain and the spontaneous spectrum numerically. Since the spectrum is the result of interference of the fields radiated from different parts of the wiggler, the phase factor f(z) is far more important and sensitive than the radiation strength factor, $a_w(z)$. For simplicity, we consider the linearly tapered wiggler with the variation

$$g(z) = h + \alpha z \tag{19}$$

and calculate the spontaneous spectrum to be

$$\frac{dW}{d\Omega d\omega} = \frac{e^2\omega^2 a_w^2}{16\pi^2 c\gamma^2} \cdot \frac{\pi}{\alpha} \left\{ [C(p) - C(q)]^2 + [S(p) - S(q)]^2 \right\}$$

$$p = \sqrt{\frac{\alpha}{\pi}}\, L + \frac{h}{\sqrt{\alpha\pi}} \tag{20}$$

$$q = \frac{h}{\sqrt{\alpha\pi}}$$

where h is the initial energy detuning, α indicates the degree of linear tapering, C and S are Fresnal functions.[10] Since

$$C(-p) = -C(p);\ S(-p) = -S(p) \tag{21}$$

the spectrum is symmetric about $p = -q$, i.e.

$$h = -\alpha L/2 \tag{22}$$

which means that the wavelength at which the spectrum is centered is determined by the parameters at the mid wiggler. If we choose to fix the wiggler parameters at the entrance, as we vary the wiggler taper, it is expected that the center of the spectrum will shift to lower values of h (shorter wavelenghts for a fixed electron energy) with increasing tapering for positive α. The spectrum, for values of αL^2 = 0, 10, 20, 30, 40, 50 is shown in Figure 1. When the taper increases, we find that the peak intensity drops while the first sideband is enhanced. In particular, at αL^2 = 30, the magnitude of the fundamental and first sideband are almost the same and the spectrum shows a plateau extending over a wide range. For αL^2 larger than 30, the center intensity drops even further and the spectrum extends rather irregularly.

It is useful to relate the parameter α to the taper rate for constant amplitude or constant period wigglers. For constant amplitude

$$\alpha = \frac{k_w}{L} \cdot \frac{\lambda_w(0) - \lambda_w(L)}{\lambda_w(0)} \tag{23}$$

and for constant period

$$\alpha = \frac{a_w^2}{1 + \frac{a_w^2}{2}} \cdot \frac{k_w}{L} \cdot \frac{a_w(0) - a_w(L)}{a_w(0)} \tag{24}$$

The small-signal gain for a linearly tapered wiggler is obtained by taking the derivative of (20)

$$G = \frac{\omega_p^2 a_w^2 k_w \sqrt{\pi}}{2c^2\gamma^3\alpha\sqrt{\alpha}} \left\{ \left[\cos\frac{\pi p^2}{2} - \cos\frac{\pi q^2}{2} \right] [C(p) - C(q)] + \left[\sin\frac{\pi p^2}{2} - \sin\frac{\pi q^2}{2} \right] [S(p) - S(q)] \right\} \tag{25}$$

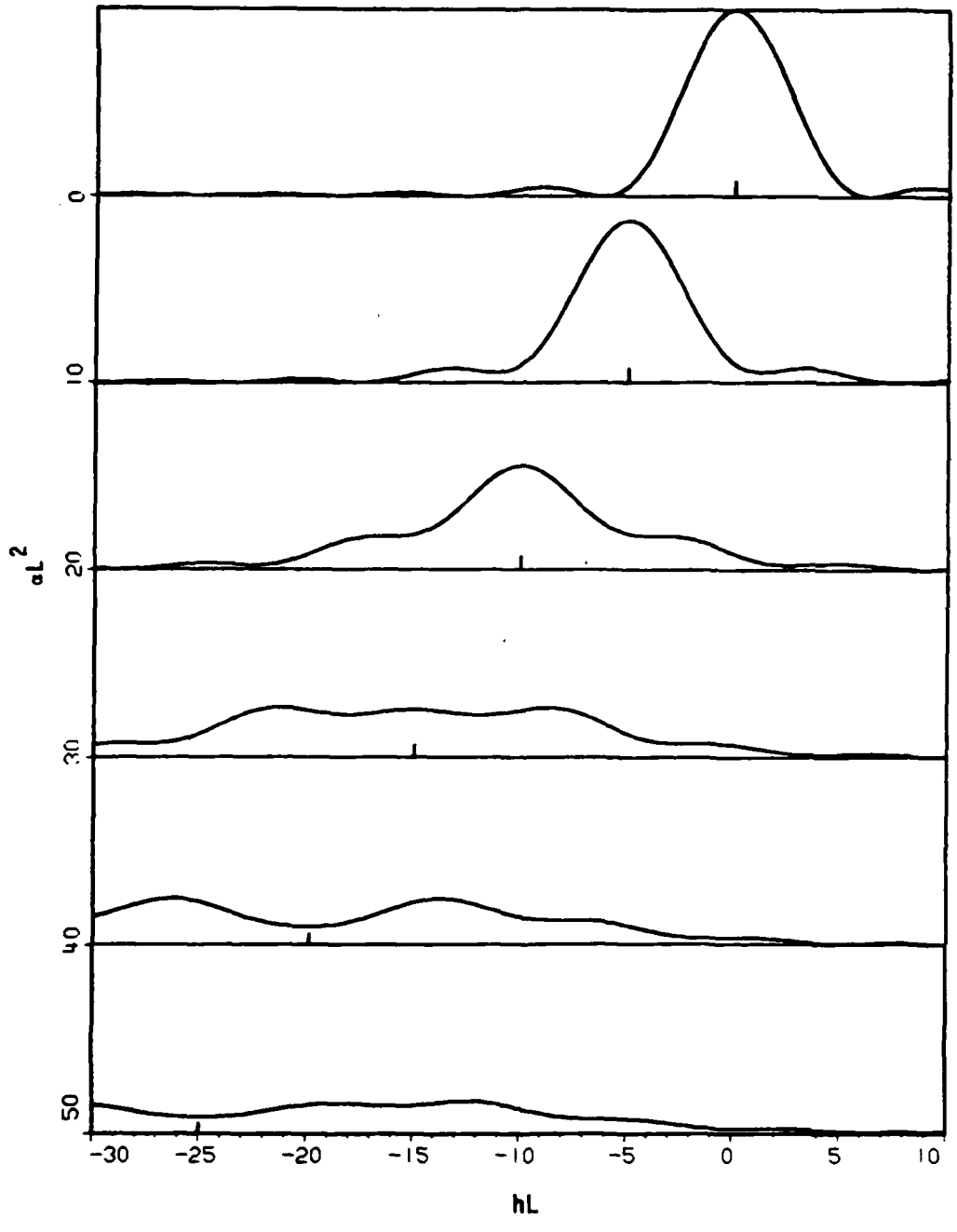

Figure 1. Spontaneous Spectrum for αL^2 = 0, 10, 20, 30, 40 and 50.

which is identical to the result obtained by C. Brau.[11] The gain spectrum is antisymmetric about the point $p = -q$ and is shown in Figure 2 as a function of the wiggler taper and the energy detuning. To simplify the figure, the negative gains are suppressed, however, they can be figured out easily from the antisymmetry relation. Figure 2 shows that the main bump in the spectrum decreases appreciably and disappears completely after $\alpha L^2 = 30$. The small bumps on the negative side of h vanishes even faster except for a rising bump within the range $-2\pi < (hL + \alpha L^2/2) < 0$. This becomes the major contribution at large tapering. It is interesting to note that the peak gain shifts toward negative h and decreases in magnitude as the taper rate increases. Eventually, the first side lobe disappears completely and it is replaced by the main peak, as the shift of the whole structure continues, the relative amplitude between the main peak and the remaining sidebands decreases and can become smaller than 1. Thus, the spectrum tends to remain rich in structure and with its maximum gain near $h \simeq 0$ ($\gamma \simeq \gamma_R$). In order to compare with Figure 1, the gain spectrum is shown explicitly in Figure 3 for the corresponding linear taperings.

In Figure 4, the relative value of the gain is shown in contours of equigain. The value indicated on each curve is the gain compared to the maximum gain (0.27) for the constant wiggler (see Eq. 18). Note that, at $\gamma = \gamma_R$, the gain can be negative for certain tapering ranges. Obviously, for the oscillator start-up at the desired wavelength, these regions should be avoided.

C. Two-Component Wiggler and Optical Klystron

A two-component wiggler device is composed of two wigglers (constant[2] or tapered[3,4]) in series with a free drift space between them (Figure 5a). For a first component or prebuncher of appropriate length, the electron bunching usually increases with the drift distance. In order to increase the drift distance without affecting the device length, dispersion magnets are introduced in the drift space. A typical arrangement is shown in Figure 5b. The free-drift space can be represented by $a_w = k_w = 0$. The phase advance of the electron relative to the radiation in the free drift space can be calculated from the phase equation. With a drift distance L_D, the phase change is

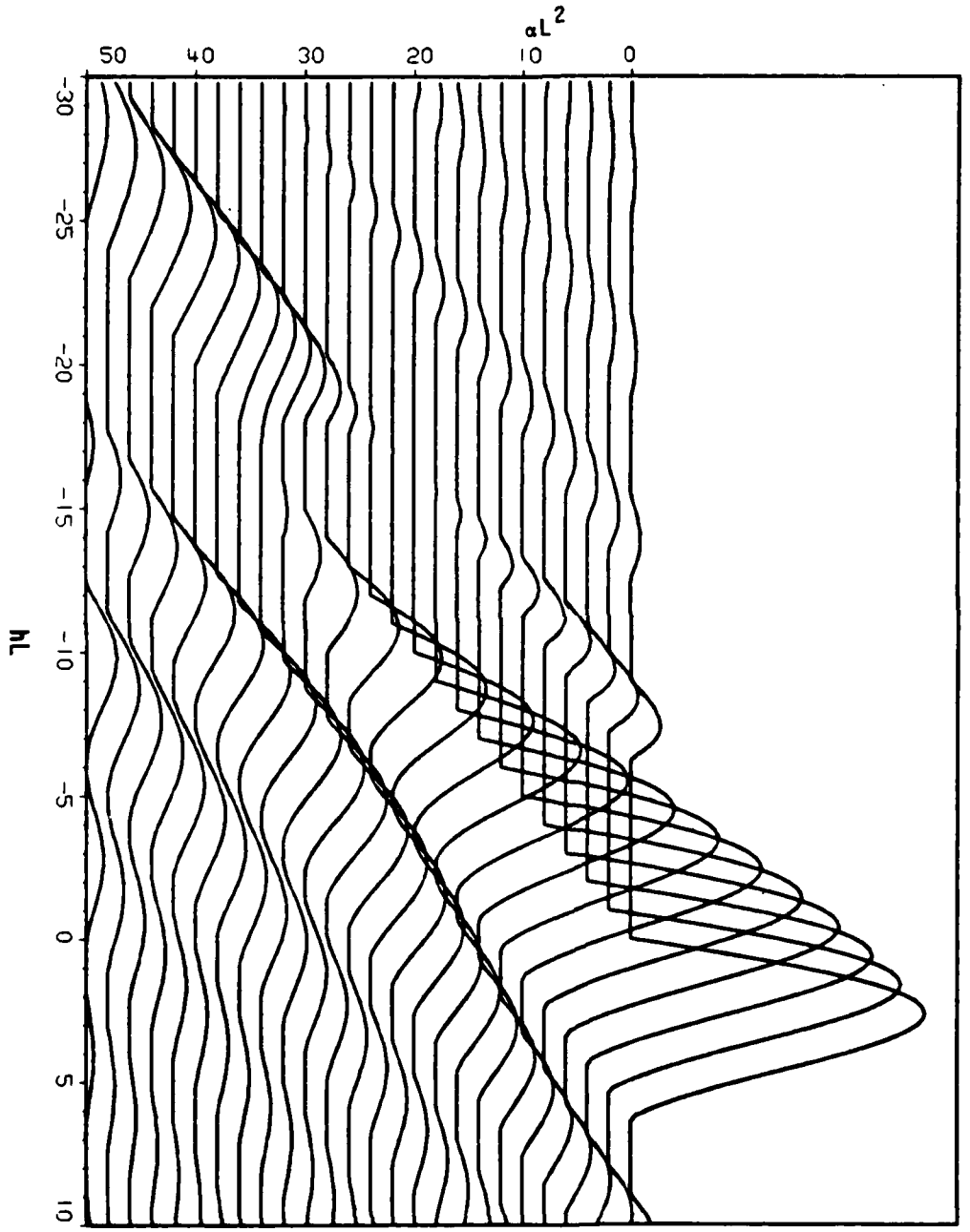

Figure 2. Gain Structure as a Function of the Taper αL^2 and the Detuning Parameter hL. The Negative Gains are Suppressed.

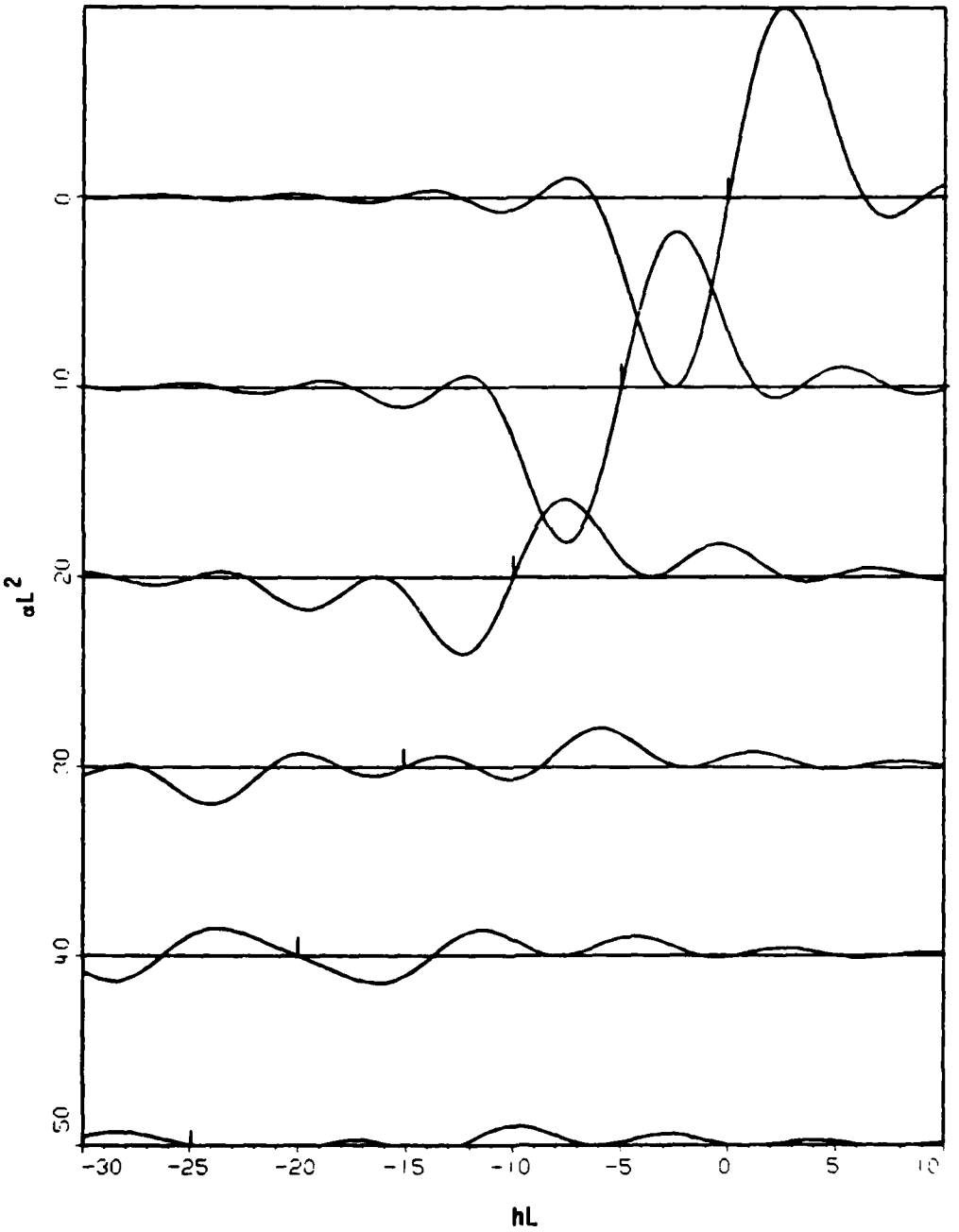

Figure 3. Gain Spectrum for αL^2 = 0, 10, 20, 30, 40 and 50.

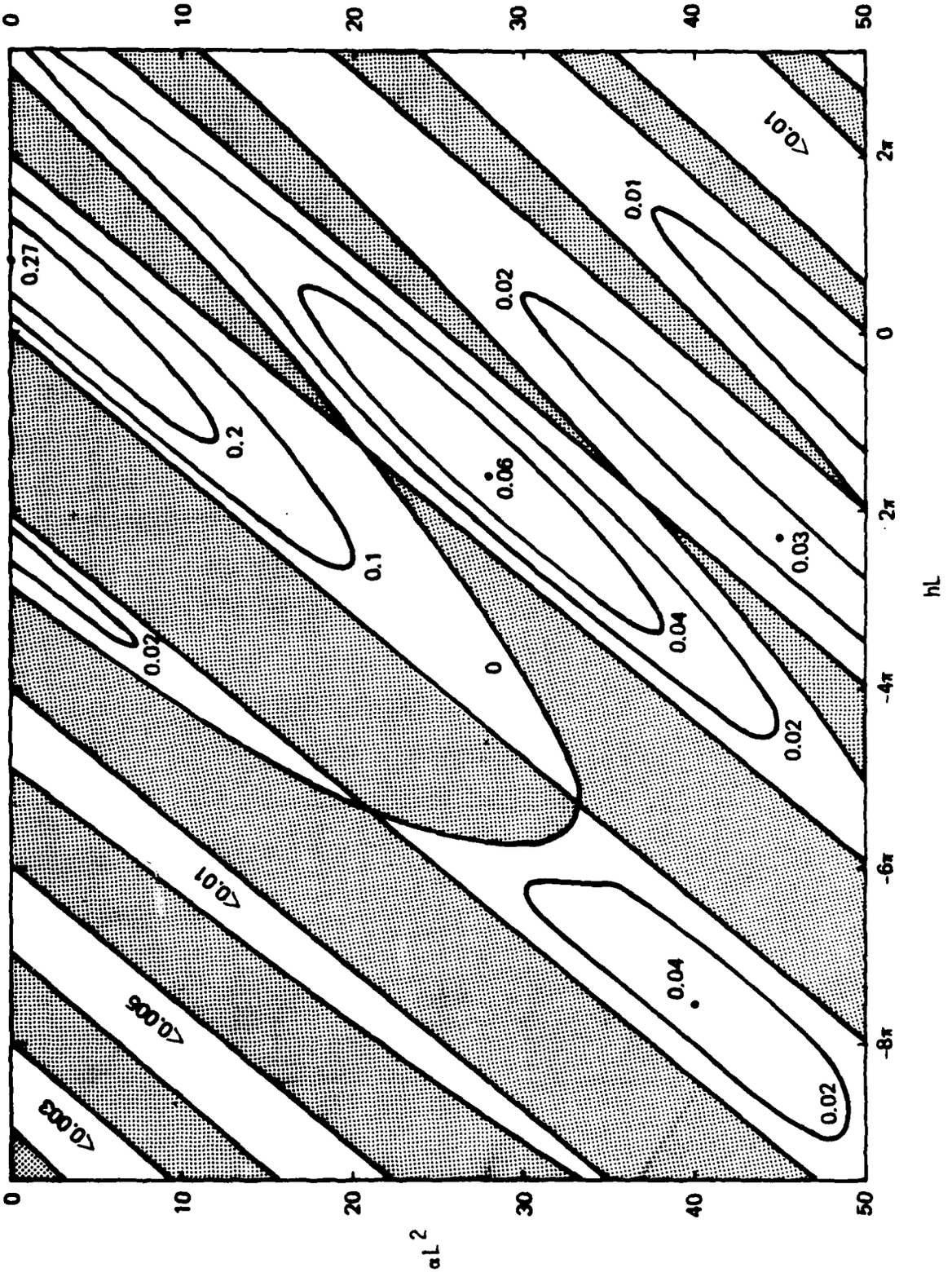

Figure 4. The Value of Gain Shown in Contours. The Value Indicated on Each Curve is the Gain Compared to the Maximum Gain of a Constant Wiggler (0.27).

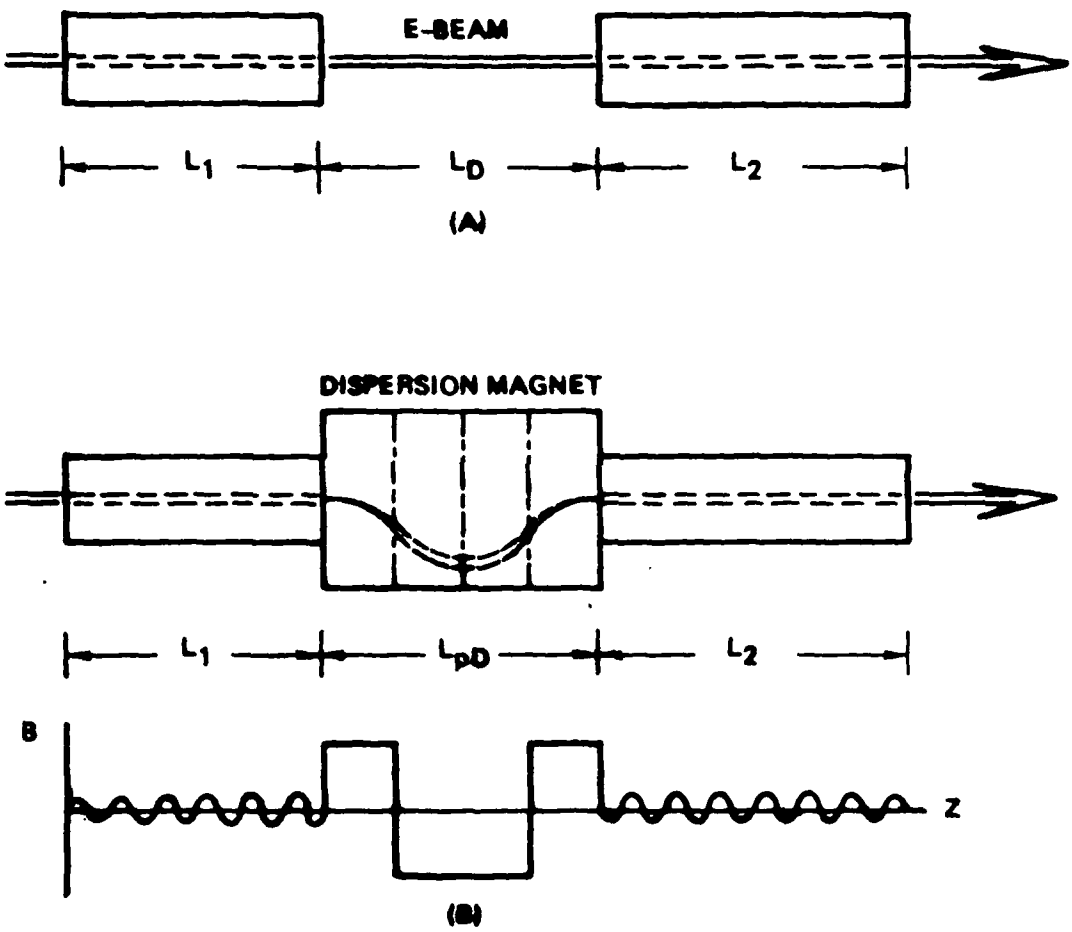

Figure 5. Typical Geometry of a Two-component Wiggler (a) and an Optical Klystron (b). The Curve Shows the Dispersion Magnetic Field in the Drift Space.

$$\psi = -\frac{k_s}{2\gamma^2} L_D \tag{26}$$

For two electrons with energy difference $\Delta\gamma$, the difference in the phase change is

$$\Delta\psi = \frac{k_s L_D}{\gamma^3} \Delta\gamma \tag{27}$$

For the dispersion magnets, the electron flight time is highly energy-dependent. For the dispersive magnetic field geometry shown in Figure (5b), the induced phase difference for $\Delta\gamma$ is found to be

$$\Delta\psi = \frac{k_s L_{pD}^3}{48\gamma^3} \left(\frac{eB}{mc^2}\right)^2 \Delta\gamma \tag{28}$$

Comparing (28) with (27), we conclude that an optical klystron with a dispersion magnet is equivalent to a two-component device with an effective drift distance

$$L_D = \frac{L_{pD}^3}{48} \left(\frac{eB}{mc^2}\right)^2 \tag{29}$$

The effective drift distance is proportional to the magnetic field squared and to the cubic of the physical distance between two sections, L_{pD}. Since these two devices are equivalent, both can be described by calculating the gain for a two component device with an effective drift distance L_D. In order to calculate the small-signal gain we first have to evaluate the integral Q in the spontaneous spectrum.

Since $|Q|^2$ is a double integral of real functions

$$|Q|^2 = \frac{1}{4\gamma^2}\int_0^L dz_1 \int_0^L dz_2 a_w(z_1)a_w(z_2)\cos\,[f(z_1) - f(z_2)] \qquad (30)$$

The integration can be divided into three regions: i) $0 \le (z_1, z_2) \le L_1$, ii) $L_1 + L_D \le (z_1, z_2) \le L$, iii) $0 \le z_1 \le L_1$, $L_1 + L_D \le z_2 \le L$ or $0 \le z_2 \le L_1$, $L_1 + L_D \le z_1 \le L$. The integral in the first region represents the spontaneous spectrum from the first wiggler while the integral in (ii) represents the radiation from the secnd wiggler. The integral in region (iii) represents the interference of the radiation fields radiated from different wigglers. Therefore,

$$|Q|^2 = |Q_1|^2 + |Q_2|^2 + \frac{1}{2\gamma^2}\int_0^{L_1} dz_1 \int_0^{L_2} dz_2\, a_{w1}(z_1)a_{w2}(z_2)$$

$$\cos\left[f_1(L_1) - f_1(z_1) + f_2(z_2) - \frac{k_s}{2\gamma^2}L_D\right] \qquad (31)$$

From (31), we observe that the spontaneous spectrum, in general, is not the same when we exchange the position of two wigglers unless the whole device is symmetric, i.e., $L_1 = L_2$ and

$$a_{w1}(L_1 - z) = a_{w2}(z)$$

$$g_1(L_1 - z) = g_2(z) \qquad (32)$$

where g(z) is the local detuning parameter defined in (4). The small-signal gain, which is the derivative of $|Q|^2$, is thus not the same for both cases.

In what follows, we will analyze two two-component wiggler devices: constant-constant wiggler (CCW) and constant-tapered wiggler (CTW). CCW is the usual case considered in optical klystrons while CTW is suggested

for the enhancement of the small signal gain of TWFEL. For the case of CCW with the same constant parameters a_w and k_w, $|Q|$ is calculated to be

$$|Q|^2 = \frac{a_w^2}{h^2}\left\{1 - \frac{1}{2}\cos hL_1 - \frac{1}{2}\cos hL_2 + 2\sin\frac{hL_1}{2}\sin\frac{hL_2}{2}\cos\left[\frac{1}{2}\left(hL_1 + hL_2 - \frac{k_s L_D}{\gamma^2}\right)\right]\right\} \quad (33)$$

The small-signal gain is obtained by taking the derivative of (33) with respect to γ. In the case of an optical klystron with dispersion magnets, L_D is much larger than L_1 or L_2 and we have

$$\frac{\partial|Q|^2}{\partial\gamma} = -\frac{2a_w^2 k_s L_D}{h^2\gamma^3}\sin\frac{hL_1}{2}\sin\frac{hL_2}{2}\sin\left\{\frac{1}{2}\left[h(L_1 + L_2) - \frac{k_s L_D}{\gamma^2}\right]\right\} \quad (34)$$

The values of hL_1 and hL_2 are of the order of unity. The quantity $(k_s L_D/2\gamma^2)$ can be varied within a range of 2π by just changing L_D within a magnetic period. Therefore, we can always adjust L_D such that the third sine function becomes 1. The function ($\sin hL_1/2$ and $\sin hL_2/2$) is maximum when $L_1 = L_2 = L_o$. Therefore, for the same total interaction length, we get the best efficiency when the two sections are identical. The maximum gain for an optical klystron with dispersion magnets is obtained at $h = 0$.

$$G_{max}^{OK} = \frac{a_w^2\omega_p^2\omega L_o^2 L_D}{2c^3\gamma^5} \quad (35)$$

Comparing this gain to the maximum gain of a constant wiggler of length $2L_o$, we find

$$\frac{G_{c,max}^{OK}}{G_{c,max}} = \frac{1 + a_w^2/2}{0.54} \cdot \frac{L_D}{L_o} \tag{35}$$

which shows the factor of gain enhancement by an optical klystron. The result is in agreement with previous derivations.[2] From (35), we find that the maximum gain is proportional to the interaction length squared L_o^2, and the effective drift distance, L_D. The width of the gain spectrum can be found from (34)

$$\Delta\left(\frac{k_s L_D}{2\gamma^2}\right) = \pi$$

or
$$\frac{\Delta\lambda_s}{\lambda_s} = \gamma^2 \frac{\lambda_s}{L_D} \tag{36}$$

When L_D is large, the value in (37) is very small and highly restricts the electron energy spread to avoid a decrease in gain. For example, for λ_s = 10 μm, L_D = 10 m and γ = 50; the electron energy spread is required to be less than 0.25 percent.

It has to be reminded that the introduction of L_D has two purposes. It transforms the energy modulation of the beam from the first wiggler into space modulation and places the modulated beam at the best phase position for the energy extraction in the second wiggler. The space modulation process needs a length comparable to or longer than the interaction length and is responsible for the high maximum gain in (35). The phase adjustment requires a much shorter distance, of the order of the magnetic period. It appears in the argument of the last sine function in (34). These two characteristic distances are so different in their orders of magnitude that they can be taken as independent parameters.

Next, we consider a two-component device where one of the wigglers is linearly tapered. The constant section can be put in front of the tapered section (constant-tapered wiggler, CTW) or after the tapered section (tapered-constant wiggler, TCW). Both schemes can be used to enhance the

small-signal gain over that of a tapered wiggler of the same total length. CTW is also especially useful at large signals because the constant section provides a bunched electron beam for the tapered section. By substituting the function f(z) for both sections into (31), we can calculate the interference term in $|Q|^2$

$$|Q|^2_{interf.} = \sqrt{\frac{\pi}{\alpha}} \frac{a_{wc} a_{wt}}{h_c \gamma^2} \sin \frac{h_c L_c}{2} \left\{ \cos M \left[C(p) - C(q) \right] + \sin M \left[S(p) - S(q) \right] \right\} \tag{38}$$

where α,p and q are given in (20) in terms of the parameters of the tapered section. The subscript c and t indicate the quantity for constant and tapered section respectively, and

$$M = \begin{cases} \dfrac{h_t^2}{2\alpha} + \dfrac{k_s L_D}{2\gamma^2} - \dfrac{h_c L_c}{2} & \text{for CTW} \\ \dfrac{\left(\alpha L_t + h_t\right)^2}{2\alpha} - \dfrac{k_s L_D}{2\gamma^2} + \dfrac{h_c L_c}{2} & \text{for TCW} \end{cases} \tag{39}$$

where h_c and h_t are the degree of detuning for the CW and TW respectively. Therefore, both schemes produce similar spectrum except for the argument M.

If L_D is much larger than L_c or L_t (which is the case if a dispersion magnet is used) the gain can be obtained easily by taking the derivatives of sin M and cos M in Equation 38 and discarding all terms except those proportional to L_D. In that case:

$$G = \pm \sqrt{\frac{\pi}{\alpha}} \frac{\omega_p^2 a_{wc} a_{wt} k_w L_D}{c^2 \gamma^3 h_c} \sin \frac{h_c L_c}{2} \left\{ \sin M \left[C(p) - C(q) \right] - \cos M \left[S(p) - S(q) \right] \right\} \tag{40}$$

where positive and negative signs are for CTW and TCW respectively. The gain becomes maximum at $h_c = 0$. If h_t is also chosen to be zero and αL^2 is a large number, we have $C(p) \approx S(p) \approx 1/2$ and $C(q) = S(q) = 0$. The functions sin M and cos M are fast oscillating as L_D varies. The value in the curled bracket in (40) can be maximized by adjusting the drift distance within a magnetic period. The maximum gain for both schemes becomes

$$G = \frac{\omega_p^2 a_{wc} a_{wt} L_c L_D k_w}{2c^2\gamma^3} \sqrt{\frac{\pi}{2\alpha_t}} \tag{41}$$

Note that the length of the taper enters in the gain expression through α_t. From (25), we find that the maximum small signal gain for a tapered wiggler of length $(L_c + L_t)$ is:

$$G^T_{max} = \frac{(\sqrt{2} - 1)\omega_p^2 a_w^2 k_w}{2c^2\gamma^3} \sqrt{\frac{\pi}{\alpha_{ct}^3}} \tag{42}$$

To simplify the comparison between (41) and (42), we assume that $a_{wc} = a_{wt}(0) = a_w(0)$ and $a_{wt}(L_t) = a_w(L_c + L_t)$, i.e. both tapered wigglers have the same percentage change in a_w or $\alpha_t L_t^2 = \alpha_{ct}(L_c + L_t)^2$. The gain-enhancement factor is then obtained by taking the ratio of (41) and (42)

$$\frac{G}{G^T_{max}} = \frac{k_w L_c L_D a_w^2 \delta}{(2 - \sqrt{2})\ \mu^2 (L_c + L_t)} \sqrt{\frac{L_t}{L_c + L_t}} \tag{43}$$

where δ is the percentage change in a_w for both tapered wigglers. For example, if we have $L_c = L_t$ and $a_w = 1$, the enhancement factor becomes

$$\frac{G}{G^T_{max}} \simeq 2.5\delta \frac{L_D}{\lambda_w} \tag{44}$$

Thus, the enhancement could be orders of magnitude large.

In order to simplify the analytical expression, we have calculated the small-signal gain enhancement of a tapered wiggler by using dispersion magnets, with $L_D >> L_c, L_t$. However, if an enhancement of gain by about ten times is sufficient for our purpose, we find that a two-component device without drift space is good enough. For example, if the small-signal gain of a 3-meter long tapered wiggler is to be enhanced, it can be broken into a 1-meter constant section and a 2-meter tapered section with the same percentage change in a_w. We keep a small gap between the two sections. The gap, which is about the distance of a magnetic period, works as a phase adjustor such that the modulated electron beam that comes out of the constant section can be placed at the optimum phase for the energy extraction in the tapered section at large signals. The details of this configuration are explained in the next section (IV).

III-5. MAXIMUM GAIN

The gain expression has been obtained in a double integration of real functions

$$G = \frac{\omega_p^2 \omega_w}{4\gamma^3 c^3} \int_0^L dz_1 \int_0^L dz_2 a_w(z_1) a_w(z_2)(z_1 - z_2) \sin [f(z_1) - f(z_2)] \tag{45}$$

where for the purpose of this discussion we have neglected the term $(2/\gamma)$ compared to $(\partial/\partial\gamma)$. From (45), an upper bound for the small-signal gain can be set easily because the absolute value of a sine function cannot be larger than one.

$$\begin{aligned} G \leq G_{limit} &= \frac{\omega_p^2 \omega_w}{4\gamma^3 c^3} \int_0^L dz_1 \int_0^L dz_2 a_{w,max}^2 |z_1 - z_2| \\ &= \frac{\omega_p^2 \omega_w}{4\gamma^3 c^3} \cdot \frac{a_{w,max}^2 L^3}{3} \end{aligned} \tag{46}$$

where $a_{w,max}$ is the maximum value of $a_w(z)$. Comparing (46) to (18), it is found that the upper limit for the small-signal gain can exceed the maximum gain for a constant wiggler only by less than 25 percent if no dispersion magnets are used. An interesting question is: within this small margin is there any other wiggler variation which can give a higher gain than the maximum gain of a constant wiggler with the same total length?

This question can be answered by using an approach similar to the calculus of variation. For simplicity, we consider that a small perturbing variation is introducted to the phase factor but not to the radiation strength of the constant wiggler

$$f(z) = hz + \delta\eta(z) \; ; \; a_w \text{ is constant} \tag{47}$$

where δ is a very small constant and $\eta(z)$ is an arbitrary function. After substituting (47) into (42), the gain can be expanded in power series of δ. If there is no other variation which can give a higher gain than the maximum gain of the constant wiggler, the following condition must be satisfied for any function $\eta(z)$

$$\left.\frac{\partial G}{\partial \delta}\right|_{hL = 2.6;\ \delta = 0} \equiv 0 \tag{48}$$

This identity requires the following function to be zero

$$J = \int_0^L dz_1 \int_0^L dz_2 (z_1 - z_2)\,[\eta(z_1) - \eta(z_2)] \cos\left[h(z_1 - z_2)\right]$$

$$= 2\int_0^L dz_1 \eta(z_1) \int_0^L dz_2 (z_1 - z_2) \cos[h\,(z_1 - z_2)] \tag{49}$$

Since $\eta(z)$ is arbitrary, it can be chosen to be a set of orthogonal functions in the interval $[0, L]$ (For example, $\eta(z)$ can be the Legendre functions if the integration range is properly transformed into $[-1, 1]$).

From the completeness of orthogonal functions, the following integral has to vanish for any value of z_1

$$\int_0^L dz_2(z_1 - z_2) \cos [h (z_1 - z_2)] = 0 \tag{50}$$

It is straight forward to check that (50) can not be satisfied. Therefore, the conclusion is that the constant wiggler gain is not the maximum gain that can be obtained. By properly recontouring the wiggler variation, we expect that the gain can be increased although the proof does not show a best way to change the tapering. It is interesting to point out that the linear taper given in (19) does satisfy the condition (48). However, if the perturbing function $\eta(z)$ is chosen to be cubic, the condition (45) is not satisfied and we obtain a gain higher than (18). The increase in the gain is obviously due to the generation of complex structures in the spontaneous spectrum. The change in its slope cannot be very big and thus the increase in gain is very limited.

The analysis can be generalized to the perturbation on any given wiggler variation. For example, consider a wiggler with the variation $f(z)$. Following a similar procedure, we can prove that the gain for that wiggler is a maximum only when

$$\int_0^L dz_2(z_1 - z_2) \cos [f(z_1) - f(z_2)] = 0 \tag{51}$$

for any value of z_1. Again, it is straight forward to show that (48) cannot be satisfied for any variation $f(z)$. Therefore, a generalized conclusion is that there is no wiggler variation which can be claimed to give a maximum gain. The gain can always be increased, within the 25 percent margin over the maximum constant-wiggler gain, by properly changing the tapering.

III-6. SUMMARY

We have completed a small-signal theory for an arbitrary FEL wiggler. The spontaneous spectrum and the small-signal gain are derived analytically. Madey's theorem is then proved in a most general situation. The gain experession is applied to special cases such as: constant wiggler, linear tapered wiggler, two-component devices and optical klystron. An upper limit is found for the small-signal gain of any wiggler configuration which can exceed the maximum gain of a constant-wiggler of the same length by less than 25 percent. The significance of its implication is discussed. For an optical klystron with dispersion magnets, it is found that the upper limit is determined from the equivalent device length which is much higher than the value determined from its physical length. The gain is thus possible to be highly enhanced with dispersion magnets in the drift space.

REFERENCES III

1. N.R. Kroll, P.L. Morton and M.N. Rosenbluth, in Physics of Quantum Electronics, Vol. 7, Edited by S.F. Jacobs, H.S. Pilloff, M. Sargent III, M.O. Scully and R. Spitzer (Addision-Wesley, Reading, Mass.) 1980.
2. C. Shih and A. Yariv, Opt. Lett., 5, 76 (1980).
3. M.Z. Caponi and C. Shih, presented at IEEE International Conference on Plasma Science, Santa Fe, New Mexico, May 18-20, 1981, Bull. Am. Phys. Soc. 1981 Plasma Annual Meeting, New York, Oct. 12-16, 1981. Also, submitted for publication to Phys. Rev. A.
4. C. Shih and M.Z. Caponi, Bull, Am. Phys. Soc., 1981 Plasma Annual Meeting, New York, Oct. 12-16, 1981 and J. Edighoffer, Private Communication.
5. V. Stagno, G. Brautti, T. Clauser and I. Boscolo, Nuovo Cimento 56B, 219, (1980).
6. J. Boscolo and V. Stagno, Nuovo Cimento, 58B, 267 (1980).
7. J.D. Jackson, Classical Electrodynamics, (wiley, New York) 1976.
8. J.M.J. Madey, Nuovo Cimento, 50B, 64 (1979).
9. N.M. Kroll, P.L. Morton, M.N. Rosenbluth, JASON Technical Report JSR-79-01, Appendix A, SRI International, February 1980.
10. W. Gautschi, Handbook of Mathematical Functions, 9th edition, Edited by M. Abramowitz and I.A. Segun, Chapter 7, (Dover, New York) 1970.
11. C.A. Brau, IEEE, J. Quan. Elect., 16, 335 (1980).

IV. GAIN AND EFFICIENCY ENHANCEMENT BY A MULTICOMPONENT WIGGLER FREE ELECTRON LASER

IV-1. INTRODUCTION

Recently, there has been a large research effort towards the development of the FEL as a high average power source of high frequency electromagnetic radiation.[1-5] It has been demonstrated theoretically that the inherently low efficiency of a FEL at high input power and small output wavelengths ($\lambda_s \leq 10.6_\mu$), can be increased by appropriately tapering the wiggler field.[3,4] In this form, an efficient FEL amplifier could be obtained. A number of experiments are in progress to validate this theory.[5,6]

The efficiency of a FEL with a tapered wiggler, however, is enhanced only at a given input power for which the taper is optimum; it can decrease or even be 'negative' at other input powers.[7] Further, the output radiation frequency at which the gain is maximum as well as the gain spectrum width changes as a function of input power for a given taper.[8] Thus, a tapered wiggler free electron laser (TWFEL) becomes less attractive as an oscillator.

The unusual behavior of the TWFEL gain and gain spectrum as a function of increasing power in the cavity results in difficult or impossible start up from noise or with small input powers, low gain and efficiency at the oscillator saturation power, and a delay, due to the possibility of mode jumping, in reaching steady state. In this section we discuss how these unwanted oscillator characteristics might be eliminated by substituting the

tapered wiggler by a more complex multi-component wiggler configuration. The multi-component wiggler (MCW) configuration is based on the physical principles of both the TWFEL and the constant (untapered) wiggler free electron laser (CWFEL). Thus, in order to understand the mechanism of the MCWFEL we first summarize briefly the characteristics of both the TW and the CWFEL.

In a TWFEL, the electrons are trapped in the ponderomotive potential well ("bucket") associated with the beating wave formed by the wiggler and the radiation field. A "resonant" or synchronous particle can be defined that has the same longitudinal velocity V_z as the phase velocity V_{ph} of the ponderomotive wave ψ and with an initial phase relative to the beating wave such that energy is extracted from the particle. By keeping the rate of change of the phase velocity of the ponderomotive wave equal to that of the initially resonant electron longitudinal velocity, the phase of the electron relative to the ponderomotive wave remains constant and the extraction process can be continued all the way down the wiggler. If the process is sufficiently slow, (adiabatic) and the initial mean energy of the electron beam coincides with the resonant energy, the electrons that were initially trapped in the bucket, tend to remain trapped.[3] Hence, as the bucket energy decreases, the mean energy of the trapped electrons is reduced. For an electron beam with an effective energy spread smaller than the bucket height, more than 40 percent of the electrons can be trapped in the potential well. The maximum increase in energy of the untrapped electrons is of the order of the bucket height. Thus, by reducing the trapped electrons mean energy by a larger value than the bucket height, the <u>total</u> mean energy of the electron beam can be reduced. The extracted electron beam energy provides the amplification of the input laser signal. The rate of change of the difference $V_z - V_{ph}$ can be adjusted in a controlled manner by adiabatically tapering the wiggler field amplitude and/or period.

In a CWFEL, the wiggler field amplitude and period are maintained constant. Thus, an initially resonant electron can be maintained at resonance throughout the constant wiggler only if its energy remains constant (zero energy extraction). Depending on their initial phase the electrons that are initially resonant can either extract energy from or give energy to the electromagnetic wave. In order to extract energy from

the electron beam in a CWFEL the initial mean energy must be larger than the resonant energy and the effective energy spread smaller than half the bucket height.[9] In this case, as the electron beam travels through the interaction region, the electrons "bunch" in phase space at the right phase for radiation amplification. Once the electron beam mean energy is reduced to the resonant energy, a large fraction of electrons starts to gain energy from the wave and the amplification process stops. A CWFEL can be thought as a special case of the TWFEL for which the wiggler taper is zero.

From the previous description it can be concluded that different tapers might require different initial electron mean energies for optimum operation. Further, for a fixed taper, there is an optimum initial difference between the longitudinal mean velocity of the electron beam, V_b, in the direction of propagation and the ponderomotive potential well phase velocity, V_{ph}, for radiation amplification at a given wavelength. For example, for a CWFEL of a given interaction length L, the optimum electron initial energy is such that a) is sufficiently close to the energy of the potential well that the electrons orbit is perturbed by the presence of the ponderomotive potential but b) sufficiently far that the electron energy is reduced to the resonant energy and the maximum energy extracted from the electron beam at a distance $z = L$ from the origin. For a TWFEL, the maximum trapping occurs when the taper is such that the electron beam energy rate of change remains the same as the ponderomotive potential energy rate of change. In this case, the optimum initial electron beam energy is the resonant energy. However if the bucket energy rate of change is, say, faster than that of the electron beam, larger trapping might occur by starting the electron beam at an energy below resonant. In both cases, (CWFEL and and TWFEL), the optimum depends on the amplitude of the ponderomotive potential well that in turn depends on the radiation power in the interaction region. As this power varies, the required initial electron beam energy for maximum gain operation also varies. Since it is very difficult if not impossible to vary the initial electron beam energy as the power in the cavity builds up, what in fact occurs is a variation in the gain spectrum and the frequency that corresponds to maximum gain. Thus, the output frequency will vary and it might become very difficult to reach steady state in a high power FEL oscillator.

IV-2. PARAMETRIC DEPENDENCE OF GAIN SPECTRUM WITH INPUT POWER AND TAPER

In order to be able to design an appropriate high power FEL it is then important to investigate and find ways to modify the parametric dependence of the gain spectrum on the wiggler taper and radiation power as well as the input electron beam energy. This dependence can be investigated through the equations of motion for the electrons coupled to Maxwell's equations for the fields.[3,4,9] In this subsection we discuss in more detail the physical mechanisms that determine the optimum electron beam initial energy for a given taper. The interaction of an electron with the radiation inside the wiggler can be described in a simplified manner by the one dimensional equations of motion averaged over the fast oscillations of the electron motion[3,4] as follows,

$$\frac{d\gamma^2}{dz} = - k_s a_s a_w \sin \psi \tag{1}$$

$$\frac{d\psi}{dz} = k_w - \frac{k_s}{2\gamma^2}[\mu - a_s a_w \cos \gamma] \tag{2}$$

where $\mu = 1 + a_w^2/2$ for a sinusoidal wiggler field, $\psi = \int(k_w + k_s)dz - \omega_s t$ is the phase position of the electron in the ponderomotive potential well and $d\psi/dz$ is proportional to the difference between the longitudinal particle velocity $v_z = dz/dt$ and the phase velocity of the ponderomotive potential $V_{ph} = \omega_s/(k_w + k_s)$.

In Equations (1) and (2), a_s and a_w are defined respectively as,

$$a_s = \frac{e E_s}{mc^2 k_s} \quad , \quad a_w = \frac{e A_w}{mc^2} \tag{3}$$

where $E_s \sim P_s^{1/2}$ is the radiation field amplitude, P_s is the radiation power, A_w is the vector potential associated with the wiggler field B_w and k_w and $k_s \simeq \omega_s/c$ are the wiggler and radiaton wavector respectively. Equations

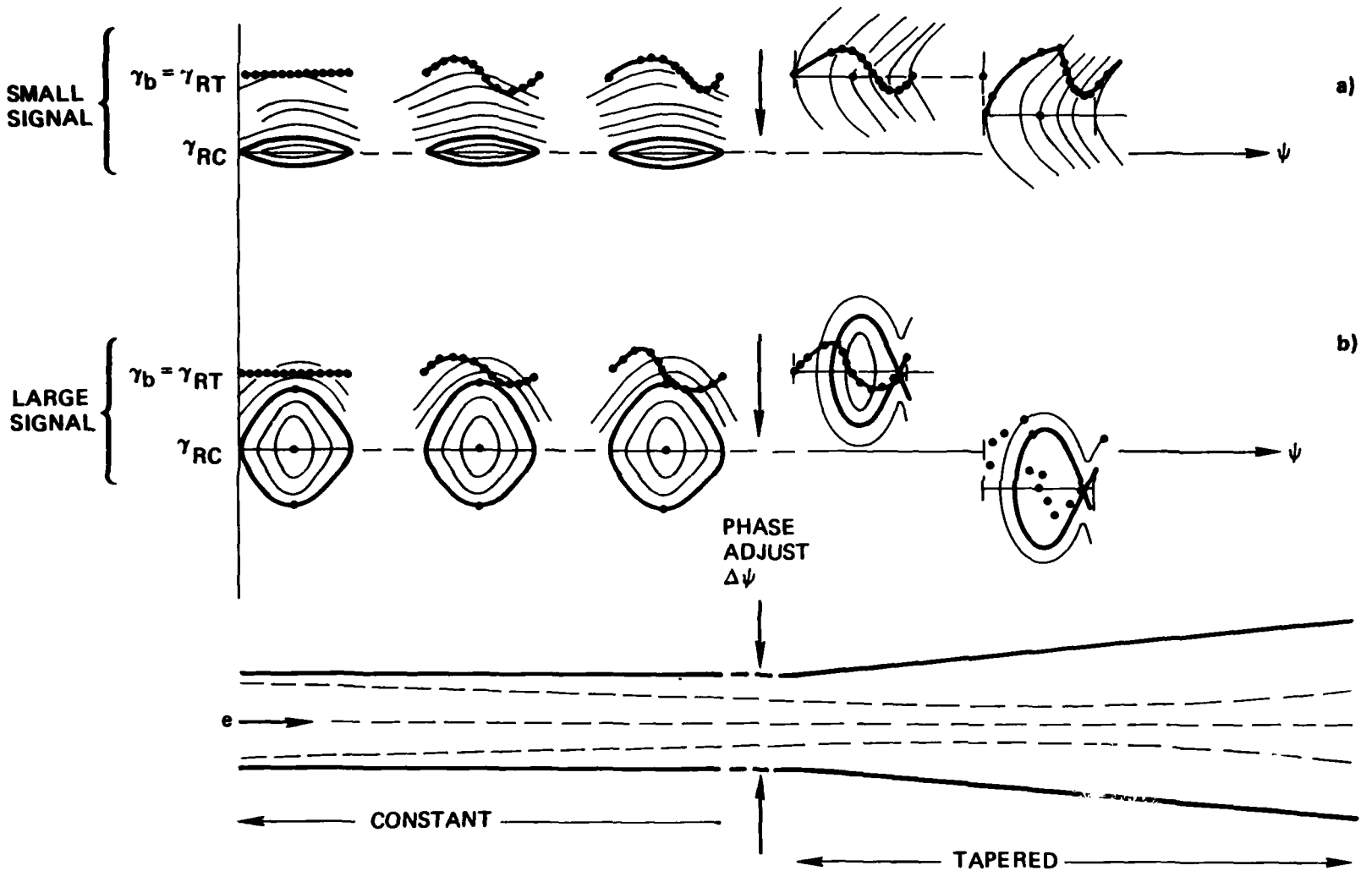

Figure 1. Schematic of Small - Signal Gain Enhancement (a) and Large Signal Gain Characteristics (b) for a Two Component Wiggler FEL

(1) and (2) can be combined to study the electrons orbit in phase space: ψ, $\delta\gamma = \gamma - \gamma_r = (d\psi/dz)[\gamma_r^3 / \mu\,(k_w + k_s)]$ where γ_r is the energy associated with the ponderomotive potential well or resonant energy; to yield:

$$\frac{d^2\psi}{dz^2} = -\frac{k_w}{2\mu}\frac{da_w^2}{dz} - \frac{2a_s\,a_w\,k_w^2}{\mu}\sin\psi \qquad (4)$$

Equation (4) has been derived assuming no spatial dependence of the wiggler wavelength ($dk_w/dz = 0$) and sufficiently small gain that the spatial variation of the radiation wavelength and amplitude can be neglected relative to the variation in the wiggler amplitude. In addition, terms of the order of $\delta\gamma/\gamma_r$ and $d\psi/(dz\,k_w)$ have been taken to be much smaller than 1 and neglected to first order. The simple orbit equation (4) can be utilized to describe the dominant mechanisms that determine the parametric behavior of a typical TWFEL, a more general expression can be found elsewhere.[11]

The previous qualitative description of the CWFEL and TWFEL behavior can be more clearly understood in the light of Equations (1) through (4). The first term in Equation (4) is due to the presence of a wiggler taper: $\Delta = [a_w(z) - a_w(o)]/a_w(o)$, a similar term occurs for the case in which the wiggler wavelength is tapered. For a zero taper FEL, $\Delta = o$, Equation (4) yields the well known pendulum equation that describes the behavior of the electrons in a CWFEL.[9,10] The trajectories of the electrons in this case are periodic and correspond to either open orbits (untrapped) or closed ones (trapped). The motion is symmetric and centered about $\psi = \psi_r = 0$. The first section (lefthand) of Figure 1, marked 'constant' in the bottom diagram, shows a schematic of the separation between open and closed orbits for a small signal (a) and for a large signal (b) case. The maximum height of the separatrix, that corresponds to the maximum $\delta\gamma_M$ for which a particle mey be trapped, is proportional to $(a_s\,a_w)^{1/2} \propto (P_s^{1/4}\,a_w^{1/2} / k_s^{1/2})$. The frequency of oscillation Ω of the particles in the well is also proportional to $\delta\gamma_H$. The maximum width of the trapped orbit is 2π.

From the orbit equations (1) through (4) it is clear that electrons injected at the resonant energy ($\gamma_{inj} = \gamma_{RC}$ in Figure 1) and uniformly distributed in phase space will have their energy oscillate about the resonant value, if $\Delta = o$. No net deceleration will occur in this case as as many

electrons will gain and lose energy and the behavior of the electrons will be symmetric about γ_R ($d\psi/dz = o$). In order to obtain maximum net deceleration of the electrons when $\Delta = o$, the electron beam must be injected above the resonant energy. Equation (1) shows that electrons uniformly distributed in phase space, will increase and decrease in energy in a sinusoidal manner about the initial γ_{inj}. Because $\gamma_{inj} > \gamma_R$, the electrons with phase near $\pi/2$ will be closer to γ_R and therefore increase slower in phase than those with other phases (Equation (2)). Hence, a bunching in phase near $\pi/2$ where the deceleration is maximum will occur. In order to extract the maximum energy, the electrons must be injected at an optimum injection energy such that after bunching they only complete a fraction (approximately 1/2) of the periodic oscillation during the length of the interaction. Because the time it takes to execute this fraction of an oscillation ($t = \Omega^{-1}$) is proportional to $P_s^{-1/4}$, the optimum injection energy required for a fixed length CW will increase with increasing radiation power.

Equation (2) shows that there is a direct correspondence between the electron resonance energy such that $d\psi/dz = o$ and the output frequency. For a practical CWFEL device the electron beam injection energy remains fixed and therefore the output frequency will shift in such a way to "reaccommodate" the resonant energy until the difference $\gamma_{inj} - \gamma_R$ has the optimum value for maximum gain. In addition, since the single pass efficiency η of a CWFEL is determined by the amplitude of the $\gamma_{inj} - \gamma_R$ difference which for operation at maximum gain will increase as $P_s^{1/4}$, the actual gain of the system $[\Delta P_s/P_s(o)) \simeq \eta/P_s(o)]$ will decrease as $P_s^{3/4}$. Thus, although the output frequency will shift as a function of power, the maximum gain for the initial small signal mode will be higher than for the other possible modes at higher power, and the initial mode might dominate as the power in the cavity builds up. The disadvantage of course is that the gain is too small at the large power of interest and the CWFEL has to be operated at moderated to low powers.

For a very small input power and a finite taper ($\Delta \neq o$), the first term in Equation (4) will dominate. This case corresponds to a small signal TWFEL and if we assume a linear wiggler taper the orbits correspond to paraboles, $\psi \sim (d\psi/dz)^2$. The effect of the second term in Equation (4) is to introduce some periodicity in the motion in such a way that parabolic

lines will be distorted as shown in the second section of Figure 1, marked "tapered" in the bottom diagram for a frame moving with γ_R. Further if the second term is suffuciently large, closed regions (buckets) will exist where the particle orbits are trapped (Figure 1b). These buckets are now asymmetric and centered at a phase $\psi = \psi_R$ that remains constant ($d\psi_R/dz = o$). The value of ψ_R and size of the bucket depends on the relation between the taper and radiation power as shown by Equation (4).

In a TWFEL, the system is prepared in such a way that the taper is "optimum" for a given radiation power of sufficiently large value. That is, the wiggler taper is made proportional to the change in γ_R in such a way that there is a phase ψ_R for which $d\psi_R/dz = o$ all through the interaction length. In addition, for maximum efficiency ψ_R has to be such that not only the deceleration is large but the "bucket size" is sufficiently large to trap the maximum number of electrons. Equation (1) shows that the deceleration is maximum for maximum sin ψ_R. On the other hand, Equation (4) shows that the largest bucket area occurs when $\psi_R = 0$. The optimum therefore occurs for ψ_R close to 40^o.[12] Since the rate of change of γ_R depends on $P_s^{1/2}$, it is clear that for a given taper there will be only one radiation power that is optimum.

If the radiation power is <u>larger</u> than this optimum, the ψ_R that corresponds to a rate of change in the energy such that $d\psi_R/dz = 0$, will be <u>smaller</u> than the optimum. In this case, a slight increase can occur in the number of trapped electrons (a maximum increase by a factor of 2 can occur only if $\psi_R \simeq 0$ that corresponds to $P_s \to \infty$) and the deceleration efficiency remains the same to match the fixed taper. Thus, for a sufficiently large increase in power from the optimum, the overall gain will decrease although the overall efficiency will remain approximately the same. For the case where the radiation power is smaller then the optimum, the corresponding ψ_R will be larger than the optimum, up to a value of 90^o, that corresponds to a decrease in the radiation power from the optimum by a factor of less than 5. For smaller radiation powers, no ψ_R can be defined, and the purely open orbits begin to resemble the open paraboles of the small signal case. Therefore, if P_s is much smaller than the optimum one (P_{sop}) for a given taper, most of the particles remain untrapped. In order to understand how the energy extraction can occur, a frame moving with γ_R that corresponds to

optimum power can be defined. In the second section of Figure 1a, the motion of the particles in this frame is shown at $z = 0$ and at $z = z_1$ assuming that initially $\gamma = \gamma_R$ and $P_s \leq P_{sop}/10$. In this figure the motion of γ_R in the laboratory frame is also shown. The particles move clockwise and <u>increase</u> in energy relative to γ_R. Due to the change of slope of the orbits, the particles move faster when moving away from γ_R than towards γ_R. Further, they move slower the closer their energy is to γ_R. Energy extraction can occur if the average increase in energy relative to γ_R occurs at a slower rate than the decrease in γ_R due to the wiggler taper. This requires that γ_{inj} be quite close to γ_R as well as a sufficiently small interaction length so that most of the particles remain in the vicinity of γ_R and do not reach the fast energy increasing region of the orbits. Further, for a given interaction length, there will be an optimum initial γ_{inj} for maximum gain, Figure 1a shows that $\gamma_{inj}^{opt} < \gamma_R$ for $P_s < P_{sop}$. For $P_s = P_{sop}$, the γ_{in}^{opt} is equal to γ_R to insure maximum electron trapping. In addition, the maximum gain for $P_s < P_{sop}$, will always be smaller than the maximum gain for $P_s = P_{sop}$. Hence, if the initial γ_{inj} is chosen to maximize the gain for $P_s = P_{sop}$, the initial ($P_s << P_{sop}$) output frequency of the oscillator will be quite different from that growing at saturation, where $P_{sat} < P_{sop}$. The problem is exacerbated for very small output wavelengths were even the maximum small signal can be below threshold for a practical cavity loss. From the above discussion we conctude that for <u>any</u> taper Δ there is an optimum power for maximum gain operation and this power increases with Δ^2. Thus, the CWFEL can again be considered as a special case of a TWFEL with zero taper and optimum operation power in the small signal regions. In addition, for any Δ the gain spectrum shifts and changes its width as a function of increasing power with larger shifts and widths occurring for larger tapers where the small signal gain is made smaller than the high (optimum) signal gain.

IV-3. MULTICOMPONENT WIGGLER SCHEME

An ideal FEL oscillator will saturate at high powers with sufficient gain and efficiency to be of practical interest. At the same time, it will have a high small signal gain, a monotonically decreasing gain curve (gain vs. cavity power) and the peak of the gain spectrum will remain at the same frequency. In this way only a minimum number of photon passes in the inter-

action region will be required to obtain saturation and the system can be started up from noise or very low powers. A MCWFEL operates as an ideal FEL by utilizing the properties of a TWFEL with different tapers to its advantage.

The basic idea is to find a system that uses a number of wiggler components in such a way that each component operates at its own optimum power and either is transparent at other powers or enhances the performance of the corresponding component. In addition, the "optimum" output frequency of all the components should be the same. This system can be found due to the fact that, as discussed before, some of the most important physics mechanisms determining the FEL characteristics depend on the initial electron beam parameters (γ_{inj}/γ_R) and the amount of taper that determines the phase ψ at which bunching occurs. The resonant energy, γ_R, is in turn determined by λ_w and B_w for a fixed λ_s. Thus, we can think of a system formed by various wiggler components with different λ_w and B_w to provide different γ_R for each component and separated by proper amounts of drift space in such a way that the electron beam enters bunched at the right phase in each section.

The simplest MCW combination is then a two component one consisting of a constant wiggler (CW) followed or following a tapered wiggler (TW) as illustrated in Figure 1. In order to obtain $\gamma_{inj} > \gamma_R^{CW}$ but $\gamma_{in} \simeq \gamma_R^{TW}$, λ_w and B_w should be chosen in such a way that $\gamma_R^{CW} < \gamma_R^{TW}$. If the constant wiggler is located before the tapered wiggler, and is of the optimum length for maximum small signal gain, that means that the electrons are bunched at the end of the wiggler. For a CW, the bunching occurs at a phase near $\pi/2$. The TW operates with the electrons bunched at a phase $\psi = \psi_r \simeq 40^\circ$. Thus, in order to introduce the electrons in the TW in a proper fashion a very small drift space is required. In this drift space, the electrons should move a distance d given by:

$$d = \left[\left\{ (90^\circ - 40^\circ) \times \frac{\pi}{180} \right\} + n \right] \lambda_s \qquad (5)$$

where n is an integer number. By using a sufficiently large n, d can be of the order of a centimeter that is experimentally possible. On the other

hand, if the CW is located after the TW, due to the very low small signal gains of the TW, no large bunching occurs in the electrons before entering the CW at low input powers. However, the possibility exists that if the gain is negative or even positive but very small, the energy spread of the electrons could be increased by a small amount, decreasing the overall small signal gain of the CW. None of these two wiggler arrangements increases the high signal gain, however, they do not reduce it either since the CW is practically transparent for high powers.

If in addition we wish to enhance the large signal gain, the system should be operated in a fashion similar to an optical klystron. In the optical klystron a wiggler is made of two elements or components of say, length L_1 separated by a length L. The first element acts as a "prebuncher" and the second element as a "radiator". A system thus composed if the lengths are appropriately chosen will have larger high signal gain than one composed of a single element of length $2L_1$. The reason for this behavior is that in a single element wiggler, the electrons are modulated in the initial part of the wiggler, and afterwards they spread as they bunch. The bunching is never as effective as if after an initial velocity modulation they drift in free space and are introduced into the second element only after appropriate bunching has occurred. In this manner, the number of trapped electrons can be increased for TW operation. The drift length necessary to achieve bunching is calculated as the length that it takes particles separated in energy by $\delta\gamma/\gamma$ and in space by half a radiation wavelength to come together. This length is:

$$L_D = \lambda_s \, (n + 1/2) \, \gamma^2/(\delta\gamma/\gamma) \qquad (6)$$

where n is is integer number of wavelengths. $\delta\gamma$ can be identified with the electron beam energy modulation in the prebuncher section in order to predict L. Further, the drift length L can be substituted by a dispersion magnet of amplitude B which produces an "effective drift distance" proportional to L^3[7] (c.f. Section III) and therefore could permit to enhance the gain with shorter devices.

IV-4. NUMERICAL RESULTS

In order to obtain quantitative confirmation of these ideas, they were numerically investigated utilizing the TRW 1-D code (described in Section II of this report) that includes diffraction effects of the input Guassian optical beam and finite electron beam emittance according to the formulation described in Section II of this report. The numerical results presented here utilize the optimum parameter of the present TRW experiment: $\lambda_s = 10.6\mu$, electron beam energy $E_b \simeq 25$ MeV, electron beam peak current $I \simeq 40A$, electron beam radius $\simeq 2.25$ mm $\simeq$ photon beam waist, total interaction length < 4m, energy spread $\Delta\gamma/\gamma = 0.5\%$ and $a_w \simeq 0.98$. Numerical analysis, however, were made for a shorter wavelength case[13] ($\lambda_s = 1\mu$) and a number of different characteristic parameters and the same basic results were obtained.

Figure 2 shows the gain spectrum obtained for a simple L = 4 m tapered wiggler FEL for different input powers. The large taper ($\Delta = 35\%$) is required to obtain sufficiently high gain (>8%) at 500 MW. The gain is below 5 percent for small signal powers (P < 1 MW) and extremely wide ($\Delta\omega/\omega > 4\%$), with the peak gain frequency shifted more than 2 percent from the "resonant" output frequency. In order to test the MCW idea we first simulated a 3 m two component wiggler as illustrated in Figure 3. Case 1) corresponds to a 1 m CW followed by a 2 m TW separated by a 1 cm phase adjustment section and the order of the components is inverted for case 2). The parameters are chosen in such a way that $\gamma_R^{CW} < \gamma_R^{TW}$ and γ_{inj} = optimum for the whole system. The exact parameters utilized in the simulation are indicated in the figure. The taper utilized is $\Delta = 20$ percent that corresponds to an optimum power of $\simeq$ 500 MW for a length of 2 m and 100 MW for a length of 3 m. The gain curve (gain vs. power) for the simple TWFEL is shown in Figure 3 with dashed lines. The effect of the 1m CW section in case 1) is to increase the small signal gain over that of a simple 3m TWFEL by a factor larger than 10, that corresponds to a gain similar to that of a 1m CW. At very high powers (P > 500 MW) the system behaves as a simple 3m TW of $\Delta = 20$ percent. The gain at 100 MW is enhanced by a factor of almost 2 and the optimum power now occurs at 50 MW. For case 2), the small signal gain is also increased by almost a factor 10, however for very high powers the system behaves as a simple 2m TWFEL. Another unusual behavior in this case is the presence of a dip in the gain curve at P ~ 100 MW.

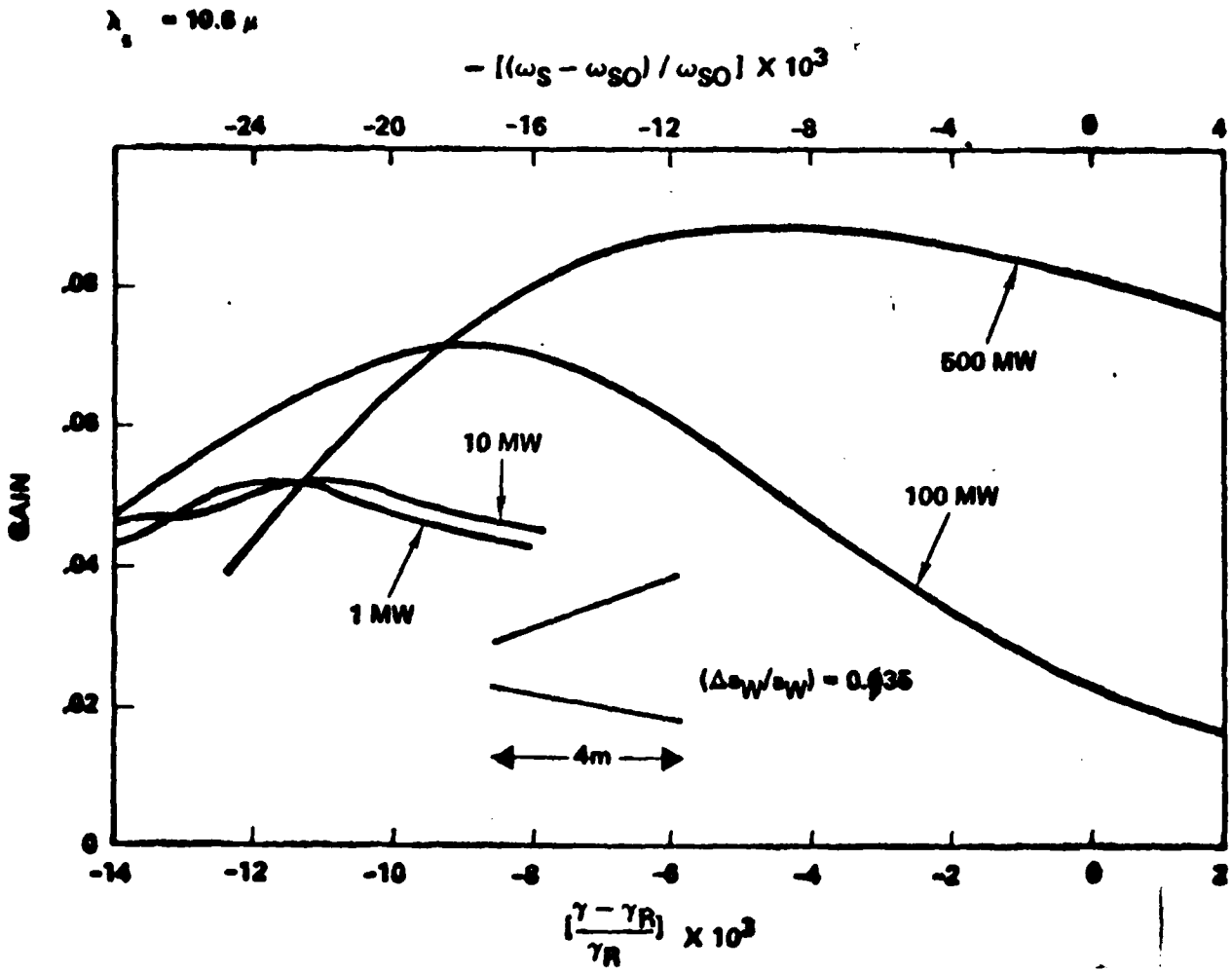

Figure 2. Gain Spectrum for Different Input Powers - TWFEL

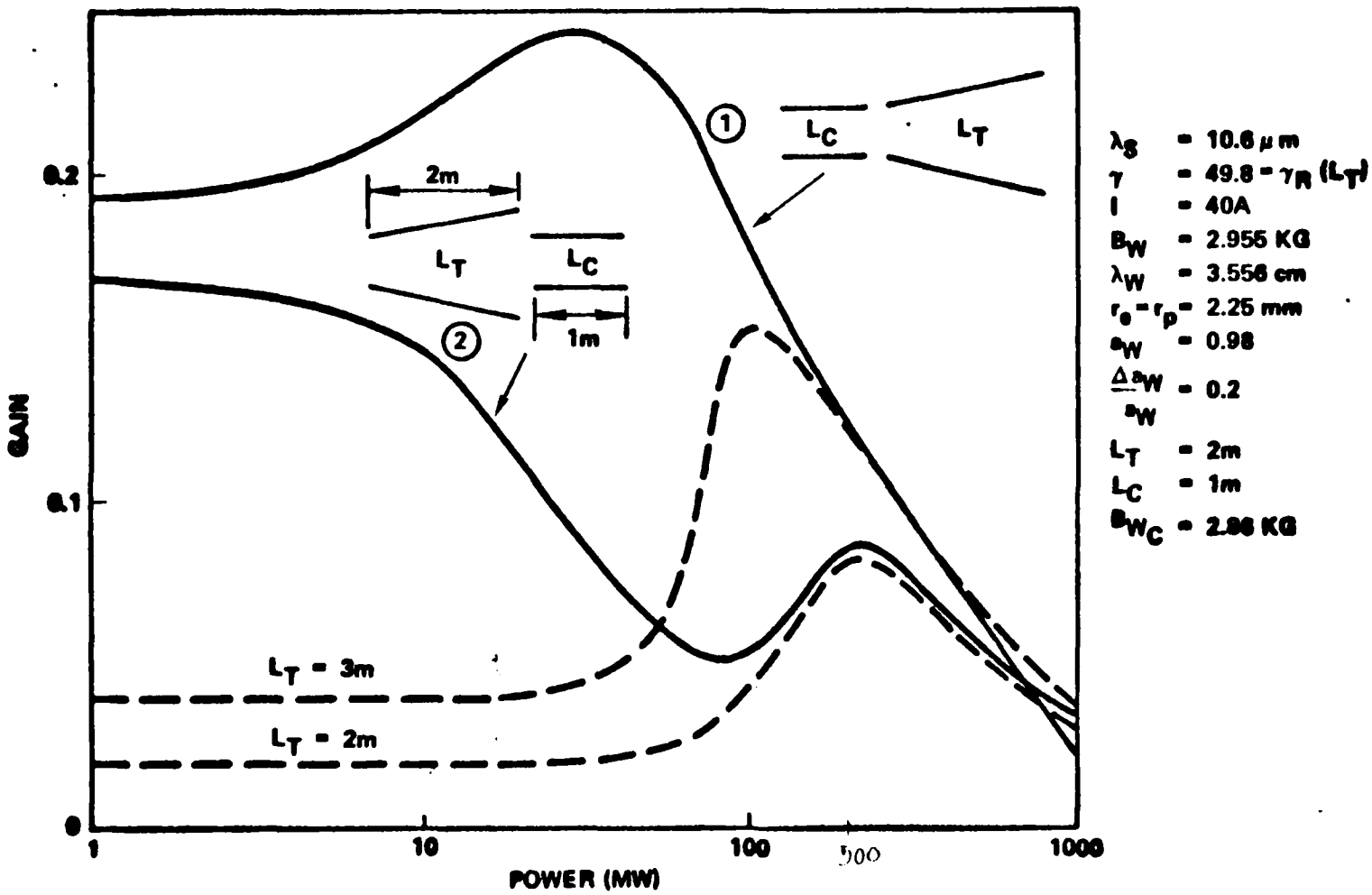

Figure 3. Multicomponent FEL (MCFEL) Gain vs. Input Power for a Two-Components Wiggler FEL

The different behavior of the gain curve at high powers for cases 1) and 2) is accounted by the "bunching" process. In a simple TW, the electrons bunch and are trapped by the potential well during the first half of an oscillation period, practically no radiation is emitted in this part of the interaction. Thus, in case 1) the initial CW is acting as the buncher section of a TW. Because the bunching in the CW is pr ably more effective than in a TW, the whole system is equivalent to a TW of length > 3m for high powers. Hence, the optimum power of this device is smaller than that of a 3m TW for the same taper Δ. For very high powers, the particles orbits show that the bunching does not play such an important role and the whole system behaves as a 3m TWFEL. For case 2), the CW is practically transparent to high powers and all the gain is determined by the 2m TW. The dip in the curve is due to the fact that this system essentially behaves like two separate components and the optimum power of the 2m TW is at those high powers for which the CW gain curve is already very small. Obviously, several possibilities can be suggested to obtain a monotonically decreasing gain curve with sufficient gain at high powers. For example, a system similar to 1) with either a shorter TW section or a very small tapered ($\Delta \sim 1\%$ or so) first section that will decrease by a very small amount the small signal gain but will increase the gain at the dip. Another possibility is to consider the effect of drift sections in the high signal gain.

In order to test the optical klystron idea for a TWFEL, a three component wiggler: CW, drift space, TW was simulated as shown in Figure 4. In this figure the results obtained for a short prebuncher CW section (L_C = 15 cm) followed by a L_D = 1m drift section and by a 2m and a 3m sections are compared with those of simple 3m and 2m TWFEL's (dashed lines). The lengths L_C and L_D were chosen to maximize the bunching at high power. Thus, the effect of the prebuncher section is to increase the bunching at the optimum power and increase the number of trapped electrons (and hence the gain and efficiency), by a factor of almost 2. This enhancement will not be effective if the electron beam has a large effective energy spread. In this case the potential well will be full from the beginning and the particles bunched in phase space will spread in energy beyond the well.

As a final demonstration of the possibilities of a MCW system for FEL oscillators, a four component system was simulated as illustrated in

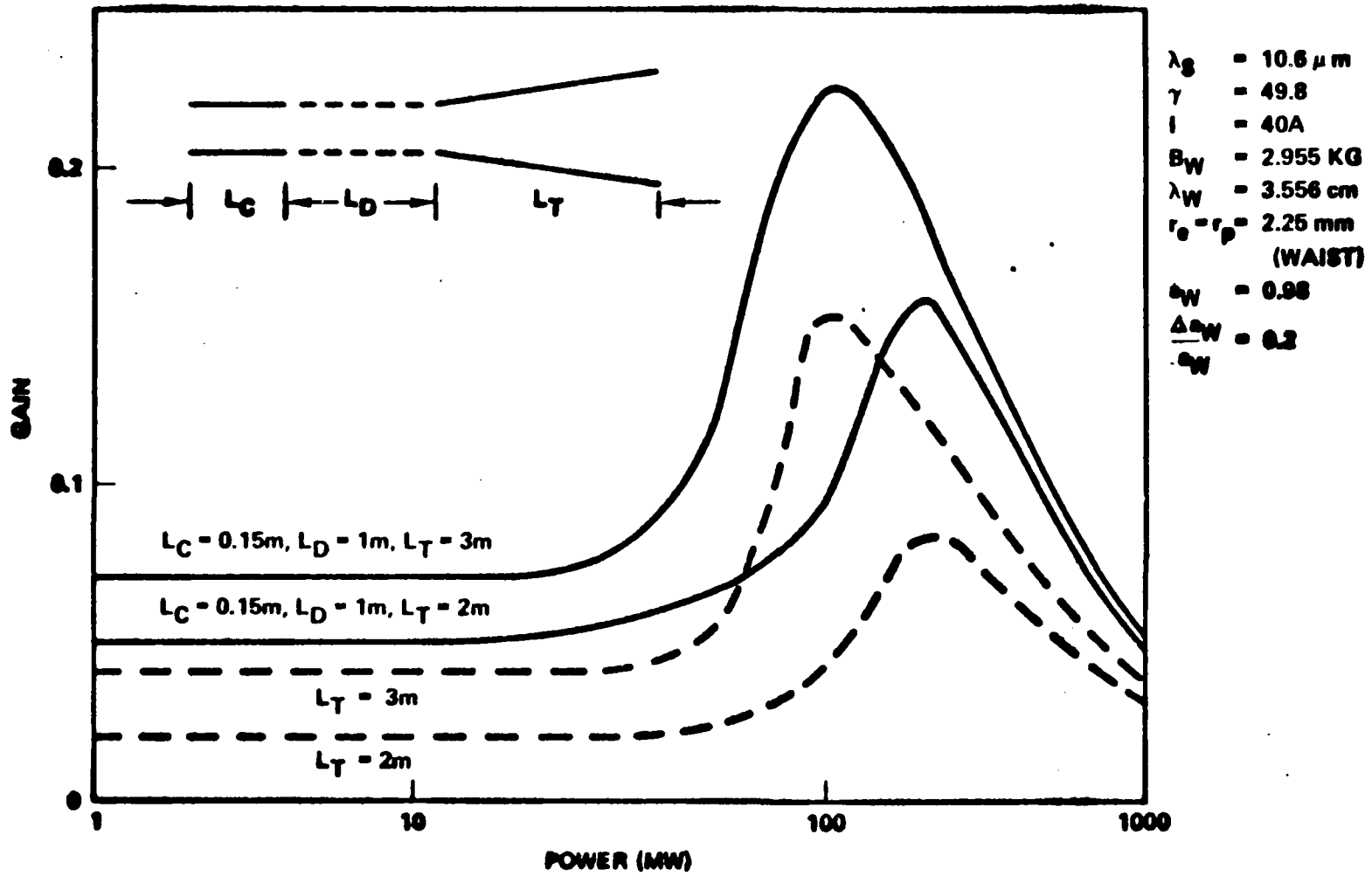

Figure 4. Multicomponent FEL Gain vs. Input Power for a TW With Prebuncher FEL (Two Components with Drift Space)

Figure 5. Essentially, a prebuncher (CW plus drift section) was added to the case 2), two component system of Figure 3. In addition, the taper was decreased to 13 percent that corresponds to a shift in the optimum power of a simple 2m TW from 500 MW to 100 MW. Essentially the same optimum power than that of a simple 3m TW with $\Delta = .20$. In this manner the small signal gain is further enhanced by utilizing now the whole initial 3m as a prebuncher for the final 1m CW secton. Note that the small signal gain is 60 percent compared to 20 percent in Figure 3 and less than 3 percent for the simple 3m TW. The high signal gain now is also increased over that of a 3m taper due to the prebuncher, however, this increase is quite small. In addition, now the whole gain curve has an almost (except for the small bump at a 100 MW) monotonically decreasing characteristic. Obviously, this system can be optimized by varying the tapers of the different sections, but the main principle here is to show that an enhancement in the gain up to the saturation power is possible to achieve. The case shown in Figure 5 has a total single pass efficient $\eta \simeq 3$ percent at $P \simeq 600$ MW which is assumed the saturation power for a cavity loss of 5 percent.

More important than to show plain gain enhancement at a given output frequency is to look at the improvement in the gain spectrum curve. Figure 6 shows the decrease in the spectrum width for small signals, the increase of the maximum gain peak and the almost negligible shift in the peak. This is due to the flexibility of choosing different γ_R for the different sections of the MCW. Again, this result can be further optimized to obtain an extremely stable output frequency and eliminate the possibility of frequency chirp that is extremely deleterious for oscillator operation. The number of photon passes calculated to obtain saturation at 600 MW assuming an injected power of 1 MW was 90 for the case shown in Figure 5. Further, the number of steps increases only in 10 by each order of magnitude that we wish to decrease the injected power if diffraction effects of the excited wave are neglected.

IV-4. SUMMARY

In conclusion, we have analyzed the main characteristics that determine the gain and gain spectrum vs. power curves for different tapers. From those characteristics we have developed a scheme that permits the operation of the FEL as an oscillator, at very high powers. The scheme, MCWFEL,

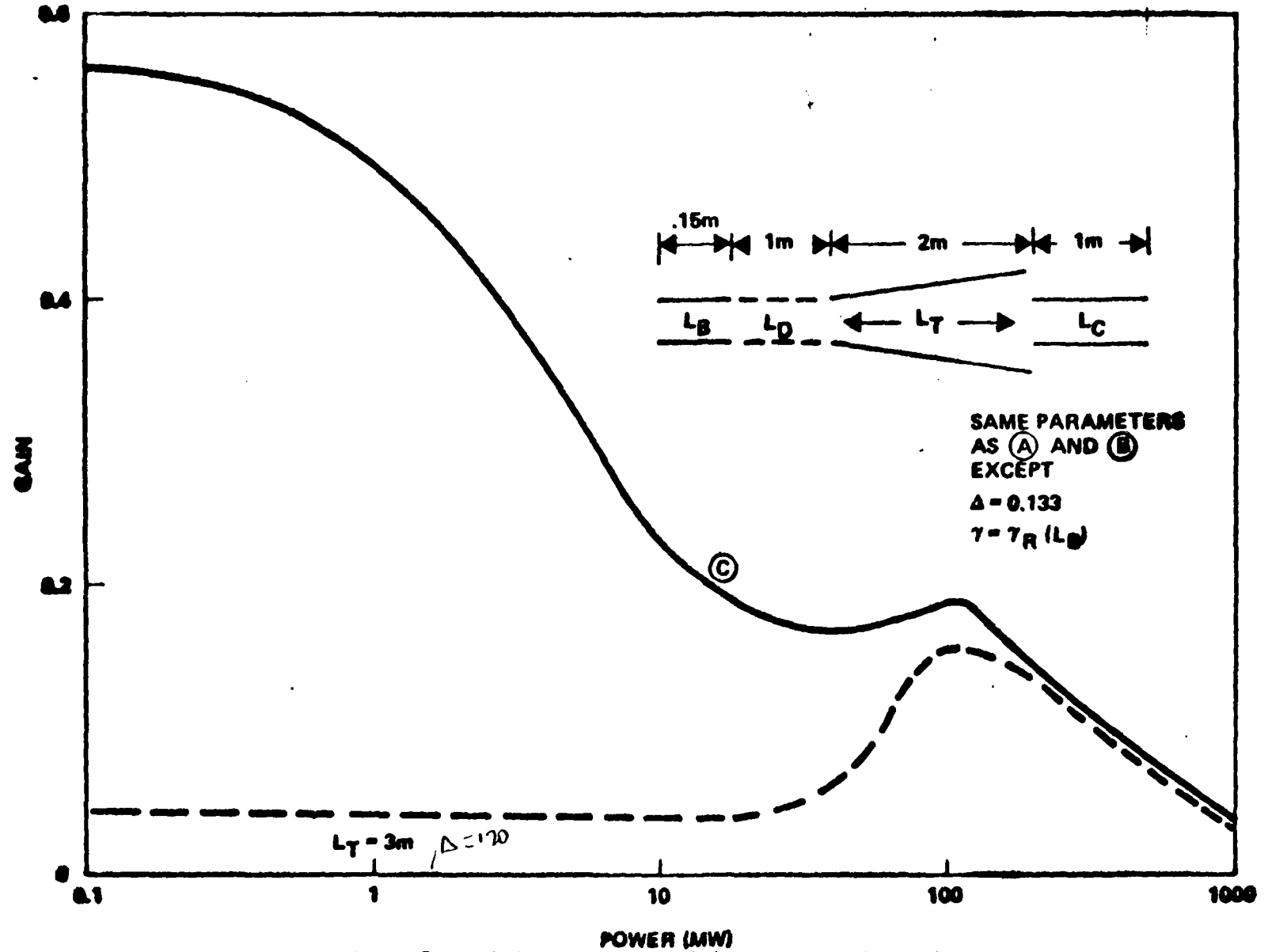

Figure 5. Multicomponent FEL Gain vs. Input Power for Three-Component Wiggler with Drift Space

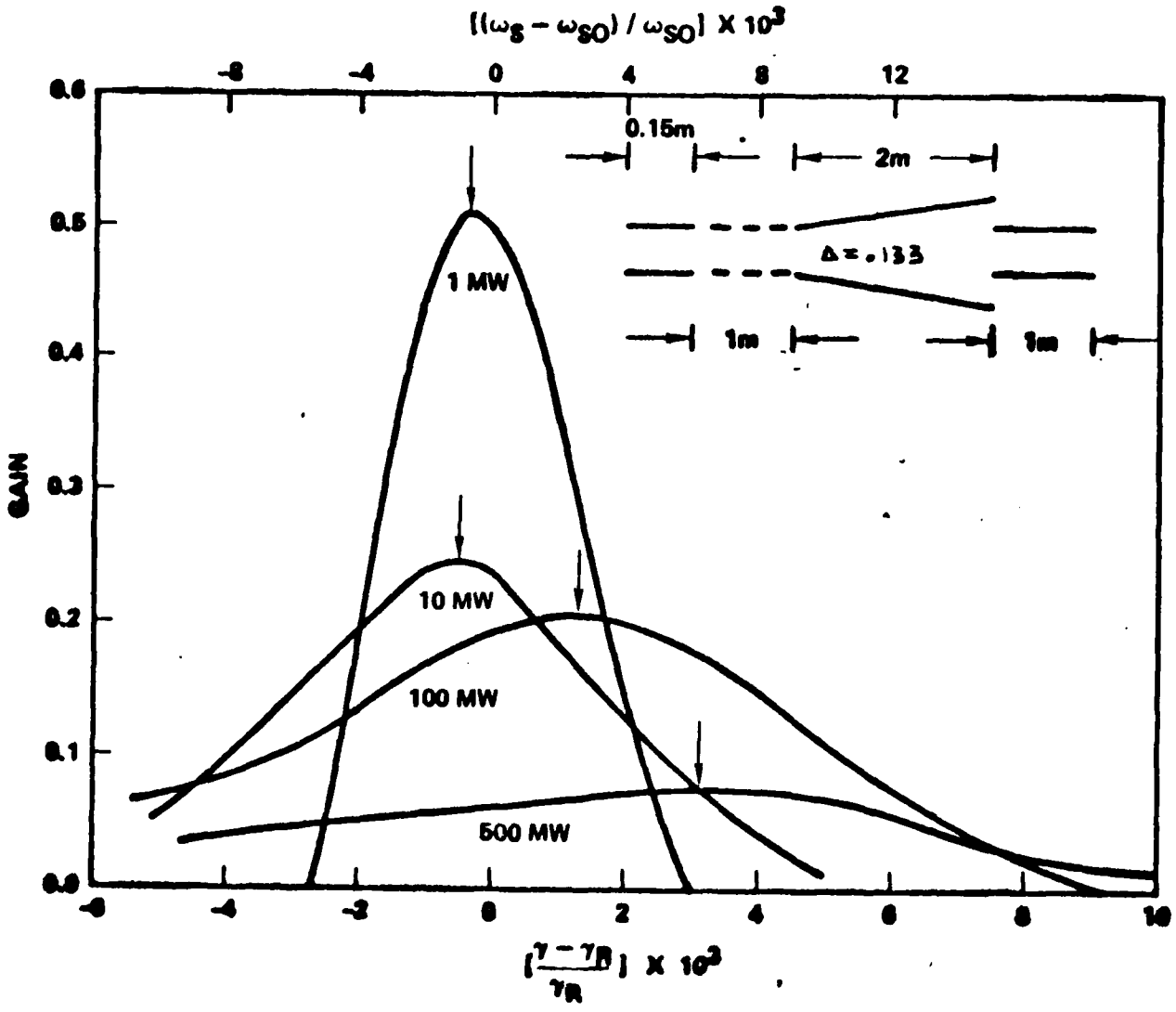

Figure 6. Multicomponent FEL Gain Spectrum for Different Input Powers MCFEL

increases the small signal gain by a factor larger than 10, provides a smooth gain curve, and decreases and/or eliminates the possibility of frequency chirp due to nonoptimum electron beam energy injection.

REFERENCES IV

1. L. Elias, W. Fairbank, J. Madey, H. A. Schwettman, T. Smith, Phys. Rev. Lett. 36, 717 (1976).

2. D. A. G. Deacon, L. R. Elias, J. M. J. Madey, G. J. Ramian, H. A. Schwettman and T. I. Smith, Phys. Rev. Lett. 38, 8921 (1977).

3. N. Kroll, P. Morton, M. Rosenbluth, J. Quantum Electronics, 7, 89, 1980.

4. P. Sprangle, C. J. Tang, W. W. Manheimer, J. Quantum Electronics, 7, 207 (1980).

5. H. Boehmer, M. Z. Caponi, J. Edighoffer, S. Fornaca, J. Munch, G. R. Neil, B. Saur and C. Shih, "Variable Wiggler Free Electron Laser Experiment" TRW, int. report, Aug 1981 accepted for publication in Phys. Rev. Lett.

6. Experiments with Tapered Wiggler FEL are in progress at LANL, MSNW and TRW

7. C. Shih and M. Z. Caponi, "General Theory of Multi-Component Wiggler Free Electron Lasers in the Small-Signal Regime", TRW int. report, Aug. 1981, accepted for publication with modifications in Phys. Rev. A

8. M. Z. Caponi and C. Shih, IEEE Int. Conf. in Plasma Sc., May 18-21, 1981, pp. 9

9. W. B. Colson, Phys. of Quantum Electronics, 5, 157 (1978)

10. W. B. Colson and S. K. Ride, Phys. of Quant. Elec., 7, 377 (1980)

11. P. Sprangle, C. M. Tang, "Formulation of Nonlinear Free Electron Laser Dynamics with Space Charge Effects and Spatially Varying Wiggler - Conference Digest of 4th Int. Conf. on Infrared and Millimeter Waves and their Applications, 1979, pp. 98-100.

12. C. Brau and R. Cooper, P. of Quant. Electr., 7, 647 (1980)

13. TRW 1981 IR and D FEL report.

V. FINITE PULSE AND PARASITIC INSTABILITIES INVESTIGATIONS (UCLA)

V-1. FINITE ELECTRON BEAM PULSE INVESTIGATIONS

TWFEL oscillators and high gain amplifiers are not well described by analyses that assume infinitely long, periodic electron beams. High peak current RF Linacs in general bunch the electron beam in 30-50 psec pulses. Therefore, the amplified radiation is also of the order of 30-50 psec long. This finiteness of the electron and optical beam pulse can modify the FEL characteristics predicted assuming infinite beam pulses. For example: 1) the longitudinal profiles are in general Gaussian. Since the radiation power for a FEL is proportional to the square of electron beam density, the excited radiation pulse profile will be similar to a Gaussian but narrower than that corresponding to the electron. Hence, "bucket height" at the edge will be smaller than at the center. If the tapers are optimized for the radiation amplified at the center, the electrons that see the edge amplitude might be detrapped, this problem will play an extremely important role for FEL oscillators; 2) the velocity of the optical pulse is larger than that of the electron beam and "slippage" effects will occur; 3) space charge fields can develop and become important at the edges of the electron beam pulse. In this case, the edge electrons will experience a dc self electric field that will modify their dynamics.

In this section we discuss our preliminary investigation of the problems related to finite electron/optical beam pulse effects. In particular, we investigate numerically the case of a 10.6μm amplifier of

the characteristics of the TRW experiment and also a high gain 10.6μm amplifier in preparation to the study of these effects on oscillators. High gain amplifiers can be obtained by either using a high density electron beam (for example, one with a density 10 times larger than the present TRW experiment) or, low input powers and small tapers, (in this case the extraction efficiency also becomes smaller) or the multicomponent wiggler FEL (MCWFEL) described in the previous section.

V-1-1 Finite-Length Simulations

We consider a relativistic electron beam with pulse length L_b and energy γ_o passing through a linear magnetic wiggler with $B = B_w \sin k_w z \hat{y}$. If $L_b >> \lambda_r$ (radiation wavelength) and both the amplitude (ε_x) and phase (ϕ) of the radiation vary slowly, the equations governing the spatial and temporal evolution of the electromagnetic wave can be derived from Maxwell's equation and take the following form

$$\left(\frac{\partial}{\partial z} + \frac{1}{c}\frac{\partial}{\partial t}\right) \varepsilon_x = -\frac{\omega_p^2 B_w}{2c^2 k_w} \cdot \frac{1}{N_o} \sum_i \frac{\cos(k_o z_i + \psi_i)}{\gamma_i} \tag{1}$$

$$\left(\frac{\partial}{\partial z} + \frac{1}{c}\frac{\partial}{\partial t}\right) \phi = \frac{\omega_p^2 B_w}{2c^2 k_w} \cdot \frac{1}{N_o} \sum_i \frac{\sin(k_o z_i + \psi_i)}{\gamma_i \varepsilon_x(z_i)} \tag{2}$$

where $\psi = k_z^2 - \omega_r t + \phi$ and ω_p is the plasma frequency of the relativistic beam. The equation of motion for each electron can be written as

$$\frac{d\gamma_i^2}{dt} = \frac{q^2 B_w \varepsilon_x}{m^2 c^2 k_w c} \cos(\psi_i + k_o z_i). \tag{3}$$

Equations (1) through (3) have a similar form to those given in Ref. 1.

In order to insure the numerical stability, Equations (1) and (2) are integrated along the characteristic curve of the electromagnetic wave; that is $\Delta x = c\Delta t$. The efficiency of a FEL decreases as the beam energy

increases. In order to enhance the efficiency, the wiggler profile should be designed in such a way that most electrons remain in resonance with the wave all the time. The resonance condition is roughly

$$k_w = \frac{k_r}{2\gamma_r^2}\left(1 + \frac{q^2 B_w^2}{2m^2c^2k_w^2}\right) \tag{4}$$

As the electron energy changes according to Equation (3), the wiggler field has to be varied accordingly so that Equation (4) remains true.

The following parameters characteristic of the 10.6μm variable wiggler experiment at TRW are used in our simulations λ_w = 3.5 cm, $\lambda_r = 1.06 \times 10^{-3}$ cm, L_b (electron beam pulse length) = 0.9 cm, L_r (signal pulse length) = 39 cm, L_w (wiggler length) = 300 cm, γ = 49.85, $\omega_p^2 = 1.69 \times 10^{20}$, $eB_w/mc = 5.2 \times 10^{10}$, and $eE_o/mc = 3.47 \times 10^{10}$, where E_o is the signal electric field amplitude. The electron beam pulse is divided into 30 grid points. Each grid contains 30 radiation wavelengths. The time step Δt is taken so that $\Delta z = c\Delta t = \lambda_w$ and the resonant phase ψ_r of the particle for determining the wiggler profile is taken to be 40^o. The simulation results of the spatial distribution of electron density and radiation amplitude at two different locations are shown in Figure (1a) ($z = 50\lambda_w$) and Figure (1b) ($z = 100\lambda_w$). To display the electron distribution function, the electron pulse is divided into five spatially equal regions and three of them are shown in Figure (2a) ($z = 50\lambda_w$) and Figure (2b) ($z = 100\lambda_w$). Obviously the resonant condition can only be maintained for a given position in the pulse, in this case we chose the particle located at the center of the beam pulse. As the radiation amplitude is increased along the length of the system, the inhomogeneity in the total electromagnetic field along the beam pulse becomes more enhanced which causes the ratio between the total trapped to untrapped electrons to drop.

The gain and particle energy averaged over the beam pulse versus distance are shown is Figure (3). Since the gain is moderate (≈15%), the

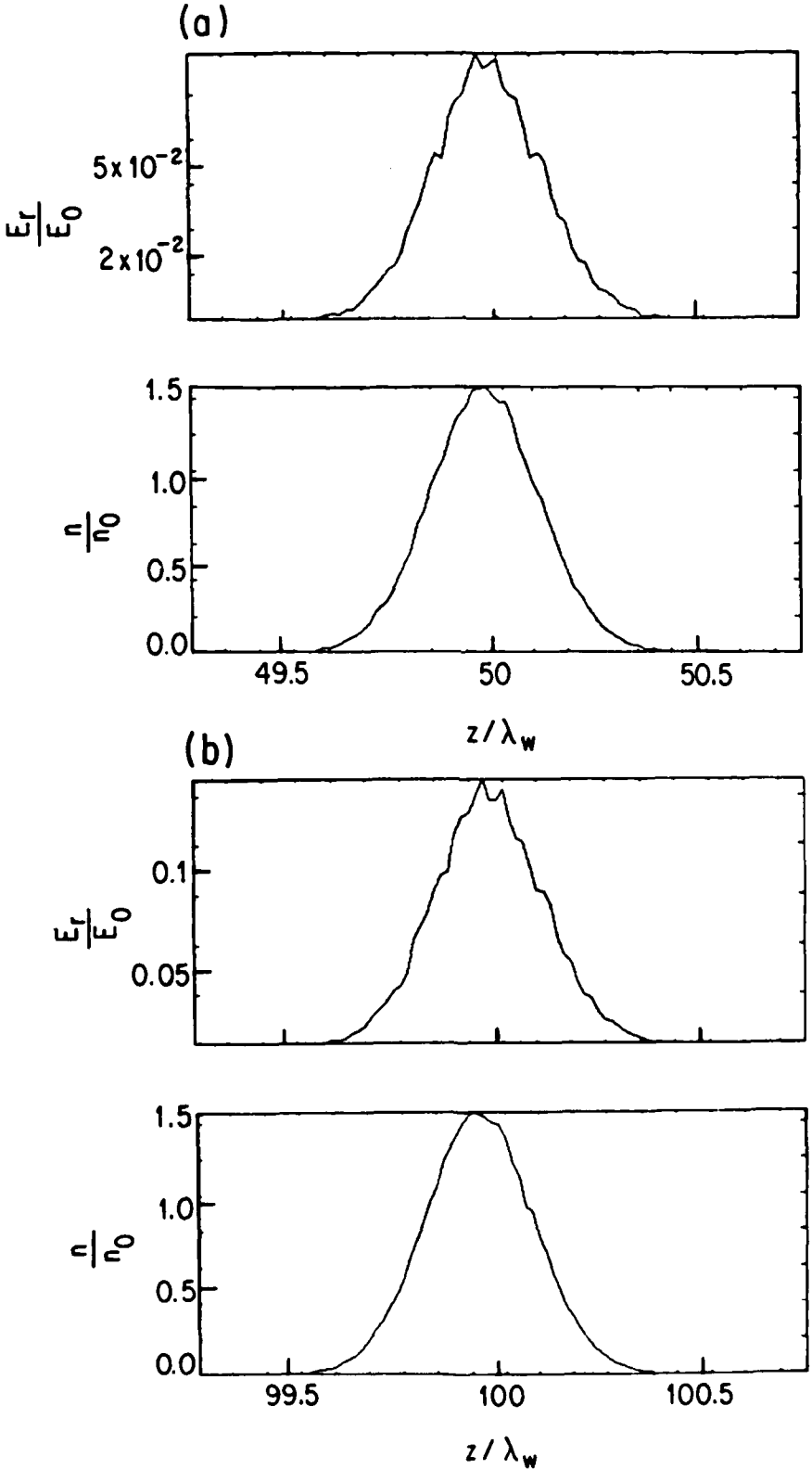

Figure 1. The Spatial Distribution of the Radiation Amplitude and Electron Density a) $z = 50\lambda_w$, b) $z = 100\lambda_w$.

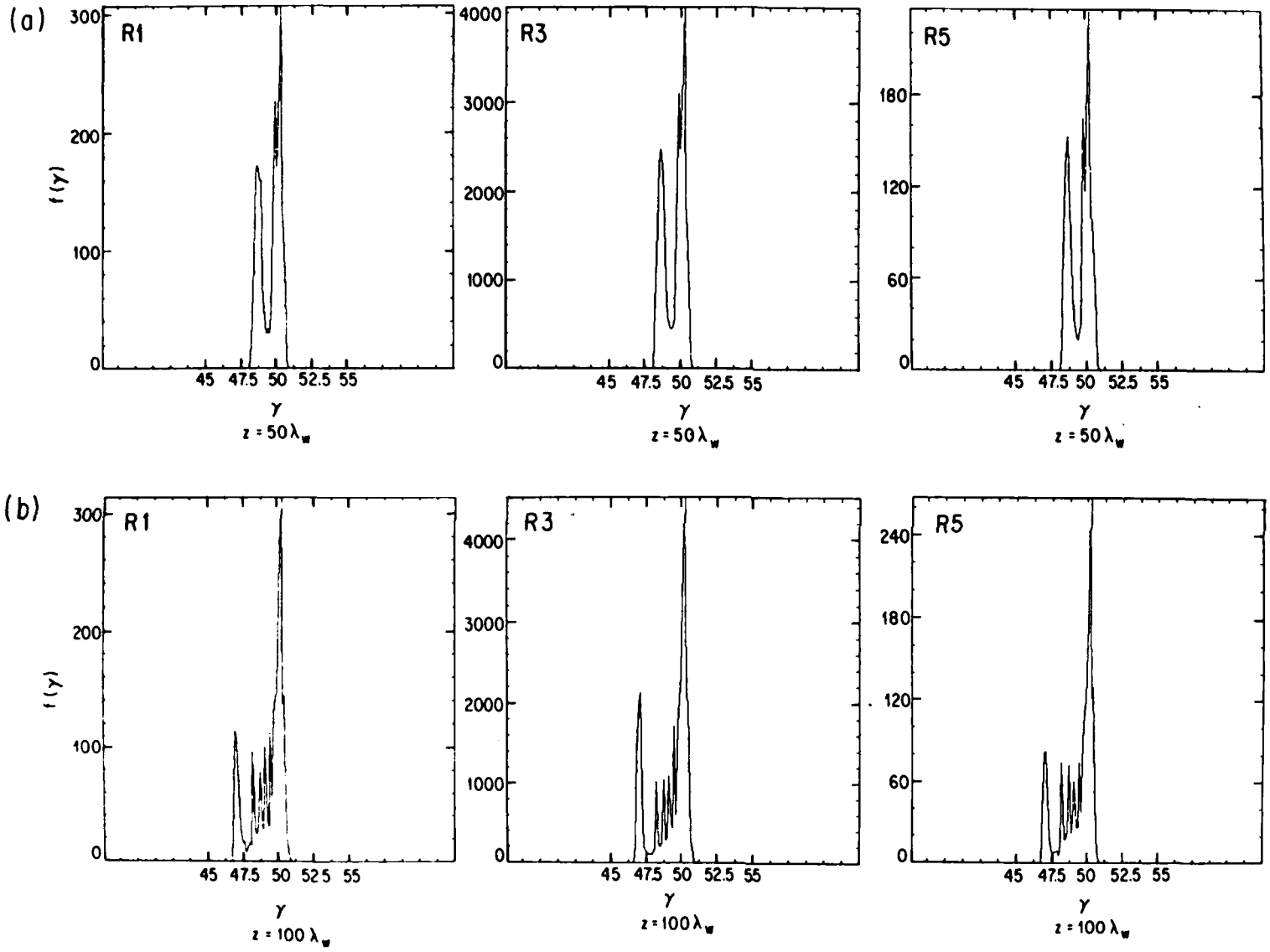

Figure 2. The Electron Energy Distribution Function a) $z = 50\lambda_w$, b) $z = 100\lambda_w$.

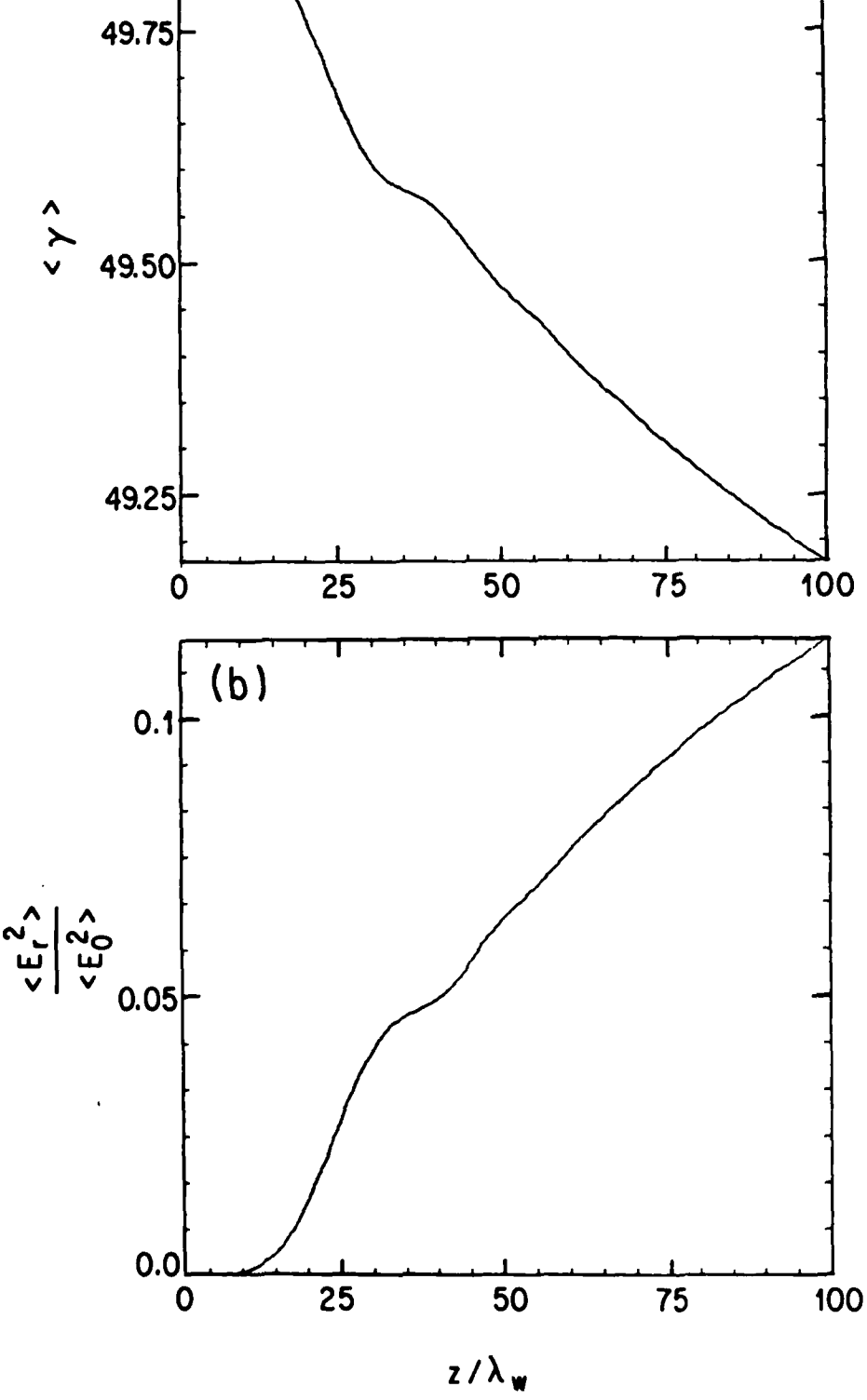

Figure 3. The Spatial Evolution of a) Averaged Electron Energy
b) Radiation Intensity

electron dynamics is dominated by the input laser. The edge effect will not play an important role in this situation, however, for a high gain or high electron density FEL, the bucket height at the edge and at the center can be substantially different from each other. In this case, the calculation using the periodic condition is not a good representation.

In order to investigate this effect, the beam density is increased by a factor of 10. The results at $z = 100\lambda_w$ are shown in Figures (4) and (5). The peak radiation amplitude is increased by approximately 10 times but the averaged gain is enhanced by only a factor of 12 (instead of 100 as it would be predicted with the infinite electron beam code). This is due to the fact that because of the strong inhomogeneities in this case, none of the electrons at the edges can remain trapped. This effect will occur also for the small signal gain part of an oscillator start up and it will be exacerbated by the presence of multimodes except if a MCWFEL is used (as shown in Section IV) .

V-1-2 Space Charge Effects

The space charge effects from one-dimensional calculations are exaggerated because the electric field lines are forced to go to either left or right. In a realistic situation the finite transverse dimension of the electron beam allows the electric field lines to go also sideways. To investigate this effect, the electron beam is divided into a collection of charged disks. The space charge electric field at z on the beam axis due to all the other charged disks can be expressed as

$$E_{s.c}(z,t) = 2\pi \int_{-\infty}^{\infty} \rho(z',\, t)dz' \left[\frac{|z-z'|}{\sqrt{|z-z'|^2 + \frac{b^2}{\gamma^2}}} - 1 \right] \mathrm{sgn}(z-z') \tag{5}$$

where b is the beam radius and

$$\mathrm{sgn}(z-z') = -1 \quad \text{if} \quad (z-z') < 0$$

$$\mathrm{sgn}(z-z') = 1 \quad \text{if} \quad (z-z') > 0.$$

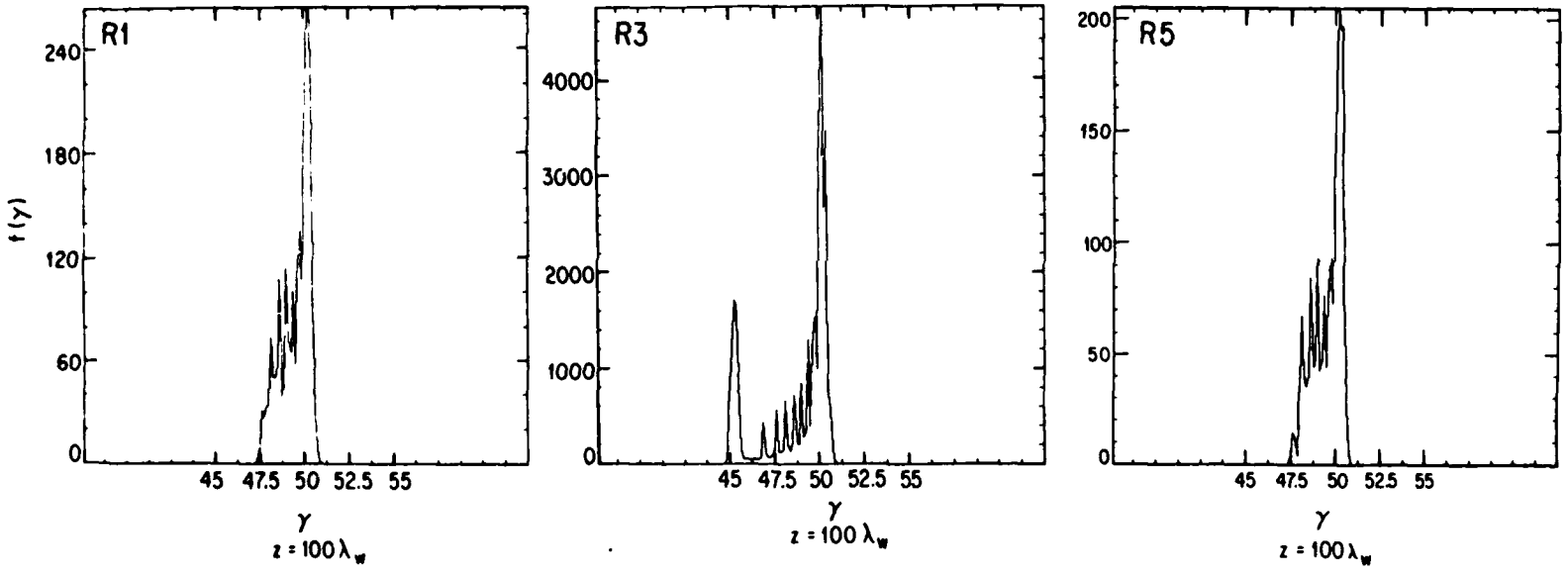

Figure 4. The Electron Energy Distribution at $z = 100\lambda_w$ With Electron Density Increased by a Factor of 10.

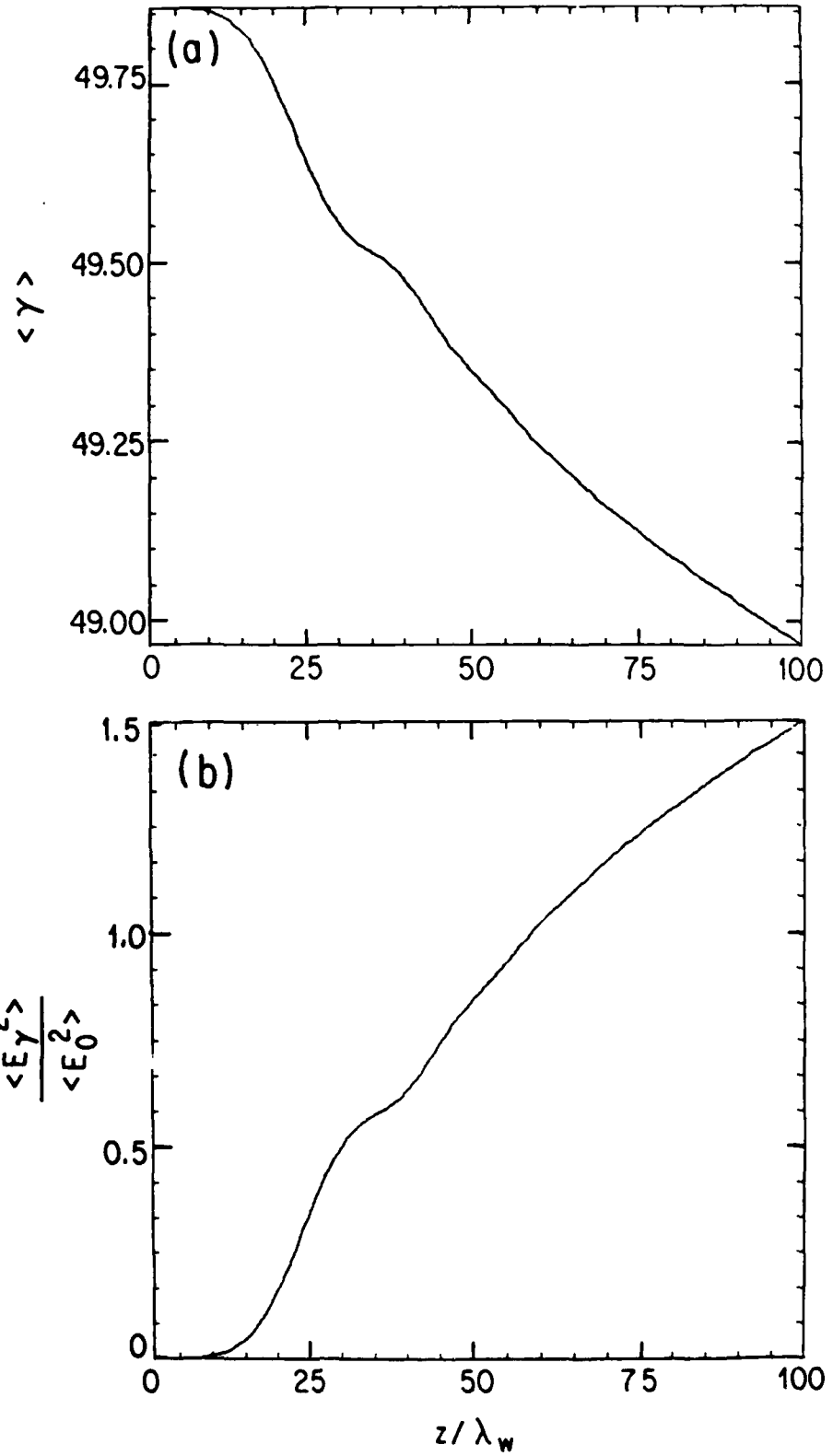

Figure 5. The Spatial Evolution of 1) Averaged Electron Energy, b) Averaged Radiation Intensity.

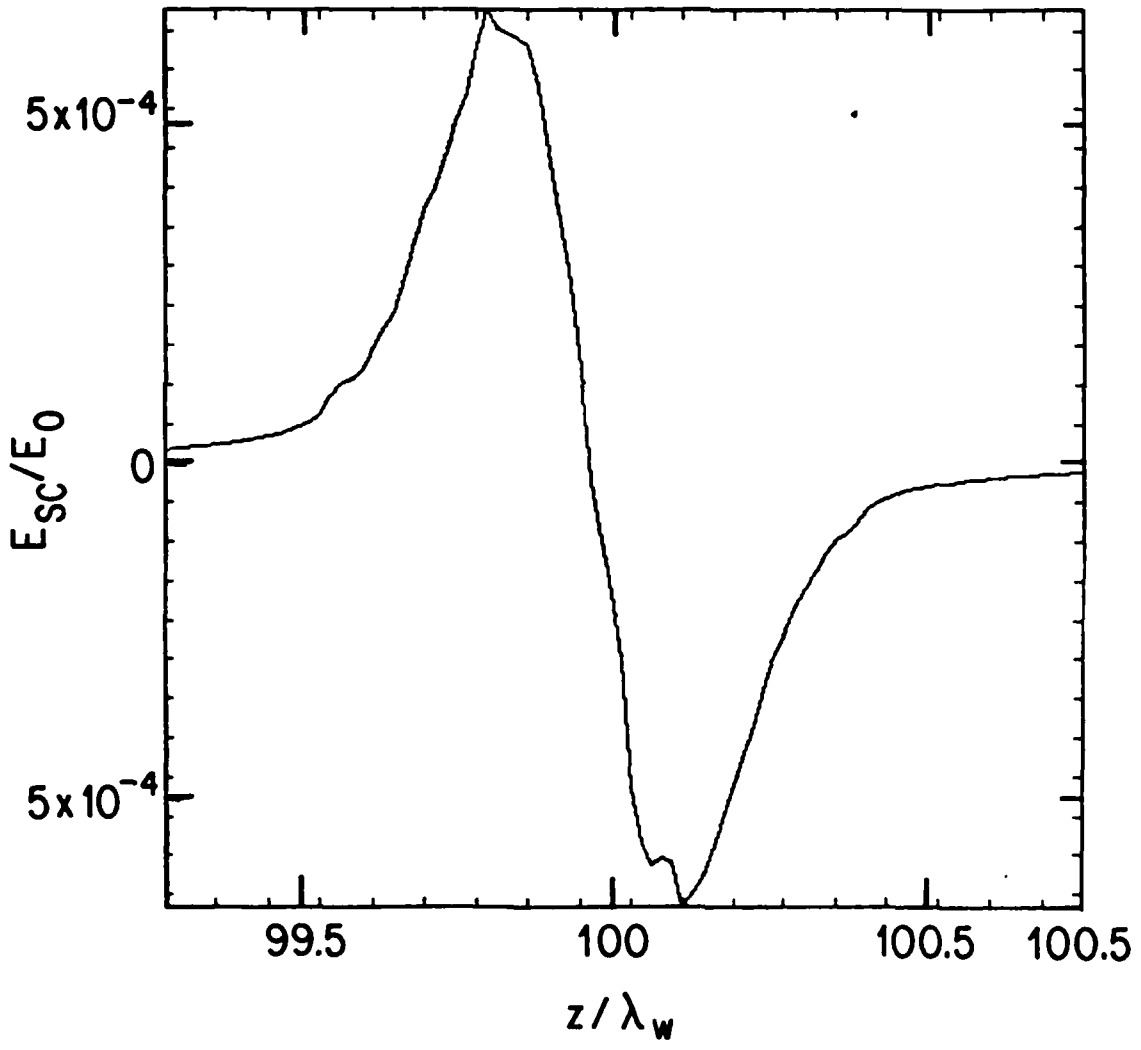

Figure 6. The Self-Consistent Spatial Space Charge Distribution at $z = 100\lambda_w$.

The spatial distribution of the space charge electric field at the end of the system is shown in Figure (6). Since the space charge force is much less than the ponderomotive force produced by the input laser and the wiggler field, the effects of the space charge on the output power are negligible. This agrees with an analytical calculation of the effect of space charge in the increase in energy spread. This calculation shows that only if the electron beam pulse is allowed to drift between the source and the interaction region for more than 50 m with I = 100A the effect can become important.

These effects, however, might play a larger role in an oscillator where small changes in the spectrum can be enhanced by the large number of round trips. At this point it should be emphazised that the code developed to perform pulse simulations is more sophisticated than other finite pulse codes previously available[1] and can follow the evolution of multimodes and density variations in a detailed manner. We think that it will prove very useful to utilize this code to study the start up, evolution and saturation of MCWFEL.

V-2 KINETIC THEORY OF THE SIDEBAND INSTABILITY IN FREE ELECTRON LASERS

In the oscillator mode of operation of a Free Electron Laser, electrons trapped in the troughs of the ponderomotive potential wells can interact coherently to produce the growth of sidebands at frequencies separated from the signal waves by multiples of the bounce frequency in the ponderomotive potential well. A kinetic treatment of this sideband instabilities for low γ Free Electron Lasers is given. It is expected that the treatement can be generalized to high γ Free Electron Lasers.

V.2-1 Introduction

The stability of a large amplitude, monochromatic plasma wave in a collisionless, one-dimensional plasma has been considered previously by many authors[2,3,4]. Because of the coherent resonant interaction between wave and electrons trapped in the troughs of the large amplitude wave, it was found that sidebands can grow exponentially.

The possibility of having these sideband instabilities in a Free Electron Laser was pointed out by N. Kroll, et al.[5] and observed in the computer simulation by A. Lin[6] (Section V.3 of this report). A kinetic treatment of this problem in a Free Electron Laser is given in this paper. The sideband instability was first investigated for electro-

static waves; the difference for the case of the Free Electron Laser is that quasi-longitudinal ponderomotive potential wells are formed by the combination of the wiggler magnetic field and the signal wave, and therefore the small amplitude sideband waves that grow are transverse, electromagnetic waves rather than electrostatic waves. Thus, instead of solving a Vlasov equation coupled with Poisson's equation as in the case of sidebands of electrostatic waves, we solve a Vlasov equation with the coupling coming from Ampere's equation.

In Section V.2-2, the Mima-Nishikawa truncation scheme[4] will be used to obtain a dispersion relation and in Section IV.2-3, the growth rates will be obtained.

V.2-2 Basic Equations

The starting equations are a 1-dimensional relativistic equation coupled with the Ampere's equation:

$$\left(\frac{\partial}{\partial z} + \dot{z}\frac{\partial}{\partial t} + \dot{p}\frac{\partial}{\partial p}\right) f(z, p, t) = 0$$

$$\left(\frac{\partial^2}{\partial z^2} - \frac{1}{c^2}\frac{\partial^2}{\partial t^2}\right)\vec{A} = \frac{4\pi e^2}{mc^2}\vec{A}\int \frac{f(z, p, t)}{\gamma}\, dp \qquad (6)$$

$\vec{A} = \vec{A}_w + \vec{A}_s + \vec{A}_R$ in equation (6) is the sum of the vector potentials for the wiggler field, signal wave and sideband which are assumed to be

$$\vec{A}_w = -\vec{e}_- a_w e^{ik_w z} + c.c \qquad (7)$$

$$\vec{A}_s = \vec{e}_- a_s e^{-i(k_s z - \omega_s t)} + c.c$$

$$\vec{A}_R = \vec{e}_- a_R e^{-i(k_R z - \omega_s t)} + c.c$$

with constant amplitude a_i. Among the terms in $\vec{A}^2$, $\vec{A}_w \cdot \vec{A}_s$ gives a bunching potential term and $\vec{A}_w \cdot \vec{A}_R$ gives coupling to the small amplitude, quasi-longitudinal test wave whose stability is to be determined.

The linearized Vlasov equation is

$$\frac{\partial f^1}{\partial t} + v \frac{\partial f^1}{\partial z} - eE^o \frac{\partial f^1}{\partial p} = eE \frac{\partial f^o}{\partial p} \tag{8}$$

where

$$E^\circ = E_o^+ e^{i[k_s + k_w) z - \omega_s t)]} \quad c.c$$

and

$$E_o^+ = \frac{ea_w a_s (k_w + k_s)}{2mic^2\gamma}$$

using Fourier-Laplace transforms of f° , f^1 , E in Equation (8) and keeping E(k) and $E(k - 2k_o)$, and $f^1(k)$, $f^1(k - k_o)$ and $f^1(k - 2k_o)$ where $k_o = k_s + k_w$, we have

$$f^1(k - k_o) + \omega_B^2 \frac{\partial}{\partial \xi} \frac{1}{\Omega^2 - \omega_B^2 \xi^2} \frac{\partial}{\partial \xi} f^1 (k - k_o)$$

$$= \Omega^{-1} (A^+ E(k) + A^- E (k - 2K_o)) \tag{9}$$

where

$$\Omega = \gamma[(\omega - \omega_o) - (k - k_o)v]$$

$$\omega_B^2 = \sqrt{2} \frac{e|E_o| \; k_o}{m\gamma}$$

$$\xi = \frac{\gamma k_o}{\omega_B} (v - \frac{\omega_o}{k_o})$$

AD-A110 306 TRW DEFENSE AND SPACE SYSTEMS GROUP REDONDO BEACH CA F/G 20/5
FREE ELECTRON LASER THEORETICAL STUDY.(U)
NOV 81 M Z CAPONI, C SHIH, J DAWSON, T LIN F49620-80-C-0079
UNCLASSIFIED FEL-27R AFOSR-TR-81-0889 NL

END
DATE FILMED
10-82
DTIC

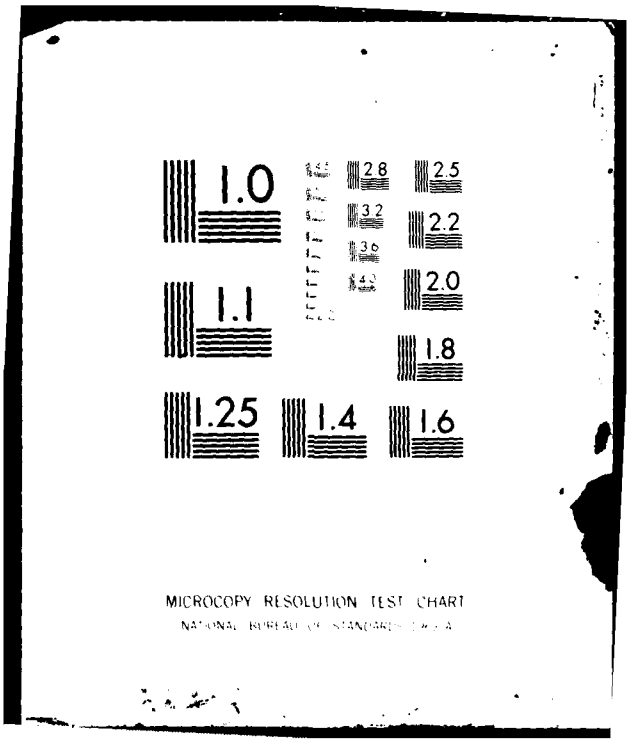
1.0
1.1
1.25
2.8
3.2
3.6
4.0
2.5
2.2
2.0
1.8
1.4
1.6
MICROCOPY RESOLUTION TEST CHART

$$A\pm = e\left[i\,\frac{1}{m\gamma^2}\,\frac{\partial}{\partial v}\,f^{\circ}_{\pm 1}\right.$$

$$-\frac{eE_o^{\pm}}{m^2\gamma^4}\,\frac{\partial}{\partial v}\,\frac{1}{\gamma[\omega-\omega_o-(k-k_o)v\;(\omega_o-k_ov)]}\,\frac{\partial}{\partial v}\;f^{\circ}_{\pm 2}$$

$$\left.-\frac{eE_o^{\mp}}{m^2\gamma^4}\,\frac{\partial}{\partial v}\;\frac{1}{\gamma[\omega-\omega_o-(k-k_o)v_{\mp}(\omega_o-k_ov)]}\,\frac{\partial}{\partial v}\;f^{\circ}_{0}\right]$$

which can be solved in terms of the parabolic cylinder function as done by Alsthul and Karpman.[7] Using the solution in Equation (6), we obtain the desired dispersion relation

$$1 = \frac{A}{\varepsilon(k-k_w,\;\omega)} + \frac{B}{\varepsilon(k-2k_o-k_w,\;\omega-2\omega_o)} \tag{10}$$

where

$$\varepsilon(k,\;\omega) = \omega^2 - k^2c^2 - \frac{\omega_p^2}{\gamma}$$

$$A = \frac{\omega_p^2}{N}\,\frac{e^2(a_w)^2\,kk_o\omega_B}{4m^2c^2}\sum_n \frac{a_nb_n}{\Omega^2-(2n+1)\omega_B^2}$$

$$B = \frac{\omega_p^2}{N}\,\frac{e^2(a_w)^2(k-2k_o)k_o\omega_B}{4m^2c^2}\sum_n \frac{c_nd_n}{\Omega^2-(2n+1)\omega_B^2}$$

$$\begin{pmatrix}a_n\\ b_n\end{pmatrix} = \int d\xi\;(1\pm\frac{\omega_B}{\Omega}\xi)\;\psi_n\;(\xi)$$

$$\begin{pmatrix} c_n \\ d_n \end{pmatrix} = \int d\xi \; (\xi^2 - 2n - 1) \; \psi_n \; (\xi) \; [\frac{E_o \pm / E_o^{\mp}}{\Omega \pm \omega_B \xi} \frac{d}{d\xi} \; f^{\circ}_{\mp 2}$$

$$+ \frac{1}{\Omega \;\; \omega_B \xi} \frac{d}{d\xi} \; f^{\circ}_o - i \; \frac{m\gamma\omega_B}{k_o e E_o^{\mp}} \; f^{\circ}_1]$$

and $\psi_n(\xi)$ is the normalized parabolic cylinder.

V.2-3 Numerical Results

Having obtained the dispersion relation, we need the zero-th order distribution function f° which gives a consistent equilibrium solution in which there is a large amplitude electromagnetic wave. Instead of following the recipe given by Bernstein, Greene and Kruskal,[8] we will use a distribution function inferred from the computer simulation.[6]

Using

$$f^{\circ} = \sum_n N_n [W - \frac{(v-v_p)^2}{c^2}]^{1/2} \quad \delta[(\frac{v-v_p}{c})^2 + (\frac{x-x_n-v_p t}{\lambda})^2 - W]$$

where N_n is the number of tapered electrons in the n-th potential trough, the dispersion relation (10) is numerically solved to obtain the curve shown in Figure 7. An unstable region is localized in k-space and occurs at frequencies $\omega < \omega_s$ (lower sideband). Figure 8 shows the bounce frequency $\omega_B \sim \sqrt{a_w a_s}$ dependence of the maximum growth rate. The decrease of the growth rate as ω_B decreases can be explained due to the disappearance of the coherence of the electrons trapped at the bottom of the ponderomotive potential well as the well becomes shallow.

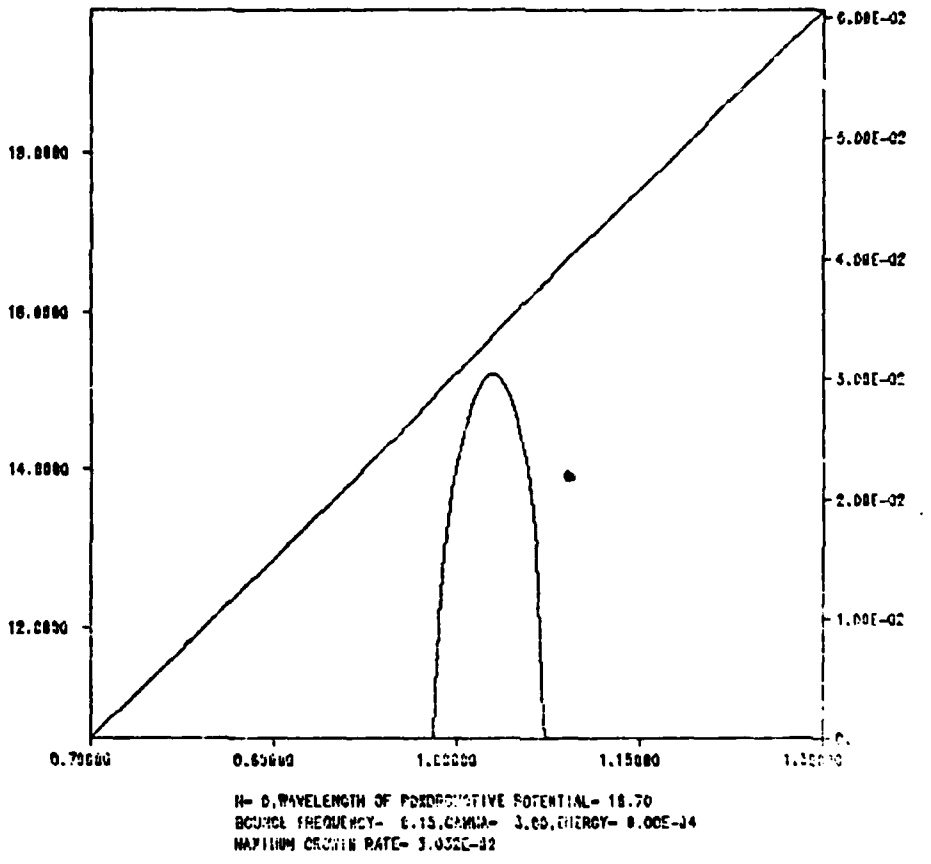

Figure 7. The real and Imaginary Parts of the Frequency Versus Wave Number for Trapped Particle Unstability.

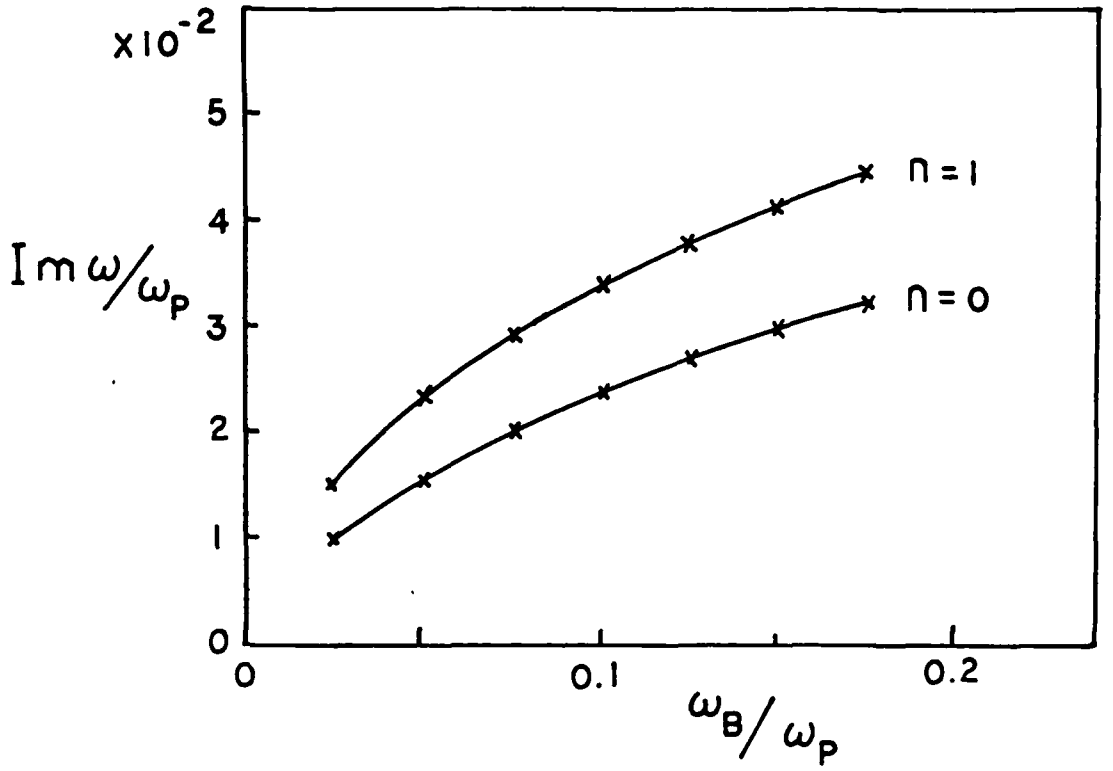

Figure 8. Growth Rate Versus Bounce Frequency for Trapped Particle Unstability.

REFERENCES V

1. W.B. Colson and S.K. Ride, Phys. of Quantum Elec. 7, 377, (1980).

2. W.L. Kruer, J.M. Dawson and R.N. Sudan, Phys. Rev, Lett. 23, 838 (1969).

3. M.V. Goldman, Ph. Z1. 13, 1281, (1970).

4. K. Mima and K. Nishikawa, J. Phys. Soc. Jap., 30, 1722 (1971).

5. N.M. Kroll, P. Morton and M.N. Rosenbluth, JASON Technical Report JSR-70-01, (1980).

6. A.T. Lin, Phys. Rev. Lett. 46, 1515 (1981).

7. L.M. Al'tshul and V.I. Karpman, Soviet Physics - JEPT 22, 361 (1966).

8. I.B. Bernstein, J.M. Greene and M.D. Kruskal, Phys. Rev. 108, 546 (1957).

V-3 Nonlinear Saturation of Parasitic Instabilities in High-Efficiency Free-Electron Lasers.

Nonlinear Saturations of Parasitic Instabilities in High-Efficiency Free-Electron Lasers

A. T. Lin
Center for Plasma Physics and Fusion Engineering, University of California, Los Angeles, California 90024
(Received 31 October 1980)

A broad spectrum of unstable parasitic waves can arise from the interaction between the trapped electrons and the radiation generated by a free-electron laser. Imposing a dc electric field with appropriate strength at the onset of trapping can substantially narrow the unstable spectrum and allows considerable enhancement in the radiation intensity. The nonlinear mechanisms which limit the enhancement process are observed to be due to nonlinear frequency shift and detrapping.

PACS numbers: 42.55.-f, 52.25.Ps

The idea[1] of generating tunable, high-power coherent radiations by passing a relativistic electron beam through a rippled magnetic field, due to the recent advance in the accelerator technology, finally becomes[2,3] a reality. The efficiency of a free-electron laser is intrinsically limited because the growth of the ponderomotive force produced by the interaction of the rippled magnetic field and the signal wave will eventually trap the electrons. There are several schemes which theoretically could substantially enhance the efficiency of a free-electron laser. For instance, if the strength of the rippled magnetic field is increased just before saturation,[4] the depth of the ponderomotive potential well becomes deeper which allows the electrons to give up more energy to photons. Another scheme, suggested by several groups,[5,6] is a variable wiggler, in which the strength and/or the period of the magnet is tapered to maintain the electrons in resonance with photons throughout the length of the device, thereby increasing energy extraction. Still another alternative[7,8] is applying a dc electric field with proper strength at the time of saturation, thereby clamping the trapped electrons in the decelerating phase which in turn transforms the dc energy into high-frequency radiations. Most of the efficiency enhancement calculations use a single-mode approximation which prohibits the parasitic instability[9,10] to occur. In this Letter, we will demonstrate, by using particle simulation (multimodes), that the enhancement process is ultimately terminated by the generation of a parasitic instability due to the interaction of the trapped electrons and the enhanced signal wave. This parasitic instability will play an important role in determining the maximum output power which can be achieved from a free-electron laser. It will be shown later that a considerable amount of improvement in output power can still be achieved by carefully choosing the strength and the turn-on time of the dc electric field.

To study the dynamics of this highly nonlinear process, a $1\frac{2}{3}$-dimensional electromagnetic particle code with periodic boundary condition is used. The parameters are the following: $\gamma_0=(1-\beta^2)^{-1/2}=3$, $ck_0=1.52\omega_p$, $P_t/P_0=10^{-3}$, and $\omega_c=qB_r/m_0c=0.53\omega_p$, where $\beta=V_0/c$, V_0 and c are, respectively, the beam velocity and speed of light, k_0 is the wave number of the rippled field, P_t is the beam momentum spread, and B_r is the rippled field strength. This set of parameters corresponds to a relativistic electron beam and a density of 10^{12} cm^{-3}, an energy of 1.5 MeV, and a current of 5 kA/cm^2. The period and the strength of the static magnetic field are, respectively, 2.2 cm and 1.2 kG. The growth rate and the efficiency of this case are $0.07\omega_p$ and 8%, respectively. The trapping of the electrons by the total longitudinal potential wave causes the saturation to occur at $\omega_p t\simeq 150$. This trapping process becomes evident in Fig. 1(a) (dashed lines) which exhibits oscillatory behavior in the time evolution of the signal wave ($ck_s=15.2\omega_p$). The oscillation frequency is at the particle bouncing frequency ω_b, which is given by

$$\omega_b=k_t(q\varphi_0/m_0\gamma_0^3)^{1/2}\omega_p, \tag{1}$$

where $ck_t=c(k_0+k_s)=16.7\omega_p$ and φ_0 is the total longitudinal potential. At the onset of trapping, a broad spectrum of parasitic waves with frequencies lower than that of the signal wave becomes unstable. The dashed line in Fig. 1(b) ($ck_a=13.7\times\omega_p$), Fig. 1(c) ($ck_s=12.2\omega_p$), and Fig. 1(d) ($ck_c=10.7\omega_p$) shows the time evolution of the three most unstable parasitic electromagnetic waves. These waves grow with a very large growth rate ($\Gamma_a=0.2\omega_p$, $\Gamma_s=0.17\omega_p$, $\Gamma_c=0.1\omega_p$) which is substantially larger than the original signal growth rate. This instability has been investigated by Kruer, Dawson, and Sudan[9] for large-amplitude electrostatic waves in plasmas and by Kroll,

Morton, and Rosenbluth[10] for high-γ_0 free-electron lasers. In this paper the dispersion relation for the parasitic instability will be derived for free-electron lasers following the approach of Ref. 9.

The instability process can be viewed as a Raman scattering of the signal wave off the electrons executing bouncing motion in the ponderomotive potential well. In the small amplitude approximation, the equation describing a driven harmonic oscillator can be used

$$\frac{d^2X_n}{dt^2}+\omega_b^2(X_n-X_{n0}-V_p t)=-\frac{q^2B_r}{m_0c^2k_0\gamma^4}\int\frac{ik_1'A_r(k',\omega')\exp(ik_1'X_n-i\omega' t)}{(2\pi)^2}dk'd\omega', \tag{2}$$

where $(X_n-X_{n0}-V_p t)$ is position of the electron relative to the nth trough, $k_1'=k_0+k'$, $V_p=\omega_p/(k_0+k_p)$ is the phase velocity of the ponderomotive potential wave which provides the trapping and A_r is the perturbing vector potential. In writing Eq. (2) the space-charge field is neglected. The density perturbation produced by the perturbed motion of the oscillators coupled with the transverse motion induced by the rippled magnetic field produced a current perturbation which is the source of the parasitic wave. By using some δ-function identities, one obtains

$$A_r(k,\omega)=\frac{\omega_b^2\omega_c^2(k_0+k)\sum_m(k_0+k+mk_p)A_r(k+mk_p,\omega+m\omega_s)}{2k_0^2\gamma_p^5(\Omega^2-\omega_p^2)\epsilon(k,\omega)}, \tag{3}$$

where $\Omega=\omega-(k_0+k)V_p$, $k_p=k_0+k_s$, and ω_b is the plasma frequency for the trapped electrons, $\gamma_p=(1-V_p^2/c^2)^{-1/2}$, and

$$\epsilon(k,\omega)=(\omega^2-c^2k^2-\omega_b^2/\gamma_p). \tag{4}$$

Retaining only the lowest-order coupling in Eq. (3), i.e., $m=0$, we obtain the desired dispersion relation

$$(\Omega^2-\omega_p^2)\left(\omega^2-c^2k^2-\frac{\omega_b^2}{\omega_p}\right)=\frac{\omega_b^2\omega_c^2}{2k_0^2\gamma_p^5}. \tag{5}$$

Substituting the appropriate parameters into Eq. (5) gives $\Gamma_3=0.12\omega_p$, $\Gamma_2=0.1\omega_p$, and $\Gamma_1=0.08\omega_p$, which is smaller than the simulation results ($\Gamma_s=0.22\omega_p$). The discrepancy could be due to the nonlinear frequency shift caused by the difference between the restoring forces for trapped electrons and for untrapped electrons. The instability tends to level off after the unstable wave energy reaches about 10^{-4} times the signal wave energy and eventually saturates because of particle diffusion and detrapping in the phase space (Fig. 2) which destroy the resonance between electrons and parasitic waves.

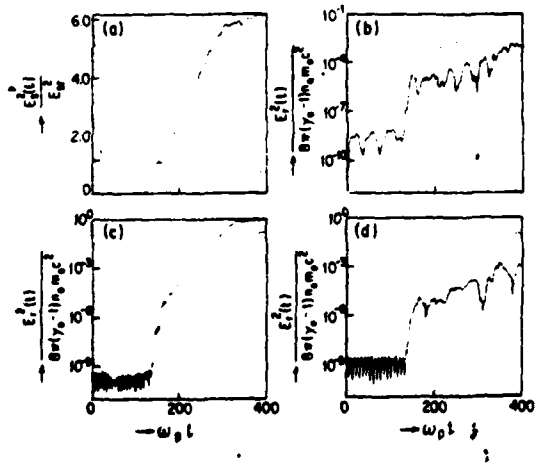

FIG. 1. Time evolution of the electromagnetic wave energies for the cases without imposing a dc electric field (dashed line) and with a dc electric field ($E_0=E_{s1}$) (a) signal wave, (b) $ck_3=13.7\omega_p$, (c) $ck_2=12.2\omega_p$, and (d) $ck_1=10.7\omega_p$.

When a dc electric field with amplitude $E_0\simeq k_1\varphi_0=E_{s1}$ where φ_0 is the saturated total longitudinal potential ($E_0\simeq 300$ V/cm) is applied at saturation, the combined action of dc and rf fields causes some of the beam electrons to become runaways while others remain clamped at the decelerating phase of the rf fields [Fig. 3(a)]. The clamped electrons transfer nearly all the dc electric field energy that went into them to the electromagnetic radiation. The escaped beam electrons are lost to the interaction. The gain in output power can in principle be extended indefinitely if the parasitic waves can be prevented from growing. The simulation results show that the unstable parasitic wave spectrum is substantially narrowed upon imposing a dc electric field at $\omega_p t=150$ (Fig. 1 solid line). This is due to the distortion of the potential well and phase shift caused by the dc electric field. In fact only the mode with $ck_2=12.2\omega_p$ remains unstable with a growth rate of $\Gamma_2=0.03\omega_p$ and the signal wave energy is increased to six times the saturation energy (E_{s0}^2) without applying the dc electric field. The en-

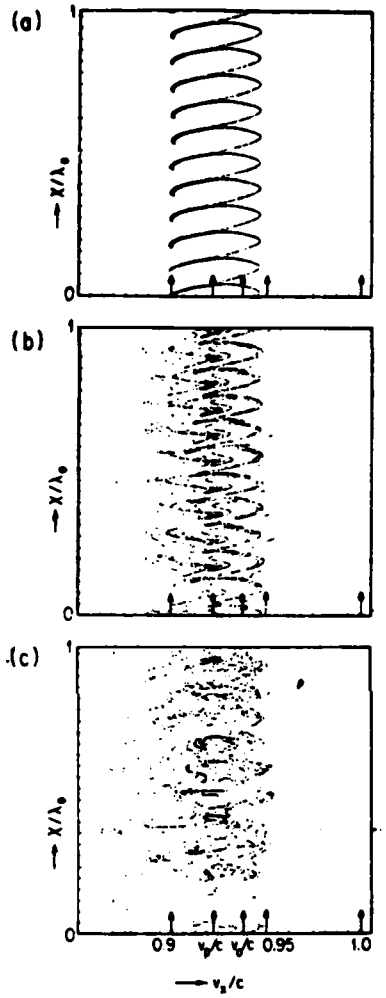

FIG. 2. Time evolution of the phase space for the case without imposing a dc electric field, (a) $\omega_p t = 145$, (b) $\omega_p t = 200$, and (c) $\omega_p t = 300$.

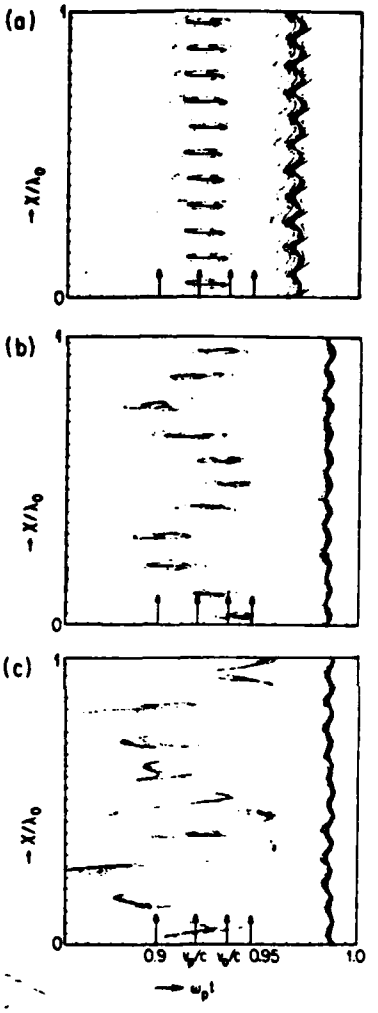

FIG. 3. Time evolution of the phase space for the case with a dc electric field of $E_0 \simeq E_{s1}$, (a) $\omega_p t = 210$, (b) $\omega_p t = 300$, and (c) $\omega_p t = 325$.

hancement process is eventually terminated due to the detrapping of resonant electrons by the ponderomotive wave with $ck_1 = c(k_0 + k_r) = 13.7\omega_p$, which is close to the original ponderomotive wave number $c(k_0 + k_s) = 16.7\omega_p$ [Fig. 3(c)]. At the same time the instability also generates a long-wavelength ponderomotive wave with wave number $c(k_s - k_r) = 3\omega_p$ [Fig. 3(b)] which does not cause any detrapping.

The results with $E_0 = 2E_{s1}$ indicate that the parasitic waves are completely suppressed for a while upon imposing the dc electric field and the mode with $ck_r = 12.2\omega_p$ begins to grow at $\omega_p t = 200$ but this mode was saturated without causing any significant detrapping. (See Fig. 4.) The saturation is due to the frequency change [Eq. (1)] introduced by the increase of φ_0. This frequency change also renders the mode with $ck_r = 10.7\omega_p$ to become unstable at $\omega_p t = 450$ and eventually detraps the resonant electrons. In this case the signal wave energy was enhanced to 25 times E_{s1}^2. However the increase rate in this case (only 25% of electrons are trapped) is lower thus requiring a longer system. The overall efficiency is small since the dc electric field spent a large amount of its energy to accelerate the runaway electrons. The efficiency enhancement factor can be substantially increased if the runaway elec-

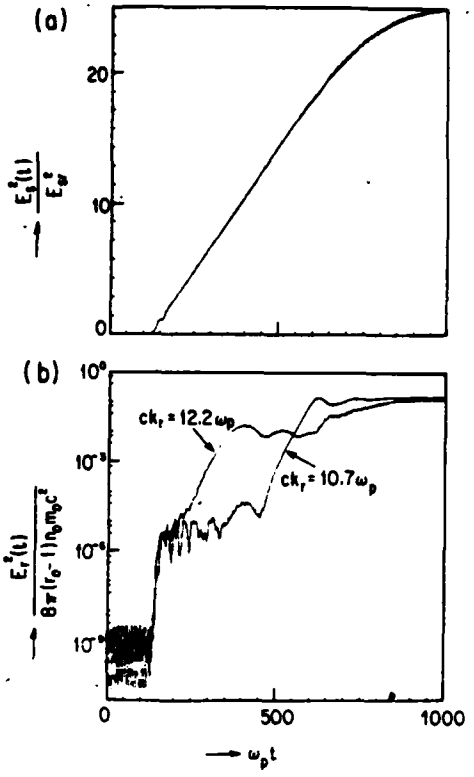

FIG. 4. Time evolution of the electromagnetic wave energies for the case with $E_0 \simeq 2E_{sl}$, (a) signal wave and (b) $ck_s = 12.2\omega_p$ and $ck_T = 10.7\omega_p$.

trons are scraped off the system.

The simulation results indicate that the output power and the efficiency of a free-electron laser can be substantially improved by applying an appropriate strength of a dc electric field at saturation. The enhancement process is ultimately terminated by the detrapping of resonant electrons caused by the parasitic instability.

The author wishes to thank Professor N. Kroll and Professor J. Dawson for many stimulating discussions and Mrs. Chih-Chien Lin for valuable numerical support. This work has been supported by the National Science Foundation under Contract No. PHY76-83686 and TRW Subcontract No. J76648DCOE, Prime Contract No. F49620-80-C-0079, and the U. S. Department of Energy under Contract No. DE-AM03-765F00010-PA-26, Task III.

[1]H. Motz, in *Proceedings of the Symposium on Millimeter Waves, Microwave Research Institute Symposia Series*. edited by J. Fox (Interscience, New York, 1960), Vol. IX, p. 155.

[2]D. A. G. Deacon, L. R. Elias, J. M. J. Madey, G. J. Ramain, H. A. Schwetman, and T. I. Smith, Phys. Rev. Lett. 38, 892 (1977).

[3]D. B. McDermott, T. C. Marshall, S. P. Schlesinger, R. K. Parker, and V. L. Granatstein, Phys. Rev. Lett. 41, 1368 (1978).

[4]A. T. Lin and J. M. Dawson, Phys. Rev. Lett. 42, 1670 (1979).

[5]P. Sprangle, Cah-Mei Tang, and W. M. Manheimer, Phys. Rev. Lett. 43, 1932 (1979).

[6]N. Kroll, P. Morton, and M. Rosenbluth, to be published.

[7]G. J. Morales, Phys. Rev. Lett. 41, 464 (1978).

[8]A. T. Lin, to be published.

[9]W. L. Kruer, J. M. Dawson, and R. D. Sudan, Phys. Rev. Lett. 23, 838 (1969).

[10]N. Kroll, P. Morton, and M. Rosenbluth, JASON Technical Report No. JSR-79-01, 1980 (unpublished).

VI CUMULATIVE CHRONOLOGICAL LIST OF WRITTEN PUBLICATIONS IN TECHNICAL JOURNALS

"Nonlinear Saturation of Parasitic Instabilities in High Efficiency Free Electron Lasers", by T. Lin. Phys. Rev. Lett 46, 1515, (1981).

"Spontaneous Spectrum and Small Signal Gain for a Tapered Wiggler Free Electron Laser", by C. Shih and M. Z. Caponi, to be published in J. of Q. Elec. V IX, 1982.

"General Theory of Multicomponent Wiggler Free Electron Lasers in the Small Signal Regime", by C. Shih and M. Z. Caponi, accepted for publication subject to revisions in Phys. Rev. A.

"Gain and Efficiency Enhancement by a Multicomponent Wiggler Free Electron Laser", M. Z. Caponi and C. Shih to be submitted for publication in Phys. Rev. A.

"Influence of Finite Emittance and Radial Profiles in the Tapered Wiggler Free Electron Laser Characteristics", by C. Shih and M.Z. Caponi to be submitted for publication

VII INTERACTIONS

1. "Free Electron Lasers at Moderate Beam Currents" M. Z. Caponi. Invited presentation at IEEE 1981 International Conference on Plasma Science, Santa Fe, New Mexico, May 18-20, 1981.

2. "Influence of the Transverse Variation of a Sinusoidal Wiggler on the Variable Wiggler Free Electron Laser Characteristics" M. Z. Caponi and C. Shih, presention at IEEE 1981 Internal Conference on Plasma Science, Santa Fe, New Mexico, May 18-20, 1981.

3. "Theoretical Studies of Free Electron Lasers at TRW" C. Shih and M. Z. Caponi, presention at Free Electron Laser Workshop, Sun Valley, Idaho, June 22-25, 1981.

4. "Small-signal Gain and the Optimization of a Tapered Free Electron Laser Wiggler", C. Shih and M. Z. Caponi, presentation at 23rd Annual meeting of the Division of Plasma Physics, American Physical Society, New York, N. Y., October 12-16, 1981.

5. "Gain and Efficiency Enhancement by a Multicomponent Tapered Wiggler Free Electron Laser", M. Z. Caponi and C. Shih, presentation at 23rd Annual meeting of the Division of Plasma Physics, American Physical Society, New York, N. Y., October 12-16, 1981.

VIII NEW DISCOVERIES

Although no invention or patent disclosure was applied for, the multicomponent wiggler scheme described in Section IV is a new discovery stemming from this research effort.

IX LIST OF THE PROFESSIONAL PERSONNEL ASSOCIATED WITH THE RESEARCH EFFORT

M. Zales Caponi: Principal Investigator and Project Manager, TRW

C. Shih: Investigator, TRW

J. Dawson: Principal Investigator, UCLA Subcontract

T. Lin: Investigator, UCLA

K. Whang: Investigator, UCLA

During the period of performance of this contract, M. Z. Caponi was awarded the independent research and development roll of honor by TRW for her work on FEL during 1980 and 1981 - In addition both TRW investigators had a strong interaction and acted in advisory capacity for the TRW FEL 10.6μm experimental program.


E
ED
82